On the applicability of post-IR IRSL dating to different environments

Inaugural-Dissertation
zur Erlangung des Doktorgrades
Dr. rer. nat.

im Fachbereich Geowissenschaften
der Freien Universität Berlin

vorgelegt von

CHRISTINE THIEL
aus Hannover

2011

Erster Gutachter: Prof. Dr. Manfred Frechen

Zweiter Gutachter: Prof. Dr. Birgit Terhorst

Eingereicht am: 05.11.2010

Tag der Disputation: 19.01.2011

Alles Wissen und alle Vermehrung unseres Wissens
endet nicht mit einem Schlusspunkt,
sondern mit Fragezeichen.

(Hermann Hesse)

Table of content

Figures

Tables

Abstract

Quaternary deposits contain detailed information on palaeoenvironmental changes, and especially terrestrial sediment archives are of great importance because these records reflect regional and sometimes even local palaeoenvironmental conditions. However, in order to apply and interpret qualitative analyses to reconstruct the palaeoenvironment, reliable chronologies are needed.

Luminescence dating techniques are suitable to set up chronological frameworks for various Quaternary deposits; however, until recently luminescence dating was restricted to the last glacial cycle. Much effort has been put into developing new luminescence dating techniques to extend the dateable age range beyond the Eemian. One promising technique to address this issue is post-IR infra-red stimulated luminescence (IRSL) dating, which makes use of an IRSL signal from feldspar which is less affected by anomalous fading, i.e. a signal decrease with time resulting in an age underestimation.

The overall objective of this thesis is to test the applicability of post-IR IRSL dating in its different forms to aeolian, coastal and shallow marine environments. In a first study, the applicability of a recently presented dating protocol (referred to as $pIRIR_{225}$) is tested on coastal and shallow marine sediments from Sardinia. The dating results suggest that the deposits under study are Eemian and older, which is in agreement with formerly published amino acid racemisation data but in contrast to radiocarbon ages.

In a second study, the $pIRIR_{225}$ dating protocol is, for the first time, successfully tested on polymineral fine grains (4-11 μm) extracted from Austrian loess. An enhanced post-IR IRSL protocol (referred to as $pIRIR_{290}$) is subsequentely applied to another loess/palaeosol sequence in Lower Austria. For the first time, a natural IRSL signal is found in saturation on a laboratory generated growth curve. This implies that for this specific signal anomalous fading is negligible, which, theoretically allows for dating up to ~300-350 ka. In the subsequent study, the two dating protocols ($pIRIR_{225}$ and $pIRIR_{290}$) are compared for several samples from three loess sections in order to investigate the differences in luminescence characteristics and age estimates for the two IRSL signals under question. Based on the new dating technique it is possible to unravel the chronostratigraphy - also beyond the Eemian - of the palaeosols preserved in the loess sequences.

However, the four presented dating studies lack reliable independent age control, and thus it is important to test the reliability of post-IR IRSL dating on known-age samples. Therefore, Japanese loess derivates, for which independent age control ranging from 25 ka to 600 ka is available, are dated using $pIRIR_{290}$. For all exept the youngest samples good agreement (within 10%) of the ages is found; for the youngest material $pIRIR_{290}$ overestimates. The overestimation might be due to a residual signal which either cannot be removed (bleached) prior to deposition or originates from thermal transfer. In order to make a statement on the

lower dating limit using post-IR IRSL dating it is crucial to investigate the cause and the size of such a residual signal. This is done on naturally bleached modern dust collected from roads in and buildings near the Chinese loess plateau and it can be shown that a great proportion of this residual signal is caused by thermal transfer; for older material such processes are of second order importance.

In conclusion, post-IR IRSL dating is applicable to all sediments under investigation. The upper dating limit is extended to ~300-350 ka for European loess; for material with lower dose rates dating beyond 350 ka is feasible. However, the lower dating limit is hampered due to residuals signals, and it is not adviseable to use the protocols presented here for Holocene samples. Future research needs to concentrate on finding an ISRL dating procedure which is neither affected by anomalous fading nor thermal transfer so that one protocol can be used to date both young and old material.

Kurzfassung

Quartäre Ablagerungen enthalten detaillierte Informationen über die Umweltveränderungen der Vergangenheit. Insbesondere terrestrische Sedimentarchive sind von besonderer Bedeutung, weil darin regionale, und manchmal sogar lokale Paläoumweltbedingungen gespeichert sind. Um die Umweltbedingungen basierend auf qualitativen Analysen rekonstruieren zu können, sind allerdings zuverlässige Chronologien unabdingbar.

Lumineszenzdatierungstechniken sind geeignet, um derartige chronologische Rahmen für zahlreiche Quartärsedimente zu erstellen, jedoch war diese Datierungemethode bis vor kurzem auf den letzten glazialen Zyklus beschränkt. In den letzten Jahren wurde viel Arbeit in die Weiterentwicklung in die Lumineszenzdatierungstechniken investiert, um Datierungen über die Eem-Warmzeit hinaus zu ermöglichen. Eine diesbezüglich sehr vielversprechende Methode ist post-IR infra-rot stimulierte Lumineszenz (IRSL). Dabei nutzt man ein IRSL-Signal von Feldspäten, welches weniger anomales Fading (Signalverlust mit der Zeit, der zur Altersunterbestimmung führt) aufweist.

Das Hauptziel der vorliegenden Arbeit ist, die post-IR IRSL-Datierung in ihren unterschiedlichen Formen an äolischen und flachmarinen Sedimenten sowie an Küstenablagerungen zu testen. Dabei wird in der ersten Studie das in der Fachliteratur vorgestellte neue Datierungsprotokoll (im Folgenden als $pIRIR_{225}$ bezeichnet) an verschiedenen Sedimenten Sardiniens getestet. Die Datierungsergebnisse zeigen, dass die Ablagerung der Sedimente im Eem oder noch davor erfolgte; dies ist in Übereinstimmung mit ehemals publizierten Ergebnissen von Aminosäurerazemisierungen, jedoch im Kontrast zu Radiokarbondatierungen.

In der zweiten Studie wird erstmalig das $pIRIR_{225}$-Protokoll erfolgreich an polyminerlischen Feinkörnern (4-11 μm) österreichischer Lösse angewendet. Ein weiterentwickeltes post-IR IRSL-Datierungsprotokoll (im Folgenden als $pIRIR_{290}$ bezeichnet) findet in der daran anschließenden Studie an niederösterreichischen Lössen seine Anwendung. Zum ersten Mal kann ein natürliches IRSL-Signal in Sättigung beobachtet werden, was impliziert, dass für das $pIRIR_{290}$-Signal kein oder nur sehr geringes anomales Fading vorhanden ist. Somit ist theoretisch eine Datierung bis ~300-350 ka möglich. In der darauffolgenden Studie werden für Lössproben aus Niederösterreich die beiden neuen Datierungsprotokolle ($pIRIR_{225}$ und $pIRIR_{290}$) im Hinblick auf Lumineszenzeigenschaften und Alter miteinander verglichen. Basierend auf den neuen Datierungstechniken ist es nun möglich, die lang umstrittene Chronostratigraphie der Löss-Paläoboden-Sequenzen auch über das Eem hinaus zu ermitteln.

Die vier vorhergehenden Arbeiten haben einen gemeinsamen Nachteil: Ihnen fehlen zuverlässige unabhängige Alterkontrollen, so dass über die Zuverlässigkeit und Genauigkeit der post-IR IRSL-Datierung keine Aussage getroffen werden kann; hierfür sind Sedimente mit Material bekannten Alters notwendig. Daher folgen $pIRIR_{290}$-Datierungen an japanischen

Lössderivaten, für die unabhänige Alterkontrollen von 25 ka bis 600 ka vorliegen. Für alle, bis auf die jüngsten Proben, stimmen die $pIRIR_{290}$-Alter innerhalb von ±10% mit der unabhängigen Alterkontrolle überein; das Alter der jüngsten Proben ist leicht überbestimmt. Ursprung der Überbestimmung könnte ein messbares Restsignal sein, welches entweder auf nicht vollständige Bleichung oder auf thermischen Tranfer zurückzuführen ist. Um das untere Datierungslimit für post-IR IRSL zu bestimmen, ist es notwendig, den Grund für sowie die Größe des Restsignals zu untersuchen. Dafür werden natürlich gebleichte ganz junge Proben benötigt, wie beispielsweise rezenter Staub von den Straßen und auf den Häusern des chinesischen Lössplateaus. Die Experimente zeigen, dass ein Großteil des Restsignals durch thermische Prozesse induziert ist; für ältere Proben sind derartige Prozesse vernachlässigbar gering.

Schlussfolgernd ist festzuhalten, dass post-IR IRSL-Datierungen auf alle untersuchten Sedimente anwendbar sind. Die obere Altersgrenze konnte für europäischen Löss auf ~300-350 ka erweitert werden; bei geringerer Dosisleistung kann es auch möglich sein, darüber hinaus zu datieren. Das untere Datierungslimit ist aufgrund von Restsignalen eingeschränkt, und es ist nicht zu empfehlen, die hier aufgeführten Datierungsprotokolle für holozäne Proben zu verwenden. Zukünftige Arbeiten sollten sich darauf konzentrieren, eine Datierungstechnik zu finden, die weder durch anomales Fading (oberes Datierungslimit) noch durch Restsignale (unteres Datierungslimit) beeinträchtigt wird, so dass ein einziges Protokoll sowohl für altes als auch für junges Material verwendet werden kann.

I

Introduction

I.1 The Quaternary and the need for reliable chronologies

The Quaternary period covers approximately the last 2.6 million years up to present (Head et al., 2008; Gibbard et al., 2010). This period is characterised by climatic changes, and can be subdivided in the prolonged glacial stages during which the continental ice sheets expanded, causing glaciation in formerly unglaciated regions, and interglacials during which the temperatures in the mid- and high latitude regions were similar to or even higher than present (Lowe and Walker, 1997). These naturally occurring climate changes have produced a geological record which exhibits diverse and manifold information on the environmental conditions at a specific time. The knowledge which can be derived from that information is important to understand the natural processes; this is a prerequisite to interpret and evaluate the influence of mankind on the present day climate.

To reconstruct and globally correlate palaeoclimatic conditions, marine cores and ice cores, which are the most continuous Quaternary records, have been investigated (Lowe and Walker, 1997). In the terrestrial realm the records are less continuous, but of great importance because these records reflect regional and sometimes even local palaeoenvironmental conditions. In order to apply and interpret qualitative analyses to reconstruct the palaeoenvironment, reliable chronologies are needed. This is not only true for the last glacial-interglacial cycle but also for the former cycles to gain more information on changes throughout the Quaternary.

However, setting up chronological frameworks is a challenging task despite manifold Quaternary dating techniques. Radiocarbon dating, which is widely used in Quaternary science, is limited to ~45 ka (e.g. Walker, 2005), and only applicable to organic material. Uranium series dating, another implemented dating technique, is restricted to carbonates, such as travertine, speleothems and corals (e.g. Scholz and Hoffmann, 2008), and certain organic material such as peat (e.g. Frechen et al., 2007). There are several other Quaternary dating methods, most of which are however only applicable to certain material are to a narrow time span; an overview of these techniques is given in e.g. Walker (2005). Among all Quaternary dating methods, luminescence dating might be the strongest technique because it determines the time elapsed since the last exposure of mineral grains to sunlight is (Aitken, 1998); this is in most sedimentary settings equivalent to the time of deposition. This technique has a large potential age range (few years to several hundred thousand years) and is applicable to a variety of sediments such as aeolian (e.g. Roberts, 2008; Singhvi and Porat, 2008), (shallow) marine (e.g. Jacobs, 2008; Sugisaki et al., 2010), fluvial (e.g. Rittenour, 2008) and glacio-fluvial and glacial (e.g. Fuchs and Owen, 2008; Lüthgens et al., 2010) deposits.

I.1.1 Luminescence dating

Luminescence dating has a scientific history of about 50 years; it started with thermoluminescence (TL) dating of heated materials such as pottery and developed towards optically stimulated luminescence (OSL) dating of sediments (see e.g. review of Wintle 2008a). In the following the basic principles of luminescence dating are briefly described and an overview on the advantages and disadvantages of the minerals used for dating is given.

I.1.1.1 Principles of luminescence dating

Mineral grains in the sediment are exposed to ionising radiation from the decay of naturally occurring radionuclides from within the sediment (external dose) and from within the grain (internal dose); the latter is of great importance for potassium feldspar, because a major contribution of the ionising radiation comes from ^{40}K. Another large part of the radiation comes from the ^{238}U and ^{232}Th decay chains; the decay of ^{87}Rb is of minor importance (Aitken, 1985). The ionising radiation causes free charge (i.e. electrons) to be trapped at defects in the crystal lattice of the minerals. When exposed to sunlight, the electrons absorb energy, which causes detrapping from their meta-stable traps and recombination in the crystal; this results in release of energy, i.e. luminescence. This process occurs under natural conditions during transport of the grains and is commonly known as bleaching or zeroing. At time of deposition the luminescence clock is thus reset, i.e. any trapped charge population is removed or at least reduced to a negligible value. This is especially true for aeolian and shallow marine sediments because of the prolonged exposure to sunlight. After burial the trapped charge population builds up again. In the laboratory, optical stimulation (in case of TL heating) of the samples frees the electrons and causes them to recombine at luminescence centres. The luminescence, which is normally visible or UV photons, can be measured using a photomultiplier. The amount of luminescence is related to the total radiation dose (palaeodose or equivalent dose, D_e) absorbed by a sample since its last exposure to daylight. Following this, both the D_e and the dose rate, i.e. the rate of energy absorption from ionising radiation during burial, have to be determined in order to derive an age estimate following the simplified formula:

$$Age\ (ka) = \frac{Equivalent\ dose\ (Gy)}{Dose\ rate\ (Gy/ka)}$$

The D_e can be determined by comparing the natural luminescence signal with that induced by laboratory irradiation (usually from a ^{90}Sr/^{90}Y beta source). In general, there are two approaches to measure the D_e: In additive dose procedures the aliquots (i.e. sub-samples), are irradiated before measurement of the luminescence signal, whereas in regenerative dose

procedures the luminescence signal is zeroed prior to irradiation. Nowadays the most commonly used procedure is the single-aliquot regenerative (SAR) dose protocol (Murray and Wintle, 2000), in which the natural luminescence signal is measured (and thus zeroed) prior to repeated irradiation and measurement on a single aliquot. Luminescence sensitivity changes are monitored and are corrected for using a known test dose. A general overview on approaches for D_e determination is given in Wintle (2008a).

For dose rate determination, either the natural radionuclides are direcetly measured or their concentrations in the sediment are determined. This is most commonly done by gamma spectrometry and/or alpha and beta counting, but other instrumental analyses such neutron activation analysis, inductively coupled plasma mass-spectrometry as well as atomic absorption spectrometry are also suitable. The measured concentrations have to be converted to individual contributions of alpha, beta and gamma dose rate using conversion factors (Adamiec and Aitken, 1998). The contribution of the cosmic rays, which is dependent on geographical position, altitude and burial depth (Prescott and Stephan, 1982), has to be added. Of importance in dose rate determination is furthermore the water content of the sediment, because water attenuates the ionising radiation. The water content is either measured using the bulk sample, or literature values are used. Even though changes in water content during burial cannot be excluded, in most cases it is assumed that the water content remained constant through time. To include uncertainties related to this issue, a large absolute error on the water content ought to be assumed, which will, however, increase the total error of the dose rate and correspondingly the total error of the age estimate.

I.1.1.2 Dosimeters in luminescence dating and possibilities to extend the age range

Since the TL studies it is known that predominantly quartz and feldspars are responsible for the luminescence signal, and hence these minerals are the main dosimeters used in OSL dating (Aitken, 1998). For feldspar infra-red stimulated luminescence (IRSL) dating of sand-sized potassium-rich feldspars (K-feldspar) are used; only a few studies have presented attempts to use plagioclase for dating (Mejdahl, 1983; Krause et al., 1997; Barré and Lamothe, 2010; Tsukamoto et al., 2010). Because feldspar can be selectively measured in the presence of other minerals using IR stimulation it is possible to use polymineral fine grain (4-11 µm) extract for dating. This is a major advantage over quartz, which cannot be measured in the presence of any other mineral; chemical or physical mineral separation is needed prior to dating. A further advantage of feldspar is the much greater luminescence intensity compared to quartz, for which only a small percentage of grains (often 5% or less) is responsible for the OSL signals from multiple grain aliquots (Duller 2008). Especially for young (Holocene) samples the quartz OSL intensity can be too small for dating (e.g. Pye et al., 1995). The dating of young quartz might furthermore be hampered by thermal transfer, which is generally of second order importance in K-feldspar dating (Aitken, 1998). Not only for dating young

samples, but especially for dating old (>70 ka) material the use of feldspar is, in principle, advantageous over quartz because the luminescence intensity saturates at much larger doses (~1.5-2 kGy; the saturation level for quartz lies at ~100-200 Gy). Therefore, feldspar has great potential to extend the age range of luminescence dating. However, feldspar suffers from anomalous fading, i.e. a decrease of the IRSL signal with time faster than expected from thermal stability measurements (Wintle, 1973; Spooner, 1994). This phenomenon can result in significant age underestimations. Corrections models have been proposed (Huntley and Lamothe, 2001; Lamothe et al., 2003; Kars et al., 2008; Morthekai et al., 2008); however, all models incorporate untestable assumptions.

Due to anomalous fading and the associated age underestimation quartz has become the preferred mineral in luminescence despite its mentioned disadvantages. Hence, over the last decade several quartz luminescence dating techniques have been investigated to extend the age range beyond the Eemian (Wintle 2008b). Jain et al. (2005) tested the potential of an isothermal TL (ITL) signal of the 325°C TL peak. When using this signal for dating Huot et al. (2006) observed a significant decrease of luminescence sensitivity during the measurement. Buylaert et al. (2006) were able to address this problem my making use of a single-aliquot regeneration and added dose (SARA) ITL procedure, and Vandenberghe et al. (2009) made use of lower measurement temperatures to solve this problem. However, even though this technique seemed very promising the ITL dose response curve did not always grow to higher doses compared to OSL. Fattahi and Stokes (2000, 2005) have presented investigations on TL signal emitting in the red part of the spectrum (red TL) rather than the near UV which has been used in conventional OSL dating. However, because of a large residual signal it has only potential for well-bleached sediments (Lai and Murray, 2006). Much effort has been put into investigating a thermally transferred OSL (TT-OSL) signal, which was first presented by Wang et al. (2006). It was suggested that this signal can in principle be used to extend the age range back to 1 Ma. Since then investigations have focussed on finding the ideal procedure to make use of the TT-OSL signal for dating (Wang et al., 2007; Tsukamoto et al., 2008; Porat et al., 2009; Stevens et al., 2009). However, TT-OSL dating is very much dependent on the sensitivity of the quartz, and not all samples show a TT-OSL signal (e.g. Schmidt et al., in press). Furthermore, the TT-OSL signal is difficult to bleach and thus can only be used for dating of well-bleached material.

Thus, the dependency on the sensitivity of the quartz has hampered most of the attempts to extend the age range using quartz as dosimeter, and hence it might be of advantage to use feldspar as dosimeter. The prerequisite to reliably date feldspar is to make use of feldspar signals that show less or no anomalous fading. One of such signals is the infra-red radiofluorescence (IR-RF) signal (Trautmann et al., 1998, 2000). During irradiation the luminescence emitted at ~865 nm is measured, and in contrast to all other luminescence techniques the IR-RF signal decreases with added doses. Even though a dating procedure for this signal was suggested (Krbetschek et al., 2000), no firm evidence is available as yet to

show the reliability of this method. Using pulsed stimulation, Tsukamoto et al. (2006) were able to show that some components of the feldspar signal fade less than others. If this is applicable to all feldspar extracts, pulsed stimulation has great potential for extending the age range. Li et al. (2007) presented a new K-feldspar dating approach named isochron dating. By making use of different grain sizes (all in the sand fraction) an isochron of equivalent dose measurements can be constructed, which is then used to obtain the burial dose of the sediment. In this procedure it is suggested that not the entire measured dose is affected by anomalous fading (Li et al., 2007) so that this phenomenon becomes of second order importance. For this method a wide range of grain sizes is needed which is apparently not present in all deposits. Much more straight forward, and in principle applicable to all deposits, is the use of a post-IR IRSL signal. Jain and Singhvi (2001) found that there is some residual trap population after an IR bleach at low temperature (50°C), which can be accessed by using high temperature (in their case 220°C) post-IR IR stimulation. This post-IR IRSL signal was systematically investigated by Thomsen et al. (2008b); they could show that the post-IR IRSL signal is less affected by anomalous fading. The basic principle is rather simple: During IR stimulation at low temperature, electrons in unstable traps recombine with holes in nearby recombination centres. This IR stimulation is followed by a second IR stimulation (post-IR IRSL) at an elevated temperature. Because the unstable traps are already empty, recombination can only take place at distant recombination centres. Thus the post-IR IRSL signal is much more stable, i.e. it fades less. The applicability of this post-IR IRSL signal to dating sand-sized K-feldspar has been tested by Buylaert et al. (2009); the observed fading rate was reduced by a factor of two, making the age correction less reliant on the untestable assumptions incorporated in any of the corrections models. This signal hence opens the opportunity to extend the age range in luminescence dating.

I.1.2 Outline of the thesis

The overall objective of this thesis is to test the applicability of post-IR IRSL dating in its different forms to aeolian, coastal and shallow marine environments, and to set up absolute chronologies for the sites under investigation. In addition to the introductory section (***Part I***), the thesis is comprised of three main chapters (***Part II*** to ***Part IV***) dealing with the application of post-IR IRSL dating, and one concluding chapter (***Part V***) which summarises the results and addresses some of the remaining questions that arose during the dissertation project. The following section gives and overview of the three main parts of thesis.

Part II: Quartz and feldspar dating of coastal deposits - When feldspar is advantageous over quartz

Preferentially quartz is used to obtain a luminescence age of sediments, because, in general, quartz OSL does not need to be corrected for anomalous fading (Aitken, 1998). However, one major drawback of quartz OSL dating is the low saturation level, i.e. the limited age range (in general ≤ 100 ka). In addition to the saturation problem, some quartz grains might have feldspar inclusions which cannot be removed by any laboratory treatment. The quartz OSL signal is then contaminated with a feldspar component, which can, in principle, be separated by making use of post-IR pulsed OSL (Denby et al., 2006; Thomsen et al., 2008a). However, when saturation of quartz is accompanied by feldspar inclusions post-IR pulsed OSL might not yield reliable ages but might underestimate the true depositional age. This was the case for several aeolian, coastal and shallow marine samples from Sardinia. In order to test whether the OSL and post-IR pulsed OSL ages are underestimates, potassium-rich feldspar extracts were dated using the post-IR IRSL measurement protocol proposed by Buylaert et al. (2009) (***Chapter II.1***).

***Part III*:** Applicability of post-IR IRSL dating to polymineral fine grains extracted from loess

The original work on post-IR IRSL dating (Buylaert et al., 2009) made use of sand-sized potassium feldspar. For loess it is difficult to extract sand-sized potassium feldspar because loess is usually dominated by the silt fraction (e.g. Pécsi and Richter, 1996); hence, most of the luminescence ages of loess have been derived from polymineral fine grains (4-11 μm) (cf. Roberts, 2008). This part of the thesis presents three studies on testing the applicability of post-IR IRSL dating to polymineral fine grains extracted from Austrian loess and associated deposits.

Firstly, the applicability of the post-IR IRSL measurement protocol presented by Buylaert et al. (2009), i.e. IR stimulation at 50°C (in the following referred to as IR_{50}) followed by post-IR IR stimulation at 225°C (in the following referred to as $pIRIR_{225}$), is tested on one fluvial layer using a sand-sized potassium-rich feldspar extract, and five loess layers using polymineral fine grain extracts from an sediment succession in Langenlois (Lower Austria) (***Chapter III.1***).

This measurement protocol was then enhanced to higher preheat and consequently higher post-IR IR stimulation temperatures based on the observations of Murray et al. (2009) that the IR dosimetry trap lies above 320°C. Following this observation, preheat temperatures up to 320°C can be used. To avoid a TL contribution contaminating the optically stimulated signal, the post-IR IR stimulation temperature should be lower than the preheat temperature and was

chosen to be 290°C (in the following referred to as $pIRIR_{290}$). Using this measurement protocol nine loess samples from a loess/palaeosol sequence in Stratzing (Lower Austria) were dated (***Chapter III.2***).

Both investigated post-IR IRSL dating protocols resulted in stratigraphically consistent ages which are considered reliable based on the good performance of the generally accepted tests (Murray and Wintle, 2003). However, nothing was known about the apparent differences of the equivalent doses, the measured fading rates and correspondingly the age estimates for the two post-IR IRSL dating protocols of interest. Therefore, both measurement protocols were applied to twelve polymineral fine grain samples from different sites in Lower Austria (***Chapter III.3***).

Part IV: Testing the reliability of post-IR IRSL dating

The major drawback in the post-IR IRSL dating studies on Austrian loess was the limited number of independent age control. Therefore it was difficult to decide on the relevance of the measured fading rates of ~1%/decade for the $pIRIR_{290}$ signal (Thiel et al., in press; Thomsen et al., in press), which contradicts the observation of an indefinitely old sample in saturation on the laboratory generated growth curve. To address this question, sediments for which independent age control is available are of major importance.

Loess derivatives in Japan are very suitable sediments for testing the reliability of post-IR IRSL dating because several tephra layers of known age (Machida and Arai, 2003) are interleaved with the loess. Two loess sequences were investigated and OSL and IRSL dated by Watanuki et al. (2005). Using the same set of samples as Wantanuki et al. (2005), post-IR IRSL dating was applied in order to test the reliability of the $pIRIR_{290}$ measurement protocol (***ChapterIV.1***).

The reliability and the age range of post-IR IRSL dating are also very much dependent on the bleachability of the signal. If the post-IR IRSL signal cannot be zeroed in nature, there will always be a residual which hampers the application of this technique to young material. Following the investigations of Thomsen et al. (2008b) there ought to be no difference in signal resetting of the IRSL and any post-IR IRSL signal. However, Buylaert et al. (2009) measured a much larger residual dose for the $pIRIR_{225}$ signal than for the IR_{50} signal in a modern sample. From that they concluded that in nature the $pIRIR_{225}$ signal bleaches much slower than the IR_{50} signal.

The post-IR IRSL dating studies on Austrian loess (*Part III*) and on the Japanese loess were also accompanied by the problem of a measured residual signal, which altered between ~5 Gy for $pIRIR_{225}$ and ~20 Gy for $pIRIR_{290}$. In any of these studies it was decided, despite any real evidence, that the measured residual signal should not be subtracted from the equivalent dose.

However, it was acknowledged that further tests on very young loess are needed to rule out any uncertainties related to the residual, which might not only originate from different signal resetting but also from thermal transfer.

Modern dust samples collected from the Chinese Loess Plateau region are the most suitable material one can think of to investigate the IRSL and post-IR IRSL residual doses: The transport mode and thus the exposure to sunlight of such material is equivalent to that of the deposit under question. Using these samples it was tested whether there is a difference in signal resetting and how much of the measured residual is caused by thermal processes (***Chapter IV.2***).

References

Adamiec, G., Aitken, M. J., 1998. Dose-rate conversion factors: update. Ancient TL 16, 37-50.

Aitken, M. J., 1985. Thermoluminescence Dating. Academic Press, London, 369 pp.

Aitken, M. J., 1998. An Introduction to Optical Dating. Oxford University Press, Oxford, 267 pp.

Barré, M., Lamothe, M., 2010. Luminescence dating of archaeosediments: A comparison of K-feldspar and plagioclase IRSL ages. Quaternary Geochronology 5, 324-328.

Buylaert, J.-P., Murray, A. S., Huot, S., Vriend, M. G. A., Vandenberghe, D., De Corte, F., Van den haute, P., 2006. A comparison of quartz OSL and isothermal TL measurements on Chinese loess. Radiation Protection Dosimetry 119, 474-478.

Buylaert, J.-P., Murray, A. S., Thomsen, K. J., Jain, M., 2009. Testing the potential of an elevated temperature IRSL signal from K-feldspar. Radiation Measurements 44, 560-565.

Denby, P. M., Bøtter-Jensen, L., Murray, A. S., Thomsen, K. J., Moska, P., 2006. Application of pulsed OSL to the separation of the luminescence components from a mixed quartz/feldspar sample. Radiation Measurements 41, 774-779.

Duller, G. A. T., 2008. Single-grain optical dating of Quaternary sediments: why aliquot size matters in luminescence dating. Boreas 37, 589-612.

Fattahi, M., Stokes, S., 2000. Extending the time range of luminescence dating using red TL (RTL) from volcanic quartz. Radiation Measurements 32, 479-485.

Fattahi, M., Stokes, S., 2005. Dating unheated quartz using a single aliquot regeneration dose red thermoluminescence protocol (SAR RTL). Journal of Luminescence 115, 19-31.

Frechen, M., Sierralta, M., Oezen, D., Urban, B., 2007. The Climate of the Past Interglacials: 8. Uranium-series dating of peat from central and Northern Europe. Developments in Quaternary Sciences, 93-117.

Fuchs, M., Owen, L. A., 2008. Luminescence dating of glacial and associated sediments: review, recommendations and future directions. Boreas 37, 636-659.

Gibbard, P. L., Head, M. J., Walker, M. J. C. and the Subcommission on Quaternary Stratigraphy 2010. Formal ratification of the Quaternary System/Period and the Pleistocene Series/Epoch with a base at 2.58 Ma. Journal of Quaternary Science 25, 96-102.

Head, M. J., Gibbard, P. L., Salvador, A., 2008. The Quaternary: its character and definition. Episodes 31, 234-238.

Huntley, D. J., Lamothe, M., 2001. Ubiquity of anomalous fading in K-felspars and the measurement and correction for it in optical dating. Canadian Journal of Earth Science 38, 1093-1106.

Jacobs, Z., 2008. Luminescence chronologies for coastal and marine sediments. Boreas 37, 508-535.

Jain, M., Singhvi, A. M., 2001. Limits to depletion of blue-green light stimulated luminescence in feldspars: implications for quartz dating. Radiation Measurements 33, 883–892.

Kars, R. H., Wallinga, J., Cohen, K. M., 2008. A new approach towards anomalous fading correction for feldspar IRSL dating - tests on samples in field saturation. Radiation Measurements 43, 786-790.

Krbetschek, M. R., Trautmann, T., Dietrich, A., Stolz, W., 2000. Radioluminescence dating of sediments: Methodological aspects.Radiation Measurements 32, 493-498.

Krause, W. E., Krbetschek, M. R., Stolz, W., 1997. Dating of Quaternary lake sediments from the Schirmacher Oasis (East Antartica) by infra-red stimulated luminescence (IRSL) detected at the wavelength of 560 nm. Quaternary Science Reviews 16, 387-392.

Lai, Z. P., Murray, A., 2006. Red TL of quartz extracted from Chinese loess: Bleachability and saturation dose. Radiation Measurements 41, 836-840.

Lamothe, M., Auclair, M., Hamzaoui, C., Huot, S., 2003. Towards a prediction of long-term anomalous fading of feldspar IRSL. Radiation Measurements 37, 493-498.

Lowe, J. J., Walker, M. J. C., 1997. Reconstructing Quaternary Environments. Longman, Essex.

Lüthgens, C., Böse, M., Krbetschek, M., 2010. On the age of young morainic morphology in the area ascribed to the maximum extent of the Weichselian glaciation in north-eastern Germany. Quaternary International 222, 72-79.

Machida, H., Arai, F., 2003. Atlas of Tephra in and around Japan. University of Tokyo Press, 337 pp. (in Japanese).

Mejdahl, V., 1983. Feldspar inclusion dating of ceramics of burnt stones. PACT 9, 351-364.

Morthekai, P., Jain, M., Murray, A. S., Thomsen, K. J., Bøtter-Jensen, L., 2008. Fading characteristics of martian analogue materials and the applicability of a correction procedure. Radiation Measurements 43, 672-678.

Murray, A. S., Wintle, A. G., 2000. Luminescence dating of quartz using an improved single-aliquot regenerative-dose protocol. Radiation Measurements 32, 57-73.

Murray, A. S., Wintle, A. G., 2003. The single aliquot regenerative dose protocol: potential for improvements in reliability. Radiation Measurements 37, 377-381.

Pécsi, M., Richter, G., 1996. Löß. - Herkunft - Gliederung - Landschaften. Annals of Geomorphology 98, 391 pp.

Porat, N., Duller, G. A. T., Roberts, H. M., Wintle, A. G., 2009. A simplified SAR protocol for TT-OSL. Radiation Measurements 44, 538-542.

Prescott, J. R., Stephan, L. G., 1982. The contribution of cosmic radiation to the environmental dose for thermoluminescene dating - Latitude, altitude and depth dependences. PACT 6, 17-25.

Pye, K., Stokes, S., and Neal, A. 1995. Optical dating of aeolian sediments from the Sefton coast, northwest England. Proceedings of the Geologists' Association 106, 281-292.

Rittenour, T. M., 2008. Luminescence dating of fluvial deposits: applications to geomorphic, palaeoseismic and archaeological research. Boreas 37, 613-635.

Roberts, H. M., 2008. The development and application of luminescence dating to loess deposits: a perspective on the past, present and future. Boreas 37, 483-507.

Schmidt, E. D., Frechen, M., Murray, A. S., Tsukamoto, S., Bittmann, F., in press. Luminescence chronology of the loess record from the Tönchesberg section: A comparison of using quartz and feldspar as dosimeter to extend the age range beyond the Eemian. Quaternary International; doi:10.1016/j.quaint.2010.07.012.

Scholz, D., Hoffmann, D., 2008. ^{230}Th/U-dating of fossil corals and speleothems. Quaternary Science Journal (E&G) 57(1-2), 52-76.

Singhvi, A. K., Porat, N., 2008. Impact of luminescence dating on geomorphological and palaeoclimate research in drylands. Boreas 37, 536-558.

Spooner, N. A., 1994. The anomalous fading of infrared-stimulated luminescence from feldspars. Radiation Measurements 23, 625-632.

Stevens, T., Buylaert, J.-P., Murray, A. S., 2009. Towards development of a broadly-applicable SAR TT-OSL dating protocol for quartz. Radiation Measurement 44, 639-645.

Sugisaki, S., Buylaert, J.-P., Murray, A., Tsukamoto, S., Nogi, Y., Miura, H., Sakai, S., Iijima, K., Sakamoto, T., 2010. High resolution OSL dating back to MIS 5e in the central Sea of Okhotsk. Quaternary Geochronology 5, 293-298.

Thomsen, K. J., Jain, M., Murray, A. S., Denby, P. M., Roy, N., Bøtter-Jensen, L., 2008a. Minimizing feldspar OSL contamination in quartz UV-OSL using pulsed blue stimulation. Radiation Measurements 43, 752-757.

Thomsen, K. J., Murray, A. S., Jain, M., Bøtter-Jensen, L., 2008b. Laboratory fading rates of various luminescence signals from feldspar-rich sediment extracts. Radiation Measurements 43, 1-13.

Thomsen, K. J., Murray, A. S., Jain, M., in press. Stability of IRSL signals from sedimentary K-feldspar samples. Geochronometria.

Trautmann, T., Krbetschek, M. R., Dietrich, A., Stolz, W., 1998. Investigations of feldspar radioluminescence: Potential for a new dating technique. Radiation Measurements 29, 421-425.

Trautmann, T., Krbetschek, M. R., Dietrich, A., Stolz, W., 2000. The basic principle of radioluminescence dating and a localized transition model. Radiation Measurements 32, 487-492.

Tsukamoto, S., Denby, P. M., Murray, A. S., Bøtter-Jensen, L., 2006: Time-resolved luminescence from feldspars: New insight into fading. Radiation Measurements 41, 790-795.

Tsukamoto, S., Duller, G. A. T., Wintle, A. G., 2008. Characteristics of thermally transferred optically stimulated luminescence (TT-OSL) in quartz and its potential for dating sediments. Radiation Measurements 43, 1204-1218.

Tsukamoto, S., Duller, G. A. T., Wintle, A. G., Frechen, M., 2010. Optical dating of a Japanese marker tephra using plagioclase. Quaternary Geochronology 5, 274-278.

Vandenberghe, D.A.G., Jain, M., Murray, A. S., 2009. Equivalent dose determination using a quartz isothermal TL signal. Radiation Measurements 44, 439-444.

Walker, M. J. C., 2005. Quaternary dating methods. John Wiley & Sons Ltd., Chichester, England.

Wang, X. L., Wintle, A. G., Lu, Y. C., 2006. Thermally transferred luminescence in fine-grained quartz from Chinese loess: Basic observations. Radiation Measurements 41, 649-658.

Wang, X. L., Wintle, A. G., Lu, Y. C., 2007. Testing a single-aliquot protocol for recuperated OSL dating. Radiation Measurements 42, 380-391.

Watanuki, T., Murray, A. S., Tsukamoto, S., 2005. Quartz and polymineral luminescence dating of Japanese loess over the last 0.6 Ma: Comparison with an independent chronology. Earth and Planetary Science Letters 240, 774-789.

Wintle, A. G., 1973. Anomalous fading of thermoluminescence in minerals. Nature 245, 143-144.

Wintle, A. G., 2008a. Fifty years of luminescence dating. Archaeometry 50, 276-312.

Wintle, A. G., 2008b. Luminescence dating: where it has been and where it is going. Boreas 37, 471-482.

II

Quartz and feldspar luminescence dating of coastal deposits - When feldspar is advantageous over quartz

II.1 Geochronology for some key sites along the coast of Sardinia (Italy)

Thiel, C.[1], Coltorti[2], M., Tsukamoto, S.[1], Frechen, M.[1]

[1] Leibniz Institute for Applied Geophysics (LIAG), S3 Geochronology and Isotope Hydrology, Stilleweg 2, 30655 Hannover
[2] Dipartimento di Scienze della Terra, Via di Laterina 8, 53100 Siena, Italy

Quaternary International (2010) 222, 36-47 (http://dx.doi.org/10.1016/j.quaint.2009.12.020)

Abstract

Recent stratigraphic surveys and facies analyses have questioned long-held interpretations of the development and furthermore the age of Quaternary sediments along the coast of Sardinia. The matter of debate is whether the investigated sediments were deposited during the Late Würmian and Holocene or during marine isotope stage (MIS) 5 and older stages. Optically stimulated luminescence (standard blue optically stimulated luminescence (OSL), post-infrared (IR) pulsed blue OSL and post-IR infrared stimulated luminescence (IRSL)) dating was applied to shallow marine and aeolian deposits as well as radiocarbon dating to bulk organic material in palaeosols. Radiocarbon dates suggest sedimentation during the Late Würmian and Holocene, whilst the luminescence results for both quartz and potassium feldspar indicate a depositional age for most of the investigated sites prior to and during MIS 5. From a geochronological point of view the luminescence ages are considered reliable because they passed all quality tests; furthermore there is good agreement of two dosimeters with different bleaching and luminescence properties. The radiocarbon ages might suffer from underestimation due to some contamination with young carbon, which however cannot be large enough to yield such young ages.

Keywords: radiocarbon dating; post-IR IRSL; post-IR pulsed blue OSL; coastal environment; Sardinia

II.1.1 Introduction

The island of Sardinia has been considered tectonically stable and has therefore been used to model the sea level changes in the Mediterranean Sea during the Last Interglacial (Antonioli et al., 1999; Lambeck et al., 2004). The elevation of the Last Interglacial sea level high stand (marine isotope substage, MIS 5e) is characterized by morphological and stratigraphical markers such as notches and beach deposits that often contain the typical warm-fossil fauna association (Senegalese fauna) including *Strombus bubonius* (Issel, 1913; Ozer et al., 1980; Hearty et al., 1986; Lambeck et al., 2004). These beach sediments as well as the marine notches occur at elevations of 3.5-11 m above sea level along the Sardinian coastline (Ozer et al., 1980; Ulzega and Ozer, 1982; Antonioli et al., 1999). The elevation on its own or in combination with the occurrence of the Senegalese fauna has often been used to correlate deposits to MIS 5e, based on the assumption that the sea level of MIS 5e has been the highest ever since. Carboni and Lecca (1985), Davaud et al. (1991) and most recently Andreucci et al. (2009) have presented another interpretation and state that at least two sea level high stands during MIS 5, most likely during substages 5e and 5c, can be found in Sardinian coastal sediments. Recently, stratigraphical surveys, facies analyses and geological mapping of some key sites along the coast of Sardinia have favoured attribution to the Holocene and Late Würmian of the deposits under study (APAT, submitted a, b; Coltorti et al., 2007, 2010) and thus question the former assumptions and the proposed sea level models.

To address the debate geochronological data are needed because stratigraphical investigations and correlations on its own are not sufficient. Apart from amino-acid racemisation (AAR) data, which are relative age attributions, and some radiocarbon and U/Th ages (Belluomini et al., 1986; Ulzega and Hearty, 1986; Coltorti et al., 2007) a reliable chronological framework has not yet been established for most of the Quaternary sediments along the Sardinian coast. Most recently, Andreucci et al. (2009) presented quartz luminescence ages for a sediment succession at San Giovanni di Sinis (western Sardinia) showing the applicability of this dating method for the deposits under investigation.

Luminescence dating techniques determine the time passed since the last exposure of mineral grains to sunlight, and thus enable to constrain the time of deposition (Aitken, 1998). Furthermore, luminescence dating spans a wide time range (few years to, theoretically, several hundred thousand years) and is suitable for a variety of sediments, e.g. aeolian, (shallow) marine, fluvial and glacio-fluvial deposits. Therefore, this dating method is a valuable tool to address the debate whether the deposits are Holocene (Coltorti et al., 2007, 2010) or MIS 5 (Belluomini et al., 1986; Ulzega and Hearty, 1986; Andreucci et al., 2009). If these sediments are Holocene or slightly older, as suggested by Coltorti et al. (2010), radiocarbon dating is another suitable method to determine the age of the sediment. Whereas luminescence dating determines the time of deposition and therefore dates the sediment itself,

radiocarbon dating estimates the time elapsed since the death of an organism (Geyh, 2005; Hogg et al., 2006); the applicability of this method is up to about 50 ka (Hajdas, 2008).

This study presents luminescence ages for both quartz and potassium feldspar of shallow marine and aeolian deposits and radiocarbon ages of bulk organic material from four sectors along the coast of Sardinia: i) San Giovanni and Capo San Marco at Sinis Peninsula, ii) Santa Reparata near Santa Teresa di Gallura, iii) Scala é Croccas in the Orosei Gulf and, iv) Is Arenas in the Cagliari Gulf (Fig. II.1) in order to address the debate whether the sediments were deposited during the Late Würmian and Holocene or during MIS 5 and older stages.

II.1.2 Geological setting and sampling locations

The section of San Giovanni di Sinis (Location 1; Fig. II.1) is located 10 km west of Oristano. The sediment succession which has a maximum thickness of 8 m (see Fig. II.2 and Coltorti et al., 2010) has been described by Lecca and Carboni (2007 and references therein). They interpret the outcrop as a shore unit, with foreshore facies evolving into a backshore and coastal dune sand, and distinguish different transgression and regression units. Recently, Andreucci et al. (2009) have described four unconformity-bounded units with three transgressive and two regressive surfaces.

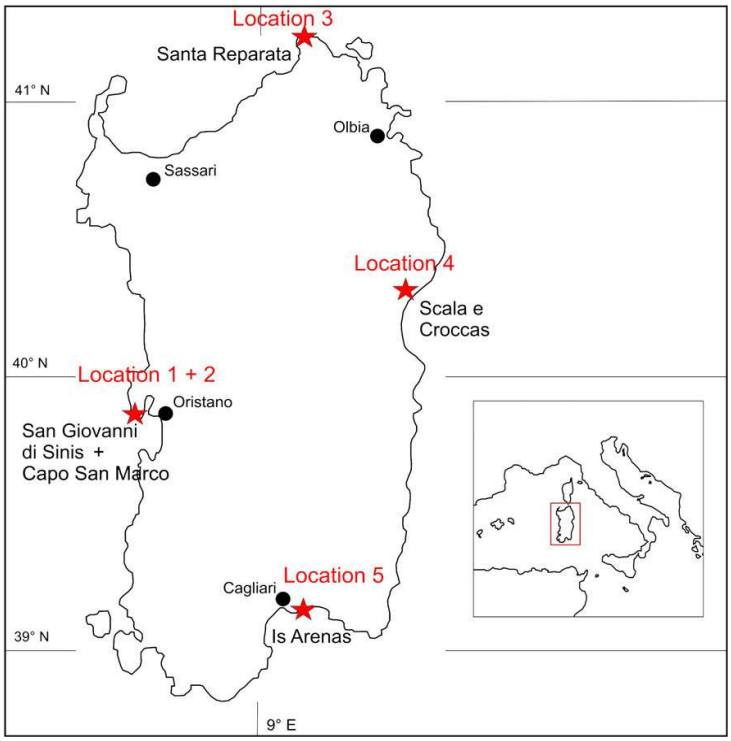

Fig. II.1: Sardinia and the study locations. 1. San Giovanni di Sinis; 2. Capo San Marco; 3. Santa Reparata; 4. Scala é Croccas, Orosei Gulf; 5. Is Arenas, Cagliari Gulf. The inset shows the location of Sardinia in the Mediterranean Sea.

Coltorti et al. (2010) interpret the sequence as aeolian in origin. In total, four samples for luminescence dating were taken from two adjacent outcrops (southern and northern outcrop, Fig. II.2). Samples SG_1 and SG_2 were taken in carbonate-rich laminated sandstone. Whereas Coltorti et al. (2010) claim that SG_1 and _2 are from the same stratigraphical unit, Lecca and Carboni (2007) allocate SG_1 to aeolian deposition and SG_2 to foreshore environment. Sample SG_3 was taken in carbonate-rich sandstone with coarse quartz pebbles.

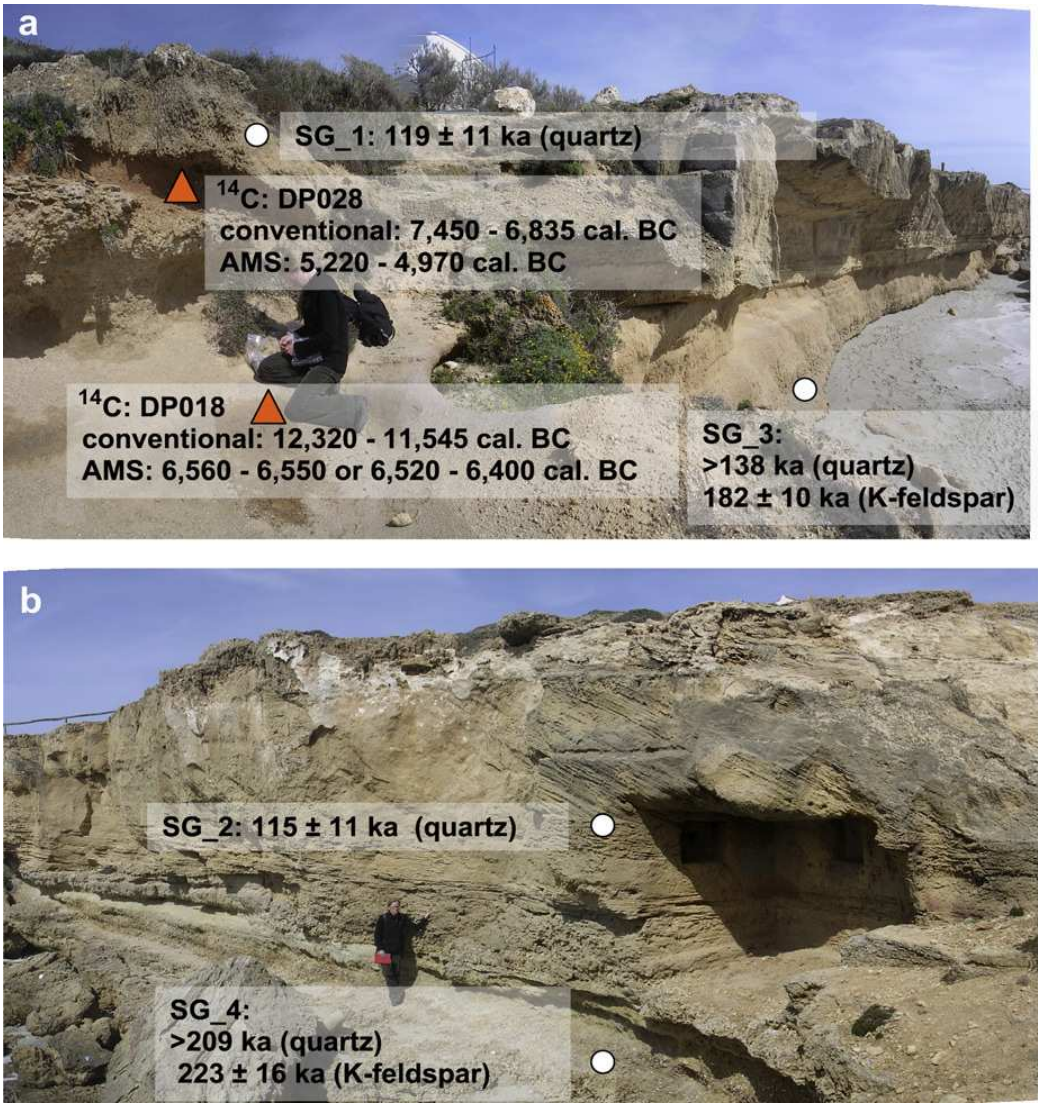

Fig. II. 2: Sampling locations and ages for San Giovanni di Sinis. a) San Giovanni northern section (Coltorti et al., 2010), where two luminescence (circle; SG_1 and SG_3) and three radiocarbon (two are indicated with triangles; DP018, DP028; the third is below and cannot be seen in the figure) samples were taken. b) San Giovanni southern section, where SG_2 and SG_4 (circles) were sampled. The presented post-IR IRSL potassium feldspar ages are fading corrected (see text). For more information on the individual samples see text as well as Lecca and Carboni (2007 and references therein), Andreucci et al. (2009), and Coltorti et al. (2010) who described the sites in more detail.

The lowermost sample (SG_4) comes from consolidated fine sands containing small shell fragments. At this site, all luminescence samples were cut off the outcrop as blocks because of the cementation. Additionally, three palaeosols were sampled for radiocarbon dating (DP018, DP028, DP029) from the northern outcrop (Fig. II.2). These palaeosols are locally consolidated (Andreucci et al., 2009); however, samples were derived from an unconsolidated part of the outcrop.

The deposits of Capo San Marco (Location 2; Fig. II.1) are located close to the San Giovanni di Sinis section on the south western side of the promontory. The sequence is composed of coarse gravels and boulders that locally created a notch in aeolianites at ca. 6-7 m asl (Fig. II.3; Coltorti et al., 2010). The aeolianite was sampled for luminescence dating (CSM_1).

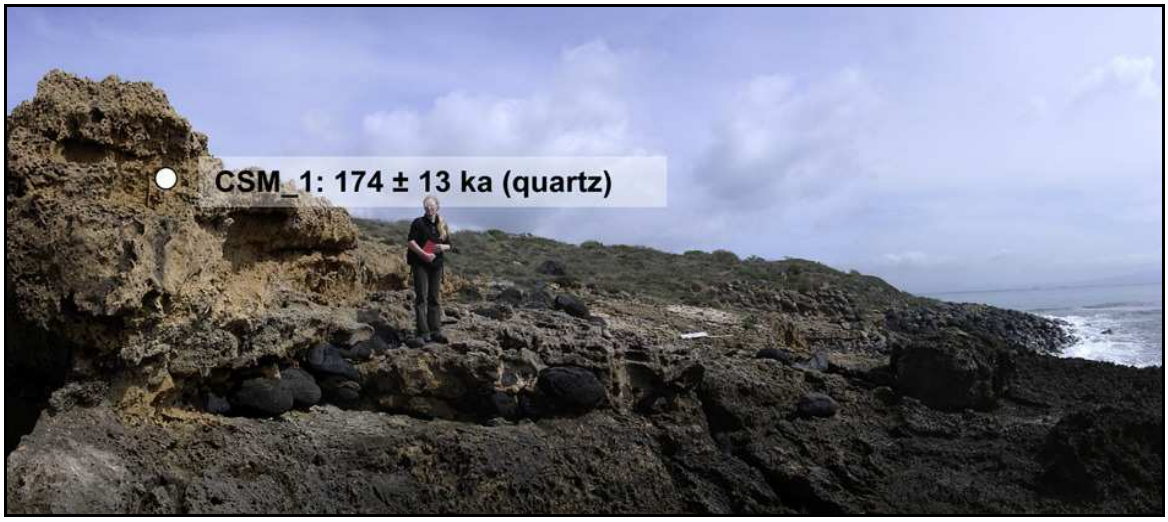

Fig. II.3: Sampling site at Capo San Marco (Sinis Peninsula), showing the luminescence dating result. More detailed geological information about this site can be found in Comaschi-Caria (1954) and Coltorti et al. (2010).

The outcrop at Santa Reparata (Location 3; Fig. II.1) is located on the east of the isthmus in the northernmost tip of Sardinia. The deposits were at first investigated by Ulzega and Ozer (1982), and later Ulzega and Hearty (1986). In their opinion the coarse beach sands and gravels rest below aeolian deposits attributed to the Last Glaciation. Further descriptions of the sediment succession of Santa Reparata are given by Belluomini et al. (1986) and Kindler et al. (1997). The latter authors distinguish three sequences formed during the last glacial period and thus revise the assumptions of Ulzega and Ozer (1982). Coltorti et al. (2010) recognize only one marine layer resting unconformably over aeolian deposits, which they attribute to Late Würmian. They state that the marine sediments are locally found in notches carved in the aeolianites and the palaeosol. Loose fine grained sand (Unit E1+2 after Coltorti et al., 2010) was sampled for luminescence (SR_1) and the pedogenized colluvium was sampled for radiocarbon dating (SR_C3), respectively (Fig. II.4).

The deposits at Scala é Croccas (Location 4; Fig. II.1) are beach ridges located about 1 km inland from the present day coastline. They are made of sandy and gravelly material reaching an elevation of ca. 4-5 m asl. Two adjacent outcrops, one of which is shown in Fig. II.5, were investigated and one sample was taken at each outcrop (SC_1, SC_2) for luminescence dating.

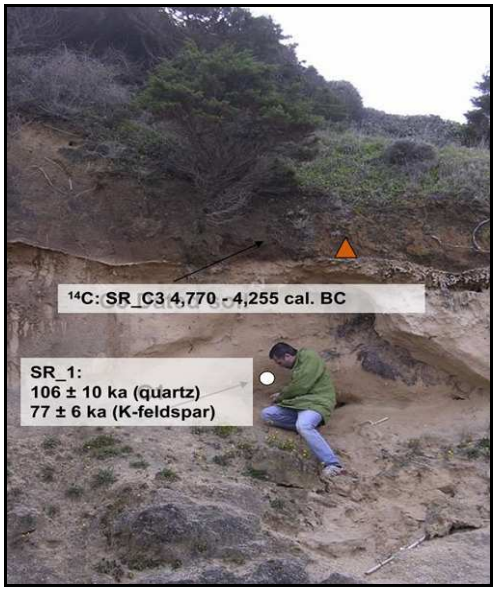

Fig. II.4: Sampling location and age estimates of Santa Reparata. The yellowish sand was sampled for luminescence dating, whereas a sample of the palaeosol was used for radiocarbon dating (triangle). A detailed site description is given by Coltorti et al. (2010).

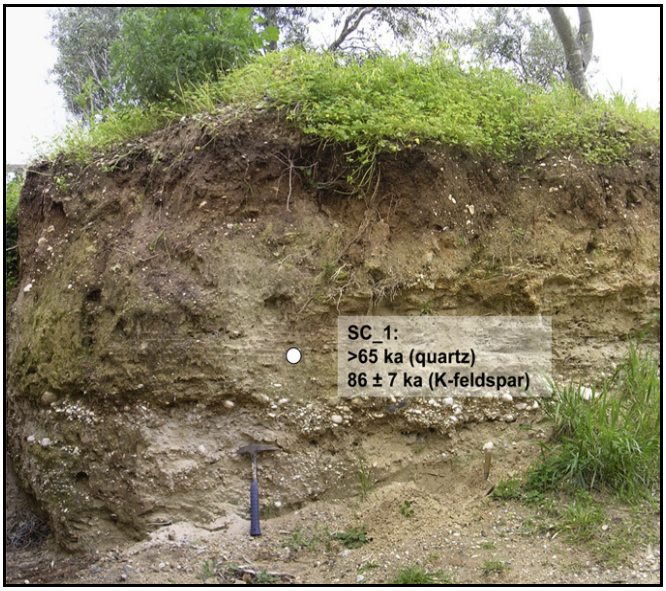

Fig. II.5: One of the sampling locations at Scala é Croccas, indicating the luminescence ages for quartz and potassium feldspar (post-IR IRSL; fading corrected). The sample was taken from a sandy layer. Description of the sedimentary composition is given by Coltorti et al. (2010).

Is Arenas (Location 5; Fig. II.1) belongs to, similar to Scala é Croccas, beach ridges succession. For luminescence dating a sand lens at the base of a clinostratified layer was sampled (IA_1). Recent excavations at the water purifier in Is Arenas, about 200 m NW of the luminescence sampling location, exposed organic mud at ca. 9 m below the surface, which was used for radiocarbon dating (IA_C1). Coltorti et al. (2010) correlate the beach ridges with washover deposits which cover the mud layer.

II.1.3 Luminescence dating

Luminescence dating methods date the last exposure of mineral grains to sunlight; most commonly quartz and potassium feldspar are used as dosimeter. As a result of environmental ionizing radiation, electrons accumulate in crystal lattice and these electrons detrap by exposure to sunlight. In an ideal case, the trapped charge population of the mineral grains was zeroed or at least reduced to a low level before deposition. After burial, electrons re-populate

in the traps due to natural ionizing radiation at a constant rate (Aitken, 1998). Light induced de-trapping causes luminescence, which can be measured in the laboratory. The amount of luminescence is proportional to the total radiation dose a sample has been exposed to since its last exposure to sunlight (equivalent dose, D_e value). The age of the deposit can then be derived by dividing this value by the radiation dose rate calculated from the radionuclide concentrations of the sediment.

II.1.3.1 Sample preparation and analytical facilities

Because of their sensitivity to light, all samples were collected either in opaque plastic tubes or as blocks (~3 kg) and were then treated under subdued red light. The outer parts (>1 cm) which might have been exposed to sunlight during sampling were removed prior to any treatment. After drying at 50°C and sieving the material with grain sizes of 100–200 μm was treated with hydrochloric acid (HCl), sodium oxalate and hydrogen peroxide in order to remove carbonates, clay coating and organic material. Quartz and potassium feldspar were separated by heavy liquid separation using sodium polytungstate. The quartz grains were additionally etched in 40% hydrofluoric acid for at least 1 h to remove any remaining feldspar grains and the alpha-irradiated outer layer (Lang et al., 1996). The etched samples were re-sieved to ensure the removal of any grains smaller than 100 μm.

The light-exposed parts of the cemented blocks of San Giovanni di Sinis and Capo San Marco were sawed under subdued red light. Afterwards, the blocks were placed in 10% HCl until the carbonate was dissolved (Sivan and Porat, 2004). The grains were repeatedly washed with water and dried before sieving. Subsequently, the above mentioned laboratory procedures were applied.

The quartz grains were mounted on stainless-steel discs using silicon oil as adhesive, whereas for the potassium feldspar grains stainless-steel cups (0.1 mm thick) were used. Medium sized aliquots, 6 mm in diameter (i.e. few hundreds of grains), were used for all measurements unless otherwise specified. Luminescence measurements were made with an automated Risø TL/OSL reader (DA-20 and DA-15; Bøtter-Jensen et al., 2003) using a calibrated $^{90}Sr/^{90}Y$ beta source (~0.15 Gy/s and ~0.08 Gy/s, respectively). For the standard quartz measurements blue light emitting diodes (LEDs), and for post-IR pulsed blue measurements additionally infrared LEDs were used for stimulation. The quartz signal was detected in UV through a 7.5 mm Hoya U-340 filter. The potassium feldspar was stimulated with infrared LEDs, and the luminescence was detected in the blue-violet region through a Schott BG39/ Corning 7-59 filter combination.

II.1.3.2 Equivalent dose measurements

II.1.3.2.1 Standard blue and post-IR pulsed blue OSL measurements of quartz

First, the purity of the quartz was checked by applying an IR depletion measurement, i.e. feldspar contamination check, on the quartz grains (Duller, 2003). The equivalent doses of the San Giovanni di Sinis and Capo San Marco samples, which showed no IR depletion, were obtained by a standard blue light single aliquot regenerative dose (SAR) protocol (Murray and Wintle, 2000). A preheat temperature of 240°C was employed, and the cut heat was set to 200°C. To minimize the effect of recuperation, a high temperature optical stimulation at 280°C for 40 s was conducted after each measurement of the test dose signal (Table II.1; Murray and Wintle, 2003). The dose response curves of SG_2 and SG_3 are shown in Fig. II.6a.

Table II.1: Quartz single aliquot regenerative dose (SAR; Murray and Wintle, 2000, 2003) and post-IR pulsed blue SAR protocol (Thomsen et al., 2008a).

Step	Treatment	Observed
1	Give dose, D_i	
2	Preheat, 240°C*, 10 s	
3**	IR stimulation, 40 s at 125°C	
3a	blue stimulation, 40 s at 125°C	L_i
4	Give test dose, D_T	
5	Cutheat, 200°C*, 0 s	
6**	IR stimulation, 40 s at 125°C	
6a	blue stimulation, 40 s at 125°C	T_i
7	blue stimulation, 40 s at 280°C	
8	Return to 1	

* For SC_1 and IA_1 a preheat and cutheat of 260°C and 220°C, respectively, was applied.

** Steps 3 and 6 are part of the post-IR pulsed blue SAR procedure. The stimulation mode is pulsed for both IR and blue stimulation. These steps are not incorporated in the SAR protocol used for the samples at San Giovanni di Sinis and Capo San Marco. For more details see text.

All other quartz samples (SR_1, SC_1, SC_2, and IA_1) exhibit feldspar contamination, which could not be removed by further etching with hydrofluoric acid. Hence, post-IR pulsed blue stimulation was applied in order to minimize feldspar contribution to the quartz signal (Denby et al., 2006; Thomsen et al., 2008a). To find the ideal setting for the pulsing measurements, the ratio of the pulsed IRSL to the [post-IR] pulsed OSL signal after giving 50 Gy was compared between different on-times ranging from 5 to 200 μs with a fixed off-time of 100 μs using SR_1 and SC_2. The total ontime for both IRSL and [post-IR] OSL

measurements was fixed to be 40 s, while the stimulation time was varied between 800 to 60 s. The lowest IRSL/[post-IR] OSL ratio was obtained between 10 and 50 µs for both samples (Fig. II.7). Thus 20 µs on-time (100 µs off) was employed for the post-IR pulsed blue OSL measurements, which is equivalent to a total stimulation time of 240 s. The settings of the pulsing measurements clearly reduce the feldspar contribution to the quartz signal, which can be seen in Fig. II.8. A preheat temperature of 240°C was chosen for SR_1 and SC_2, whereas for SC_1 and IA_1 it was set to 260°C. A cut heat of either 200°C (SR_1, SC_2) or 220°C (SC_1, IA_1) was applied, and a clean-out of 280°C was conducted at the end of each measurement cycle (Table II.1). The dose response curves for IA_1 and SC_2 are shown in Fig. II.6b.

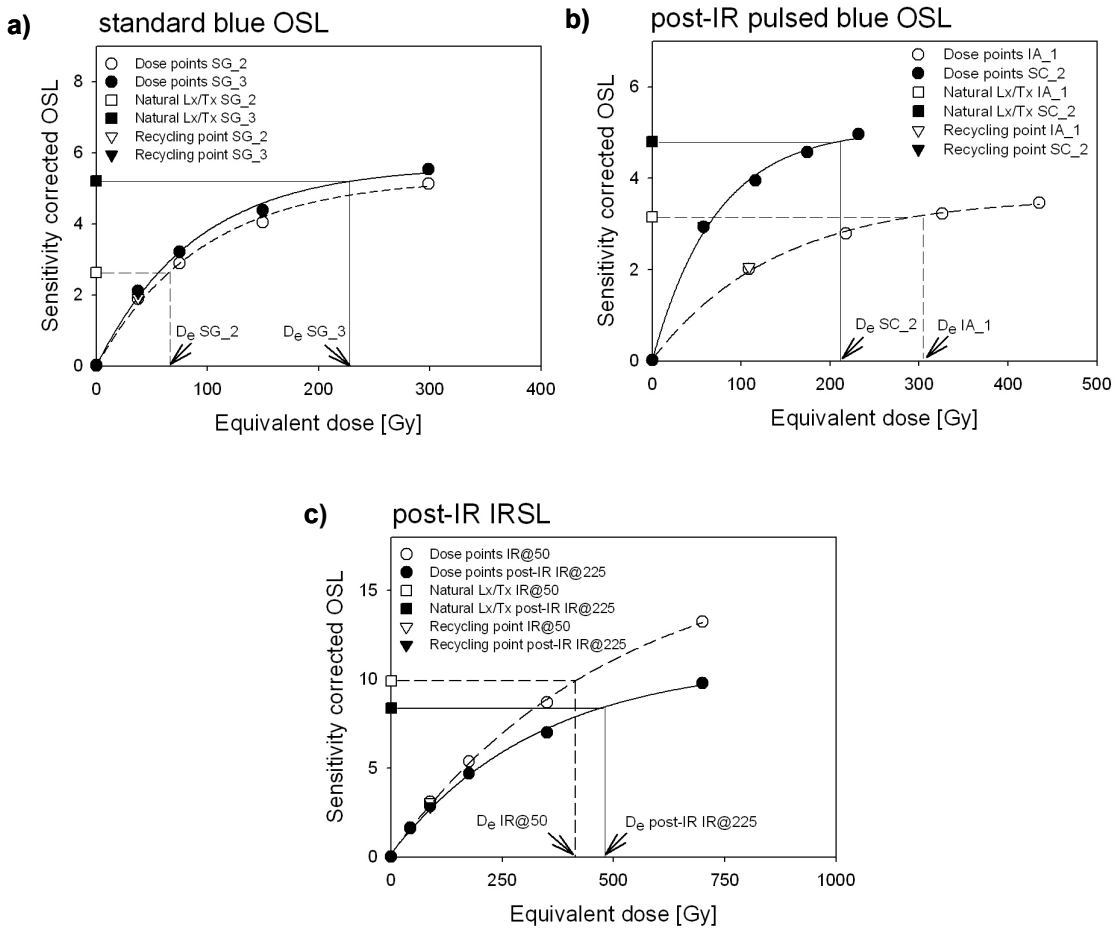

Fig. II.6: Dose response curves for a) standard blue OSL measurements of SG_2 and SG_3, b) post-IR pulsed blue OSL measurements of IA_1 and SC_2 (decay curves for pulsed OSL can be seen in Fig. 8), and c) post-IR IRSL measurements for SG_3. The dose response curves and naturals for both the IR signal at 50°C and the post-IR IR signal at 225°C are shown.

The age range of OSL dating of quartz is limited by a saturation of the signal intensity towards high doses, and the saturation dose varies between different samples (Wintle and Murray, 2006). Hence, the dose response curve obtained from each aliquot was fitted to a single saturating exponential,

$$I = I_0 (1-e^{-D/D0}),$$

where I is the sensitivity-corrected OSL for a given dose D, I_0 is the value of OSL at saturation, and D_0 is the characteristic saturation dose. Wintle and Murray (2006) suggest that it is possible to obtain a D_e value when the natural signal is no more than 85% of the maximum achievable value (I_0), which corresponds to two times D_0. Thus, the OSL ages obtained from the D_e which are beyond $2*D_0$ are regarded as minimum ages (Table II.2).

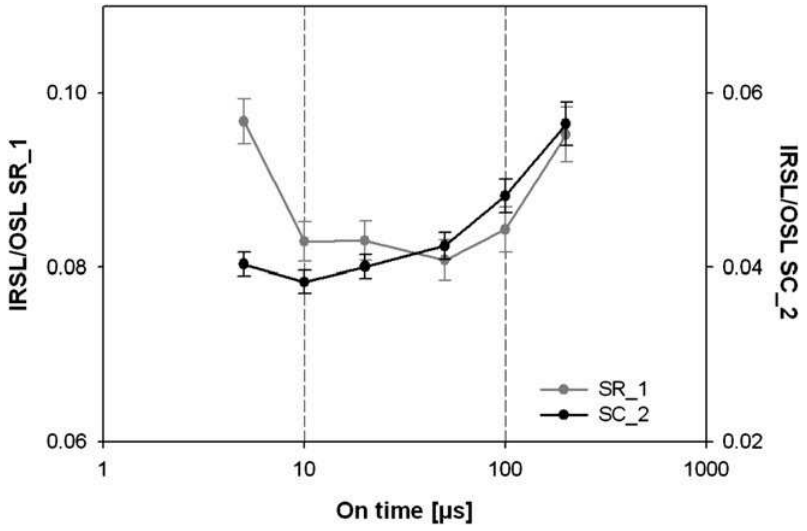

Fig. II.7: IRSL/OSL ratios for SR_1 and SC_2 using different on-times (off-time 100 µs). Based on these test measurements, 20 µs on-time was chosen for post-IR pulsed blue OSL D_e measurements. For details see text.

Dose recovery tests (Murray and Wintle, 2003) were conducted for all the samples (except SC_2). Six aliquots each for the samples were bleached twice using blue LEDs for 40 s, and were given a dose close to the De value. This dose was regarded as a surrogate of the natural dose, and the same SAR protocol was applied to check if the given dose can be accurately recovered. Dose recovery tests resulted in values between 0.90 ± 0.05 (SG_3) and 1.06 ± 0.10 (SG_1). Furthermore, recycling ratios for all quartz samples range from 0.93 ± 0.01 (IA_1) to 1.00 ± 0.01 (CMS_1) and recuperation ranges from 0.7 to 1.5%. Hence the applied protocols (standard blue OSL and post-IR pulsed blue OSL) are considered successful (Duller, 2003).

Table II.2: Summary of quartz luminescence dating results.

Location	Sample	Protocol	No. aliquots	Dose recovery	Recycling ratio	D_e value [Gy]	D_0 value [Gy]	Quartz age [ka]
San Giovanni di Sinis	SG_1	standard SAR	15	1.06 ± 0.10	0.98 ± 0.00	130 ± 7	97 ± 5	119 ± 11
	SG_2	standard SAR	18	1.01 ± 0.03	1.00 ± 0.00	82 ± 5	87 ± 4	115 ± 11
		standard SAR	60*	1.01 ± 0.03	1.01 ± 0.00	73 ± 3	85 ± 3	103 ± 9
	SG_3	standard SAR	15	0.90 ± 0.05	0.97 ± 0.00	249 ± 9	82 ± 7	> 138**
	SG_4	standard SAR	18	0.96 ± 0.07	0.99 ± 0.01	208 ± 12	97 ± 8	> 209**
Capo San Marco	CSM_1	standard SAR	18	0.97 ± 0.02	1.00 ± 0.01	183 ± 9	90 ± 6	174 ± 13
Santa Reparata	SR_1	post-IR pulsed blue SAR	23	0.96 ± 0.02	0.95 ± 0.00	199 ± 9	105 ± 6	106 ± 10
Scala é Croccas	SC_1	post-IR pulsed blue SAR	21	0.97 ± 0.01	0.97 ± 0.00	245 ± 14	100 ± 12	> 65**
	SC_2	post-IR pulsed blue SAR	19	n.a.	1.00 ± 0.00	237 ± 11	79 ± 9	> 70**
Is Arenas	IA_1	post-IR pulsed blue SAR	10	1.00 ± 0.03	0.93 ± 0.01	325 ± 34	150 ± 22	90 ± 3

* small aliquots (2mm); the median is used for equivalent dose calculation.

** minimum ages due to saturation.

Table II.3: Applied post-IR IRSL SAR protocol (Buylaert et al., 2009).

Step	Treatment	Observed
1	Give dose, D_i	
2	Preheat, 250°C, 60 s	
3	IR stimulation, 100 s at 50°C	L_i^*
4	IR stimulation, 100 s at 225°C	L_i^{**}
5	Give test dose, D_T	
6	Preheat, 250°C, 60 s	
7	IR stimulation, 100 s at 50°C	
8	IR stimulation, 100 s at 225°C	T_i^{**}
9	IR stimulation, 40 s at 290°C	
10	Return to 1	

* This is referred to as IR at 50°C.

** This is referred to as post-IR IR at 225°C.

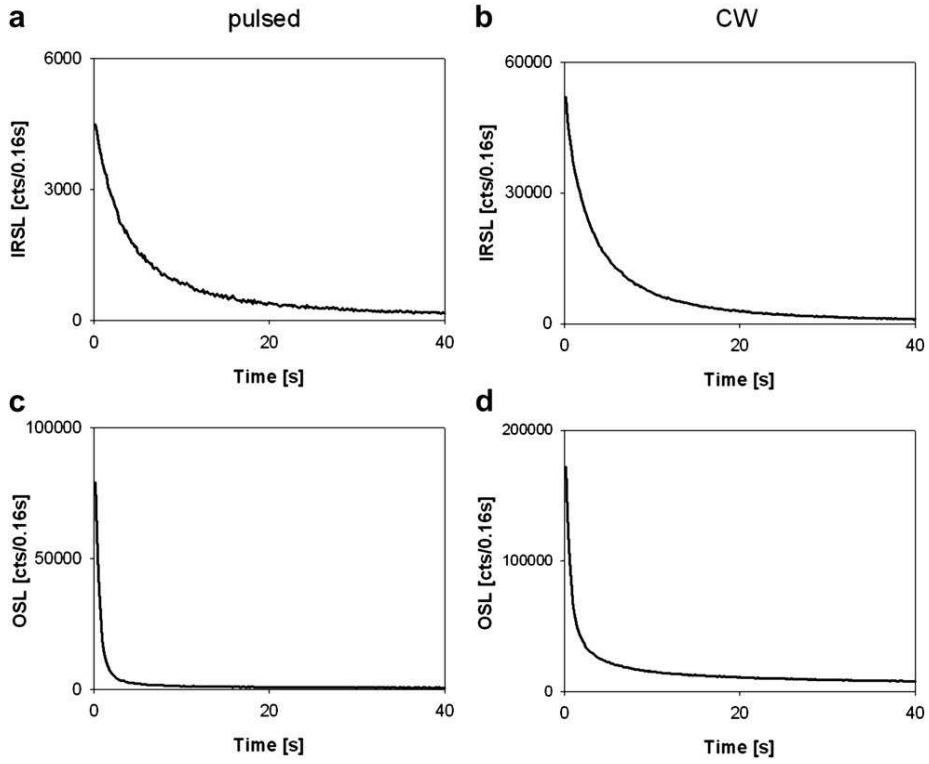

Fig. II.8: Comparison of pulsed vs. continuous wave (CW) decay curves for SR_1 (see text for details) a) pulsed IRSL signal, b) CW IRSL signal, c) pulsed OSL signal, d) CW OSL signal. The pulsed stimulation eliminates feldspar contribution to the quartz signal, indicated by the steep decay curve (fast component) of the quartz OSL signal (c), whilst CW stimulation shows a slower decay and a high background signal, indicating feldspar contribution (d).

II.1.3.2.2 Elevated temperature post-IR IRSL measurements of potassium feldspar

In contrast to quartz, potassium feldspar has a much higher saturation dose of about 2000 Gy (Aitken, 1998), and therefore IRSL dating was applied to the samples which showed saturation for the quartz. However, the applicable age range using potassium feldspar is hampered by anomalous fading (Spooner, 1994). Anomalous fading is a result of quantum-mechanical tunnelling (Visocekas, 1985), which causes a decrease of the IRSL signal with time faster than expected from thermal stability measurements; hence, IRSL ages tend to underestimate. The fading rate is expressed as signal loss in %/decade, known as *g*-value (Aitken, 1985). Corrections for this effect are needed and have been proposed by Huntley and Lamothe (2001) and Lamothe et al. (2003). Nevertheless, the corrections involve inherent assumptions, including that the fading rate observed on a laboratory timescale is relevant to geological time (e.g. Huntley and Lamothe, 2001). For standard IRSL measurements, i.e. IR stimulation at 50°C, a fading correction of up to 40% (Huntley and Lamothe, 2001) is needed

depending on the mineral provenance, which emphasises the importance of investigations focusing on more stable, i.e. less fading signals. Based on the identification of potassium feldspar signals that show less anomalous fading (Thomsen et al., 2008b), Buylaert et al. (2009) successfully applied an enhanced single aliquot regenerative dose IRSL dating protocol, termed elevated temperature post-IR IR protocol. In their study, the observed fading rates could be reduced by a factor of two, and the corrected ages agreed well with ages derived from independent age control. The measurement protocol proposed by Buylaert et al. (2009; Table II.3) was used, and the grains bleached after a preheat of 250°C for 60 s with IR diodes at 50°C for 100 s and subsequently measured the luminescence at 225°C for 100 s. The effect of recuperation was reduced by an IR illumination at 290°C (40 s) at the end of each measurement cycle. Within the post-IR IR protocol the standard IRSL signal at 50°C is also recorded and thus it is possible to compare both the D_e values and the fading rate for the two signals (Table II.4). The dose response curves for both the IRSL signal at 50°C and the post-IR IRSL signal at 225°C of SG_3 are shown in Fig. II.6c. Buylaert et al. (2009) observed indistinguishable dose response curves for the two signals for their samples, whereas for SG_3 the curve of the post-IR IRSL measurement flattens off earlier. For all samples recycling ratios are very close to 1.0 (Table II.4), and recuperation is well below 5%.

In the laboratory fading rates can be measured as an IRSL signal decrease over time on artificially irradiated aliquots. Therefore, for fading measurements the same aliquots used for D_e measurements, i.e. eight per sample, were bleached, given a dose of ~35 Gy and measured after storage ranging from repeated prompt measurements to delays of ~15 h. As suggested by Auclair et al. (2003) the preheat was applied immediately after irradiation and before storage. Fading rates for the IRSL signal at 50°C range from 2.9 ± 0.1%/decade to 5.2%/decade, whereas for the post-IR IRSL signal at 225°C they are reduced to 1.2 up to 1.8%/decade. Hence, as expected, the post-IR IRSL signal shows less fading, i.e. the post-IR IRSL signal is more stable than the standard IRSL signal. After fading correction the ages of the IRSL signal at 50°C are indistinguishable from the fading corrected ages of the post-IR IRSL signal at 225°C (Table II.4).

For the dose recovery test (Wallinga et al., 2000) six aliquots for each sample were bleached for 4 h in a Hönle SOL2, placing the aliquots at a distance of ~1.2 m from the light source to ensure the samples do not heat above room temperature. Three aliquots for each sample were then given a dose close to the D_e value and subsequently the same SAR post-IR IR protocol was applied to check if the given dose can be accurately recovered, while the other three aliquots were used for the measurement of the residual dose after bleaching. Residual doses of ~5 Gy were measured for the post-IR IRSL signal, and after subtraction of the residual the dose recovery test resulted in values ranging from 0.89 ± 0.01 to 0.96 ± 0.01. For the IRSL signal at 50°C the dose recovery is comparably less satisfactory, however, still in the accepted range of 20% (Wallinga et al., 2000).

Table II.4: Summary of potassium feldspar (IR at 50°C and post-IR IR at 225°C) dating results. Number of aliquots is eight per sample, except IA_1, where only seven aliquots were used for calculations**.**

Location	Sample	Dose recovery		Recycling ratio		D_e value [Gy]		*g*-value [%/decade]		Fading uncorr. age [ka]		Fading corr. age [ka]	
		IR@50	post-IR IR@225	IR@50	post-IR IR@225	IR@50	post-IR IR@225	IR@50	post-IR IR@225	IR@50	post-IR IR@225	IR@50	post-IR IR@225
San Giovanni di Sinis	SG_3	0.96 ± 0.01	0.96 ± 0.01	1.00 ± 0.00	1.00 ± 0.00	343 ± 6	398 ± 6	3.0 ± 0.1	1.3 ± 0.1	142 ± 8	165 ± 9	182 ± 11	182 ± 10
	SG_4	0.93 ± 0.02	0.94 ± 0.02	0.99 ± 0.00	0.99 ± 0.00	276 ± 6	325 ± 8	2.9 ± 0.1	1.2 ± 0.0	173 ± 13	203 ± 15	220 ± 16	223 ± 16
Santa Reparata	SR_1	0.91 ± 0.04	0.94 ± 0.02	1.01 ± 0.00	1.01 ± 0.00	121 ± 2	166 ± 1	5.2 ± 0.0	1.8 ± 0.0	49 ± 4	67 ± 5	78 ± 6	77 ± 6
Scala é Croccas	SC_1	0.79 ± 0.02	0.89 ± 0.01	1.00 ± 0.00	0.99 ± 0.00	291 ± 3	342 ± 3	3.4 ± 0.0	1.4 ± 0.1	66 ± 5	78 ± 6	87 ± 7	86 ± 7
	SC_2	0.94 ± 0.00	0.96 ± 0.01	1.00 ± 0.00	1.00 ± 0.00	301 ± 3	351 ± 3	3.6 ± 0.1	1.4 ± 0.1	75 ± 5	88 ± 6	101 ± 7	97 ± 7
Is Arenas	IA_1	0.82 ± 0.02	0.93 ± 0.01	0.99 ± 0.00	1.00 ± 0.00	220 ± 3	293 ± 4	4.4 ± 0.1	1.5 ± 0.0	52 ± 7	70 ± 9	76 ± 10	78 ± 10

Table II.5: Summary of dosimetry data.

Location	Sample	U [ppm]	Th [ppm]	K [%]	Cosmic dose [Gy/ka]	Dose rate quartz [Gy/ka]	Dose rate potassium feldspar [Gy/ka]
San Giovanni di Sinis	SG_1	1.29 ± 0.01	1.99 ± 0.02	0.44 ± 0.01	0.16 ± 0.03	1.09 ± 0.11	n.a.*
	SG_2	0.69 ± 0.01	1.10 ± 0.02	0.27 ± 0.01	0.09 ± 0.01	0.71 ± 0.08	n.a.*
	SG_3	0.82 ± 0.01	2.90 ± 0.03	1.27 ± 0.01	0.13 ± 0.01	1.81 ± 0.13	2.41 ± 0.13
	SG_4	0.64 ± 0.03	1.32 ± 0.06	0.60 ± 0.02	0.12 ± 0.04	1.00 ± 0.11	1.60 ± 0.11
Capo San Marco	CSM_1	0.63 ± 0.01	1.22 ± 0.01	0.64 ± 0.01	0.18 ± 0.02	1.05 ± 0.09	n.a.*
Santa Reparata	SR_1	1.02 ± 0.04	2.65 ± 0.07	1.41 ± 0.02	0.09 ± 0.01	1.87 ± 0.19	2.47 ± 0.19
Scala é Croccas	SC_1	1.25 ± 0.03	5.28 ± 0.09	3.33 ± 0.03	0.45 ± 0.05	3.80 ± 0.34	4.40 ± 0.34
	SC_2	0.95 ± 0.05	3.23 ± 0.09	3.13 ± 0.04	0.42 ± 0.04	3.41 ± 0.27	4.01 ± 0.27
Is Arenas	IA_1	1.01 ± 0.04	2.69 ± 0.08	3.38 ± 0.04	0.42 ± 0.04	3.60 ± 0.55	4.20 ± 0.55

***** Dose rate for potassium feldspar only presented for those samples where elevated temperature post-IR IRSL measurements were applied.

II.1.3.3 Dosimetry

The dose rates were derived using high-resolution gamma-ray spectrometry. Depending on the available amount of material, either 50 g or 700 g of the dry sample material were filled in N-Type or Marinelli beakers, respectively, and stored at least one month before measurements to build up equilibrium between radon and its daughters. Radioactive disequilibrium was not observed.

For the calculations, the water content for the cemented blocks of San Giovanni di Sinis and Capo San Marco was set to 5 ± 2% (Sivan and Porat, 2004) and to 10 ± 2% for all other samples. This is in agreement with measured water contents presented by Andreucci et al. (2009). A possible geochemical alteration of the cemented samples was neglected, as it is assumed that the cementation happened within a comparably short time period (a few hundreds of years after deposition of the sand). Hence, no changes in water or air content and thus in dose rate as suggested by Nathan and Mauz (2008) were incorporated, as these factors are considered as constant.

The internal beta-dose rate of the potassium feldspar grains was calculated after Mejdahl (1979; absorbed beta-dose fraction of ^{40}K), and Readhead (2002; absorbed beta-dose fraction of ^{87}Rb). The suggested mean of 12.5 ± 0.5% potassium was used for calculations (Huntley and Baril, 1997). Because the outer rim of the potassium feldspar grains was not removed, external alpha radiation was taken into account (a-value 0.08 ± 0.02). The dosimetry results are summarized in Table II.5. The quartz dose rates range from 0.71 ± 0.08 Gy/ka (SG_2) to 3.80 ± 0.34 Gy/ka (SC_1); the carbonate-rich sediments of San Giovanni di Sinis and Capo San Marco show significantly smaller dose rates than all other samples. Due to internal potassium, the dose rates for potassium feldspar are higher than the quartz dose rates and range from 1.60 ± 0.11 Gy/ka (SG_4) to 4.40 ± 0.34 Gy/ka (SC_1).

II.1.4 Radiocarbon dating

Most of the radiocarbon ages for the bulk organic material were obtained using the conventional method (gas proportional counters; Leibniz Institute for Applied Geophysics, Hannover). Three samples (DP018, DP028, DP029) were additionally measured using accelerator mass spectrometry (AMS; Beta-Lab) (Hajdas, 2008). The material used was bulk organic material from soils or sediment.

For the conventional method the calculation of the radiocarbon ages is based on the radioactive half-life after Libby, i.e. 5568-years, and the ages have been fitted to the international radiocarbon timescale by the NBS oxalic acid standard. All data are δ^{13}C corrected (Table II.6). The ages were calibrated to calendar years following Stuiver and Reimer (1993).

Table II.6:. Summary of radiocarbon ages.

Location	Sample	Lab ID	Method	Material	$\delta^{13}C$ ‰	Conventional age BP	Calibrated BC
San Giovanni di Sinis	DP 018	Hv 25676	conventional	org. matter in soil	- 24.3	11,930 ± 240	12,320 - 11,545
		Beta 250287	AMS	org. matter in soil	- 26.1	7,610 ± 50	6,560 - 6,550 or: 6,520 - 6,400
	DP 028	Hv 25677	conventional	org. matter in soil	- 26.4	8,150 ± 155	7,450 - 6,835
		Beta 250288	AMS	org. matter in soil	- 25.8	6,160 ± 50	5,220 - 4,970
	DP 029	Hv 25678	conventional	org. matter in soil	- 27,2	10,520 ± 215	10,915 - 10,160
		Beta 250289	AMS	org. matter in soil	- 26.1	4,950 ± 40	3,800 - 3,650
Santa Reparata	SR_C3	Hv 25679	conventional	org. matter in soil	- 26.6	5,655 ± 205	4,770 - 4,255
Is Arenas	IA_C1	Hv 25670	conventional	org. matter in sediment	- 25.6	2,035 ± 105	195 - 75 AD

II.1.5 Results and discussion

The lowermost sample of San Giovanni di Sinis (SG_4) resulted in a fading corrected potassium feldspar age of 223 ± 16 ka (Table II.4) and in a minimum quartz age of 209 ka (Table II.2); hence, the two dosimeters are in very good agreement. These age estimates correspond to previous interpretations (Carboni and Lecca, 1985; Davaud et al., 1991; Kindler et al., 1997), who state that these deposits are older than MIS 5. The quartz dating of the transgressive unit after Lecca and Carboni (2007) (SG_3) yielded a minimum age >138 ka (Table II.2) and a fading corrected potassium feldspar age of 182 ± 10 ka (Table II.4). These results disagree with the interpretation of the latter authors who claim attribution to MIS 5. Using petrographic indices Lecca and Carboni (2007) identified the occurrence of an intervening lowstand of the sea level between two phases, concluding that the sequence of San Giovanni di Sinis represents two distinct sea level events during MIS 5e. In their opinion, the SG_3 deposits correspond to a warming phase between 132.6 and 125.4 ka, followed by foreshore sedimentation between 123.2 ka and 119.2 ka during a cooling phase after the 128 ka insolation maximum, as described by Chen et al. (1991). Recent investigations (Andreucci et al., 2009), which were accompanied by quartz luminescence dating, allow for distinction of four units and corresponding transgressive and regressive surfaces. They dated the lowermost part of their Unit 1 to 186 ± 13 ka (quartz age), also showing that deposition started prior to MIS 5.

For the overlying laminated sediment (SG_2), interpreted by Lecca and Carboni (2007) as foreshore deposits, a quartz luminescence age of 115 ± 11 ka was obtained, which can clearly be attributed to MIS 5. The quartz OSL dating to 119 ± 11 ka of the aeolian sands (SG_1) agrees with the interpretation of Lecca and Carboni (2007), if one assumes a sea level drop shortly after the highstand. However, Ulzega and Hearty (1986), who employed AAR dating, proposed an relative age of 90 ± 15 ka, i.e. MIS 5c, for the foreshore sedimentation and assigned the overlying sequence to MIS 5a. Incorporating the errors of the age estimates of luminescence dating, a deposition age during MIS 5c is possible for the laminated foreshore sands, whereas MIS 5a for the dune succession is unlikely. Andreucci et al. (2009) allocate the laminated sediment to their Unit 3a; the lower part of that unit was quartz luminescence dated to 120 ± 10 ka, i.e. MIS 5e (125-110 ka). They furthermore attribute the aeolian sand (SG_1; their Unit 3b) to MIS 5c (110-90 ka). Hence, our luminescence dating results are in good agreement with the data of Andreucci et al. (2009). Even though an unequivocal correlation to the individual substages of MIS 5 is not possible with the data, an attribution to MIS 5 and older stages is clear for the San Giovanni di Sinis section if only the luminescence ages are considered.

However, the radiocarbon dating of the palaeosols, described by Andreucci et al. (2009) as mature colluvial deposits, resulted in Late Würmian and Holocene ages (Table II.6), which support the interpretation of Coltorti et al. (2010), who claim that the entire sequence is

aeolian in origin. Following Coltorti et al. (2010) the soils correspond to stable phases with vegetation cover. Due to the high content of modern roots in the sampled soil it is possible that these ages are underestimated because recent organic matter has been added to the original one. Furthermore the disagreement of conventional and AMS radiocarbon dating (the latter yielding even younger ages) gives rise to question the radiocarbon ages; this problem is even more underlined by the age inversion found (Table II.6). The degree of contamination with young carbon needs to be very large; and hence it is possible that the soils developed during the Early Holocene. However, the luminescence ages are very reliable because of the agreement of quartz and potassium feldspar as well as the agreement of two potassium feldspar signals. The only cause for overestimation is incomplete bleaching. If the sediment succession was aeolian one can assume sufficient resetting of the luminescence signal; the same is true for foreshore deposits (Madsen and Murray, 2009). For SG_2, which is either aeolian (Coltorti et al., 2010) or shallow marine (Lecca and Carboni, 2007), an additional D_e measurement using 60 small aliquots (2 mm diameter) was conducted to test whether there was incomplete bleaching before burial. The results (Fig. II.9) indicate that there are few subsamples which have higher D_e values and hence inhomogeneous bleaching cannot be excluded. However, this is not significant for the age estimate, which is shown by comparing median D_e value (suggested by Murray and Funder, 2003) and mean D_e value: the median D_e value is 73 ± 3 Gy, i.e. 103 ± 9 ka, whereas the mean D_e results in 79 ± 3 Gy, i.e. 111 ± 9 ka. Hence the age estimates are identical within errors.

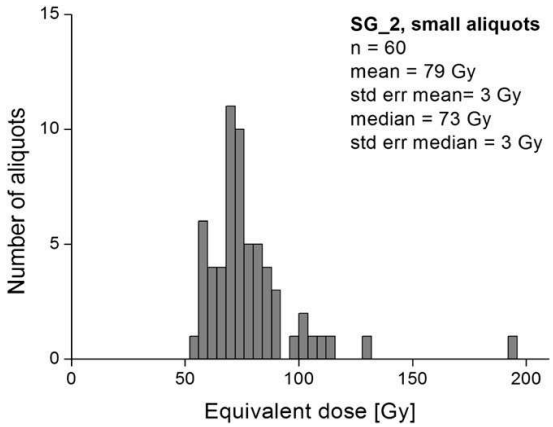

Fig. II.9: The histogram shows a distribution of the equivalent doses for 60 small aliquots measured (SG_2). The dominant peak is at about 70 Gy, with a shift towards higher doses. For details see text.

If one assumes that both the radiocarbon ages as well as the luminescence age estimates are correct, the cause for the discrepancies might be the sampling location in respect to the stratigraphical position. Coltorti et al. (2010) and Andreucci et al. (2009) state that the palaeosols are interleaved with the aeolian and shallow marine deposits. However, along most

parts of the outcrop these palaeosol are consolidated, whereas locally there are unconsolidated which indicates weathering and probably even reworking in more recent times. Such unconsolidated material was sampled for radiocarbon dating and thus makes comparison with the luminescence ages difficult.

The Capo San Marco deposits have been described by Comaschi-Caria (1954) suggesting deposition during MIS 5e because of its elevation above sea level. Consequently, the underlying aeolian deposits were attributed to older marine isotope stages. Coltorti et al. (2010) interpret the aeolian deposits as one single unit which was deposited during the Late Würmian. They claim that subsequently to the aeolian deposition gravels and boulders, which are found in the sequence, carved a notch in the aeolian unit (Fig. II.3). This interpretation assumes that the sea level during the Holocene exceeded the MIS 5e marine high stand. The quartz luminescence dating resulted in an age of 174 ± 13 ka, hence making a deposition prior to MIS 5 very likely. The age of the aeolian unit cannot give any information on when the notch was carved and when the gravels and boulder were deposited. However, following existing sea level models (Antonioli et al., 1999; Lambeck et al., 2004) it is likely that the notch was carved during the MIS 5e sea level high stand.

The sand at Santa Reparata (SR_1) was dated to 106 ± 10 ka using quartz as dosimeter (Table II.2) and to 77 ± 6 ka using potassium feldspar (post-IR IR at 255°C; Table II.4); this is a reasonable good agreement within two standard deviations. However, a clear attribution to any substage of MIS 5 is not possible. Following the interpretation of APAT (submitted a, b) and Coltorti et al. (2010), the aeolian sand was deposited during Würmian. In their opinion the palaeosol radiocarbon dated to 4,770-4,255 cal. BC (Table II.6) developed on top of the aeolian sands and was then, i.e. during the Holocene, cut by the sea which formed a notch. Coltorti et al. (2010) claim that the beach rock forming the notch filling is related to a Holocene sea level higher than the recent sea level. Unfortunately the notch filling could not be dated because of the lack of suitable material. Therefore it can only be concluded that, following the luminescence ages, the aeolian sand was most likely deposited during late MIS 5 or early MIS 4. If the palaeosol developed on such old material there ought to be a big hiatus, because the pedogenized material was dated to the Holocene. This hiatus, which should be indicated by an erosional surface, has not been described (Coltorti et al., 2010), but is an explanation for the discrepancy in ages. Another reason for the discrepancy could be the contamination with modern carbon, because nowadays the soil is rooted. However, the degree of contamination with modern carbon needs to be very large, and thus, if there is no hiatus and if the radiocarbon ages are considered reliable, the luminescence ages would have to largely overestimate the depositional age. The main reason for overestimation is incomplete bleaching (Aitken, 1998), which is negligible for the sedimentary environment under investigation (Madsen and Murray, 2009), and thus the luminescence ages (quartz and potassium feldspar) are reliable.

The sands of the Scala é Croccas outcrops yielded quartz ages of 65 ka (SC_1) and 70 ka (SC_2) (Table II.2); all D_e values of SC_1 and _2 are well above $2*D_0$ and therefore the quartz ages for these sites have to be regarded as minimum ages. The post-IR IRSL measurements resulted in fading corrected ages of 86 ± 7 ka for SC_1 and 97 ± 7 ka for SC_2 (Table II.4); within errors they are identical. Due to their elevation of approximately 5 m asl, these beach ridges have been correlated to the MIS 5e sea level highstand (Servizio Geologico d'Italia, 1967). The luminescence ages indicate a deposition after MIS 5e; possibly MIS 5c. Even though sea level models as well as tectonic interpretations neglect a higher sea level any time after MIS 5e (Antonioli et al., 1999; Lambeck et al., 2004), other authors (Carboni and Lecca, 1985; Davaud et al., 1991; Kindler et al., 1997; Andreucci et al., 2009) found indications for a transgression after MIS 5e at San Giovanni di Sinis and in Santa Reparata. In either case more investigations are needed before a conclusion can be drawn whether the sediments at Scala é Croccas result from such a sea level highstand. Coltorti et al. (2010) and APAT (submitted a, b) also state that the deposits at Scala é Croccas are the result of a sea level highstand after MIS 5e, however, attribute the formation of the beach ridges to an Early Holocene sea level highstand. This could not be confirmed by luminescence dating.

The laminated sands of the beach ridge at Is Arenas gave a quartz age of 90 ± 3 ka (Table II.2), which correlates to a deposition of the beach ridge during MIS 5, possibly MIS 5c. A similar age of 78 ± 10 ka was obtained for potassium feldspar (Table 5). This again could point to a sea level highstand during MIS 5c. Previously, the deposits were allocated to the MIS 5e marine high stand due to their elevation of ca. 5-6 m asl and the result of AAR dating (Ozer et al., 1980; Ulzega et al., 1982; Ulzega and Hearty, 1986; Hearty et al., 1986). Belluomini et al. (1986) reported younger numerical ages (AAR dating), yet attributing the deposits to MIS 5. This is in agreement with the luminescence ages. On the other hand, the organic mud layer at Is Arenas which is said to rest ca. 9 m below wash-over deposits which are correlated to the beach ridges (Coltorti et al., 2010) gave a radiocarbon age of 195 cal. BC - 75 cal. AD (Table II.6). Coltorti et al. (2007) state that the beach ridge results from long shore drifting sediments which originate from slope degradation following intense human deforestation during the Holocene. Hence, by means of stratigraphic interpretations they attribute the Is Arenas beach ridge to the Holocene.

II.1.6 Conclusions

The aim of this paper was to set up a chronological framework for Quaternary deposits along the coast of Sardinia which long-held stratigraphic interpretations have recently been questioned (APAT, submitted a, b; Coltorti et al., 2007, 2010). The matter of debate is whether the investigated sediments were deposited during the Late Würmian and Holocene (Coltorti et al., 2007, 2010) or during MIS 5 and older stages (e.g. Ozer et al., 1980; Ulzega and Hearty, 1986; Belluomini et al., 1986; Lecca and Carboni, 2007; Andreucci et al., 2009).

Therefore, radiocarbon dating was applied to palaeosols and organic rich layers, and aeolian and shallow marine deposits were dated by luminescence dating techniques using both quartz and potassium feldspar as dosimeters.

Very contrasting results were obtained using the different dating methods. The luminescence ages for both quartz and potassium feldspar clearly point to a deposition of all investigated sedimentary units during or prior to MIS 5. On the other hand, radiocarbon ages of the bulk organic material resulted in Holocene and Late Würmian ages.

In principle it is unexpected that radiocarbon and luminescence age estimates result in discrepancies of an order of magnitude. There are three explanations for the disagreements found:

i) Luminescence dating yielded the correct ages and thus, the radiocarbon ages are underestimating the true age caused by contamination with young carbon. Furthermore, if the deposits are older than 45-50 ka, as indicated by the luminescence ages and those of Andreucci et al. (2009) but also by AAR data (Ulzega and Hearty, 1986; Belluomini et al., 1986), radiocarbon dating is unsuitable due to its applicable age range (Hogg et al., 2006).

ii) The radiocarbon ages are correct, because one can argue that the degree of contamination is not large enough to yield such young ages. Thus, the luminescence ages have to largely overestimate, which can only be caused by incomplete bleaching. This is very unlikely because quartz and fading corrected potassium feldspar ages are in very good agreement, even though quartz and potassium feldspar have different bleaching behaviour (quartz bleaches faster then potassium feldspar) and luminescence properties (Aitken, 1998). An agreement of ages derived from these two minerals has to be interpreted as a reliable age estimate. Furthermore the luminescence measurements passed all quality tests (Duller, 2003).

iii) The proposed stratigraphical correlations (APAT, submitted a, b; APAT, 2005; Coltorti et al., 2010) are not appropriate and need revision despite the very thorough work. This might be especially true for San Giovanni di Sinis, where for radiocarbon dating the organic matter of an unconsolidated palaeosol, which is said to be interleaved in the consolidated dune succession (Coltorti et al., 2010), was used. At Is Arenas the correlation of the beach ridge with the wash-over deposits could be questioned, which then allows for correct age estimates, i.e. the radiocarbon dated mud is not underlying the beach ridge.

Following this, it is not possible to draw a final conclusion on the geochronology and stratigraphy of the Sardinian coastal deposits. However, the problems related to a study where controversial ages estimates are obtained using different dating methods should be considered.

Acknowledgements

This study was supported by The Leibniz Pakt Project for Research and Innovation 2008-2010 and has been carried out in connection with the works for the new geological maps of Itlay, entrusted to the Progemisa SpA (now ARPA-Sardinia). We thank the coordinators and directors of the sheets as well as the field geologists for their support. We are indebted to Karsten Vollmer and Sonja Riemenschneider for laboratory assistance and are grateful to Andrew Murray for discussions on the topic and to two anonymous reviewers, whose detailed reviews helped to improve the manuscript. We furthermore thank the Editor-in-Chief Norm Catto for English corrections and his decision to accept the manuscript for publication despite controversial reviews.

References

Aitken, M. J., 1985. Thermoluminescence Dating. Academic Press, London, 369 pp.

Aitken, M. J., 1998. An Introduction to Optical Dating. Oxford University Press, Oxford, 267 pp.

Andreucci, S., Pascucci, V., Murray, A. S., Clemmensen, L. B., 2009. Late Pleistocene coastal evolution of San Giovanni di Sinis, west Sardinia (Western Mediterranean). Sedimentary Geology 216, 104-116.

Antonioli, F., Silenzi, S., Vittori, E., Villani, C., 1999. Sea level changes and tectonic mobility: precise measurements in three coastlines of Italy considered stable during the last 125 ky. Physics and Chemistry of the Earth, Part A 24, 337-342.

APAT, 2005. Note Illustrative alla Carta Geologica alla scala 1:50.000 F.557 Cagliari. SELCA Ed., 240 pp.

APAT, submitted for publication a. Note Illustrative alla Carta Geologica alla scala 1:50.000 F.411 Santa Teresa di Gallura.

APAT, submitted for publication, b. Note Illustrative alla Carta Geologica alla scala 1:50.000 F.564 Carbonia.

Auclair, M., Lamothe, M., Huot, S., 2003. Measurement of anomalous fading for feldspar IRSL using SAR. Radiation Measurement 37, 487-492.

Belluomini, G., Branca, M., Delitala, L., Pecorini, G., Spano, C., 1986. Isoleucine epimerization dating of quaternary marine deposits in Sardinia, Italy. Annals of Geomorphology 62, 109-117.

Buylaert, J.-P., Murray, A. S., Thomsen, K. J., Jain, M., 2009. Testing the potential of an elevated temperature IRSL signal from K-feldspar. Radiation Measurements 44, 560-565.

Bøtter-Jensen, L., Andersen, C. E., Duller, G. A. T., Murray, A. S., 2003. Developments in radiation, stimulation and observation facilities in luminescence measurements. Radiation Measurements 37, 535-541.

Carboni, A., Lecca, L., 1985. Osservazioni sul pleistocene medio-superiore della penisola del Sinis (Sardegna occidentale). Bollettino Societa Geolologica Italiana 104, 459-477.

Chen, J. H., Curran, H. A., White, B., Wasserburg, G. J., 1991. Precise chronology of the last interglacial period: 234U/230Th data from fossil coral reefs in the Bahamas. Geological Society of America Bulletin 103, 82-97.

Coltorti, M., Barca, S., Melis, E., 2007. Stable or mobile sea-level, stable or mobile Sardinia during the Holocene: evidence from the Cagliari Gulf. Il Quaternario 20, 87-91.

Coltorti, M., Melis, E., Patta, D., 2010. Geomorphology, stratigraphy and facies analysis of some Late Pleistocene and Holocene key deposits along the coast of Sardinia. Quaternary International 222, 19-35.

Comaschi-Caria, L., 1954. Nuovi lembi di quaternario in Sardegna. Rendiconti del Seminario della Facoltà di Scienze dell'Università di Cagliari 24, 205-516.

Davaud, E., Kindler, P., Martini, R., Strasser, A., 1991. Enregistrement des variations eustatiques dans des dépôts littoraux du Pléistocène supérieur San Giovanni di Sinis (Sardaigne occidentale). Bulletin de la Société Géologique de France 162, 523-533.

Denby, P. M., Bøtter-Jensen, L., Murray, A. S., Thomsen, K. J., Moska, P., 2006. Application of pulsed OSL to the separation of the luminescence components from a mixed quartz/feldspar sample. Radiation Measurements 41, 774-779.

Duller, G. A. T., 2003. Distinguishing quartz and feldspar in single grain luminescence measurements. Radiation Measurements 37, 161-165.

Geyh, M. A., 2005. 14C dating - still a challenge for users. Annals of Geomorphology 139, 63-86.

Hajdas, I., 2008. Radiocarbon dating and its application in quaternary studies. Eiszeitalter und gegenwart. Quaternary Science Journal 57, 2-24.

Hearty, P. J., Miller, G. H., Stearns, C. E., Szabo, B. J., 1986. Aminostratigraphy of quaternary shorelines in the mediterranean basin. Geological Society of America Bulletin 97, 850-858.

Hogg, A. G., Fifield, L. K., Turney, C. S. M., Palmer, J. G., Galbraith, R., Baillie, M. G. K., 2006. Dating ancient wood by high sensitivity liquid scintillation counting and accelerator mass spectrometry - pushing the boundaries. Quaternary Geochronology 1, 241-248.

Huntley, D. J., Baril, M. R., 1997. The K content of the K-feldspars being measured in optical dating or in thermoluminescence dating. Ancient TL 15 (1), 11-13.

Huntley, D. J., Lamothe, M., 2001. Ubiquity of anomalous fading in K-felspars and the measurement and correction for it in optical dating. Canadian Journal of Earth Science 38, 1093-1106.

Issel, A., 1913. Lembi fossiliferi quaternari e recenti osservati nella sardegna meridionale dal Prof. D. Lovisato. Rendiconti Accademia Nazionale dei Lincei, Classe di Scierzze Fisiche, Matematiche e Naturali 23, 759-770.

Kindler, P., Davaud, E., Strasser, A., 1997. Tyrrhenian coastal deposits from Sardinia (Italy): a petrographic record of high sea levels and shifting climate belts during the last interglacial (isotopic substage 5e). Palaeogeography, Palaeoclimatology, Palaeoecology 133, 1-25.

Lambeck, K., Antonioli, F., Purcell, A., Silenzi, S., 2004. Sea-level change along the Italian coast for the past 10,000 yr. Quaternary Science Reviews 23, 1567-1598.

Lamothe, M., Auclair, M., Hamzaoui, C., Huot, S., 2003. Towards a prediction of longterm anomalous fading of feldspar IRSL. Radiation Measurement 37, 493-498.

Lang, A., Lindauer, S., Kuhn, R., Wagner, G., 1996. Procedures used for optically and infrared stimulated luminescence dating of sediments in Heidelberg. Ancient TL 14, 7-11.

Lecca, L., Carboni, S., 2007. The Tyrrhenian section of San Giovanni di Sinis (Sardinia): stratigraphic record of an irregular single high stand. Rivista Italiana di Paleontologia e Stratigrafia 13, 509-523.

Madsen, A. T., Murray, A. S., 2009. Optically stimulated luminescence dating of young sediments: a review. Geomorphology 109, 3-16.

Mejdahl, V., 1979. Thermoluminescence dating: beta-dose attenuation in quartz grains. Archaeometry 21, 61-72.

Murray, A. S., Funder, S., 2003. Optically stimulated luminescence dating of a Danish Eemian coastal marine deposit: a test of accuracy. Quaternary Science Reviews 22, 1177-1183.

Murray, A. S., Wintle, A. G., 2000. Luminescence dating of quartz using an improved single-aliquot regenerative-dose protocol. Radiation Measurements 32, 57-73.

Murray, A. S., Wintle, A. G., 2003. The single aliquot regenerative dose protocol: potential for improvements in reliability. Radiation Measurements 37, 377-381.

Nathan, R. P., Mauz, B., 2008. On the dose-rate estimate of carbonate-rich sediments for trapped charge dating. Radiation Measurements 43, 14-25.

Ozer, A., Paskoff, R., Sanlaville, P., Ulzega, A., 1980. Essai de correlation du Plèistocène supérieur de la Sardaigne et de la Tunisie. Comptes rendus de l'Académie des Sciences Paris 291 (D), 801-804.

Readhead, M. L., 2002. Absorbed dose fraction for 87Rb b particles. Ancient TL 20, 25-28.

Servizio Geologico d'Italia Regione e Autonoma della Sardegna, 1967. Carta Geologica d'Italia, Orosei, Foglio 195, scala 1:100.000, Roma.

Sivan, D., Porat, N., 2004. Evidence from luminescence for Late Pleistocene formation of calcareous aeolinite (kurkar) and paleosol (hamra) in the Carmel Coast, Israel. Palaeogeography, Palaeoclimatology, Palaeoecology 211, 95-106.

Spooner, N. A., 1994. The anomalous fading of infrared-stimulated luminescence from feldspars. Radiation Measurements 23, 625-632.

Stuiver, M., Reimer, P. J., 1993. Extended 14C data base and revised CALIB 3.0 14C age calibration program. Radiocarbon 35, 215-230.

Thomsen, K. J., Jain, M., Murray, A. S., Denby, P. M., Roy, N., Bøtter-Jensen, L., 2008a. Minimizing feldspar OSL contamination in quartz UV-OSL using pulsed blue stimulation. Radiation Measurements 43, 752-757.

Thomsen, K. J., Murray, A. S., Jain, M., Bøtter-Jensen, L., 2008b. Laboratory fading rates of various luminescence signals from feldspar-rich sediment extracts. Radiation Measurements 43, 1-13.

Ulzega, A., Ozer, A., Lecca, F., Leone, G., Pecorini, C., Spano, C., Cordy, M. J., 1982. Excursion Table-Ronde Tyrrhenian de Sardaigne (Livret-Guide). INQUA, 88 pp.

Ulzega, A., Hearty, P.J., 1986. Geomorphology, stratigraphy and geochronology of late quaternary marine deposits in Sardinia. Annals of Geomorphology 62, 119-129.

Ulzega, A., Ozer, A., 1982. Comptes-rendus de l'excursion - Table ronde Tyrrhenian de Sardaigne. April 1980. INQUA, University Cagliari, 110 pp.

Visocekas, R., 1985. Tunnelling radiative recombination in labradorite: its association with anomalous fading of thermoluminescence. Nuclear Tracks and Radiation Measurements 10 (4–6), 521-529.

Wallinga, J., Murray, A. S., Duller, G. A. T., 2000. Underestimation of equivalent dose in single-aliquot optical dating of feldspars caused by preheating. Radiation Measurements 32, 691-695.

Wintle, A. G., Murray, A. S., 2006. A review of quartz optically stimulated luminescence characteristics and their relevance in single-aliquot regeneration dating protocols. Radiation Measurements 41, 369-391.

III

Applicability of post-IR IRSL dating to polymineral fine grains extracted from loess

III.1 Sedimentation and erosion processes in Middle to Late Pleistocene sequences exposed in the brickyard of Langenlois/Lower Austria

Thiel, C.[1,2], Terhorst, B.[3], Jaburová, I.[4], Buylaert, J.-P.[2,5], Murray, A. S.[2], Fladerer, F. A.[6], Damm, B., Frechen, M.[1], Ottner, F.

[1] Leibniz Institute for Applied Geophysics, Section S3: Geochronology and Isotope Hydrology, Hannover, Germany
[2] Nordic Laboratory for Luminescence Dating, Department of Earth Sciences, Aarhus University, Risø DTU, Roskilde, Denmark
[3] Institute of Geography, Department for Physical Geography, University of Würzburg, Germany
[4] Institute of Geography and Regional Research, University of Vienna, Austria
[5] Radiation Research Division, Risø National Laboratory for Sustainable Energy, Technical University of Denmark, 4000 Roskilde, Denmark
[6] Department of Palaeontology, Geozentrum, University of Vienna, Austria
[7] Institute of Structural Research and Planning, University of Vechta, Germany
[8] Institute of Applied Geology, University of Natural Resources and Life Sciences, Austria

Geomorphology, in press (http://dx.doi.org/10.1016/j.geomorph.2011.02.011)

Abstract

The correlation of sedimentary and pedogenetic processes in Lower Austria is difficult due to significant discontinuities and local variability in soil formation. This hampers landscape reconstruction at a regional scale. However, at a local scale distinct landscape formation processes represented by a shift from fluvial to aeolian deposition can be observed in the brickyard of Langenlois, Lower Austria. Sedimentological and mineralogical analyses in combination with palaeontological finds suggest that the fluvial deposition took place during the Middle Pleistocene. This attribution is confirmed by infra-red stimulated luminescence (IRSL) dating, which gives a minimum age of 300 ka for the palaeosurface on which the fluvial sediments were deposited. This is consistent with a small faunal assemblage including *Stephanorhinus* sp., *Dama* sp. and an *Alcine* cervid. Such a fauna is previously unknown in Austria; it indicates a Middle Pleistocene interglacial period. The low degree of weathering as well as Cryosols found in the loess sequence point to loess accumulation during the Last Glacial; the dating results (35-55 ka) indicate prolonged loess deposition. No signs of pedogenesis could be found; this is surprising because in other areas this period is known for weak soil development. The lack of soil formation seems to be specific to the western part of Lower Austria, as is the complete erosion of the last glacial maximum (LGM) loess, which is not found at Langenlois.

Keywords: Lower Austria; loess stratigraphy; Middle Pleistocene fauna; post-IR IRSL dating

III.1.1 Introduction

In the terrestrial realm the complex inter-relations between topography, parent rock, geosystem and atmosphere are recorded in Quaternary sediments. Thus terrestrial sedimentary archives that represent prolonged periods of the Quaternary can provide valuable information on the palaeoenvironment. It is evident that the spatio-temporal susceptibility of morphodynamic processes depends on long-term changes in sediment budgets, erosion, weathering processes and land surface forms and structures (Terhorst et al., 2010 a). In particular, loess/palaeosol sequences and fluvial sediments record sedimentation and erosional processes and hence reflect changes in the landscape.

Loess landscapes are widespread in Europe (e.g. Haase et al., 2007) and are abundant in Lower Austria. The Kremsfeld (also Kremser Feld) in particular, with its famous sites Krems, Göttweig, Paudorf and Stratzing (Fig. III.1), has received attention because of its archaeological finds (Einwögerer et al., 2006; Neugebauer-Maresch, 2008; Händel et al., 2008). However is difficult to understand why the rather thick and manifold loess/palaeosol sequences in Lower Austria have not been the subject of further studies besides archaeological investigations since the works of Fink (1956, 1976, and 1978). Since the 1930's (Götzinger, 1936) attempts have been made to develop a common stratigraphy for 69 the area under question. This has not only been hampered by the lack of a continuous record but also by the lack of suitable dating techniques. Thus the chronological positions of many of the marker palaeosols such as the Stillfried complex (e.g. Fink 1976), the 'Göttweiger Verlehmungszone' and the 'Paudorfer Bodenbildung' (e.g. Götzinger, 1936, Fink 1976) have been the source of considerable controversy (Noll et al., 1994; Zöller et al., 1994) - it was not possible to decide which of these pedocomplexes depicted the last interglacial soil (Eemian). Using new dating techniques Thiel et al. (2010b) were able to clearly identify the 'Paudorfer Bodenbildung' at its type locality in Paudorf (Fig. III.1) as the Eemian soil. The 'Göttweiger Verlehmungszone' can most likely be attributed to marine isotope stage (MIS) 11 (Thiel et al., 2010b). These results have however only been a small step towards the reconstruction of the former landscape in Lower Austria and its evolution. Other approaches to gain more information on pedogenesis and palaeoenvironmental conditions in Lower Austria during the Quaternary have included micromorphological (e.g. Smolíková, 2003; Smolíková and Havlíček, 2007; Havlíček et al., 1998), geochemical (Haslinger and Heinrich, 2008; Haslinger et al., 2009) and palaeontological investigations (e.g. Döppes and Rabeder, 1997; Fladerer et al., 2005). Due to the topographically controlled variability of soil formation, the micromorpholocial attributes were not sufficient to allow stratigraphic correlations and palaeoenvironmental reconstruction.

Because Lower Austria is a geographical key position for the correlation of the dry loess landscape with the loess/palaeosol sequences of the east and south-east Europe it is important to derive more information on loess deposition and pedogenesis as well as erosional processes

in time and space. Therefore we investigated the brickyard of Langenlois (Fig. III.1), where fluvial and aeolian deposits are exposed (Piffl, 1976). Only very few data exist for the loess exposures around the market town of Langenlois (Fladerer, et al., 2005; Smolíková, 2003), and none of this information is sufficient to explain any of the sedimentation and erosion observed in the brickyard.

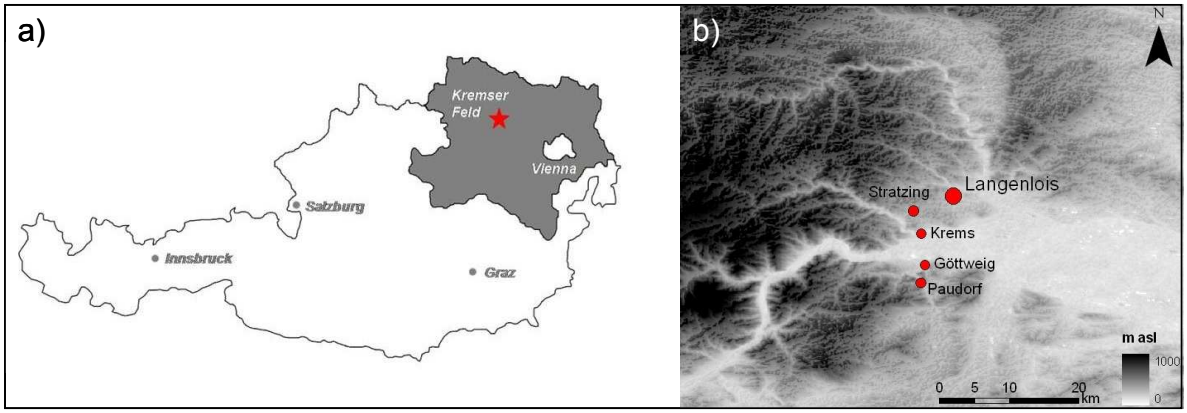

Fig. III.1: a) Map of Austria, indicating the study area (star) in Lower Austria (grey area). b) Hillshaded elevation map of the Kremser Feld (based on ASTER GDEM, Earth Remote Sensing Data Analysis Center (ERSDAC). The locations of the important loess profiles mentioned in this manuscript are shown.

In order to gain an improved understanding of the processes that formed the landscape in Langenlois, we conducted detailed logging of three profiles in the brickyard. The field survey revealed interesting palaeontological finds, and it was accompanied by sedimentological and mineralogical analyses to gain information about the sedimentation modes as well as on weathering processes and pedogenesis (cf. Terhorst et al., 2002). The depositional age of the sediments under question are derived by luminescence dating (e.g. Aitken, 1998); by making use of infra-red stimulated luminescence (IRSL) dating (Buylaert et al., 2009; Thiel et al., 2010a, b) it is possible to date not only Late Pleistocene but also Middle Pleistocene deposits.

In summary, this study allows us to constrain the local sedimentary processes in time and is hence a contribution to the reconstruction of the morphodynamics at a regional scale.

III.1.2 Site description

The study area is located at the south-eastern border of the Bohemian Massif (Waldviertel), about 7 km north-east of the city of Krems, Lower Austria (Fig. III.1); this area is referred to as Kremsfeld. The loess was deposited in a Late Neogene hollow mould („Kremser Bucht“) formed in Tertiary Molasse (Wessely, 2006). Götzinger (1936) made note of the up to 20 m thick loess sequences at the southern edge of the plateau, and Piffl (1955) observed even thicker loess deposition at the easterly slopes of the Kremsfeld.

The Kremsfeld is situated in the transition between the dry and wet loess landscape (‘trockene’ and ‘feuchte Lösslandschaft’ after Fink, 1956). The separation of these two

Austrian landscapes is based on the estimated precipitation during the Late Pleistocene, which influenced the development of the loess facies (Brandtner, 1956; Fink 1956). Based on this classification, precipitation in the Kremsfeld was equivalent to that in the dry loess landscape, but the loess was later influenced by more humid conditions. It has to be noted that this transition zone is not a separate palaeoclimatic region, but a loess region with specific genetic characteristics such as intensively weathered and coloured palaeosols which were affected by solifluction as well as by erosion processes.

The mean annual temperature of this area is 9.1°C (AD 1971-2000; meteorological station Langenlois, 204 m asl.), and the mean annual precipitation is 451 mm with more than 50% of precipitation during summer months (ZAMG 2010). The region is dominated by westerly winds, which are redirected in a north-westerly direction by the Bohemian Massive. During winter months cold and dry easterly winds prevail. The climate of the study area can thus be assigned to the transition zone between the oceanic (Atlantic) and the continental climatic regions (Zwittkovits, 1983).

The north-exposed wall of the former brickyard in Langenlois was briefly described by Piffl (1976). The base of this sediment wall is made up of Danube gravels, covered by gravels of the river Kamp (Piffl, 1976). On top of this fluvial unit, sandy and clayey-loamy fluvial sediments were deposited. Piffl (1976) furthermore noted two brown palaeosols which cover the fluvial units; these soils contain weathered rock fragments and gravels. Palaeomagnetic data, which were unfortunately not derived from high resolution sampling but only from samples, suggested that the fluvial units of the north-exposed walls were deposited during a chron of reversed magnetisation, most likely the Matuyama Chron (Piffl, 1976). Subsequent sedimentation was dominated by aeolian processes. The base of the aeolian sediments is made up of a pedocomplex. On top of this succession, in the eastern part of the north-exposed wall distinct layers of red weathered sands fill a depression, indicating an erosional phase (Piffl, 1976). Recently, the ‘Red Outcrop’ of Langenlois, situated on the Schenkenbichl hill, was investigated (Haslinger and Heinrich, 2008; Haslinger et al., 2009), and these studies suggested red soil development during the Middle to Lower Pleistocence or even Pliocence. However, a correlation with the soils found at the north-exposed in Langenlois is not possible.

Even though the east-exposed wall existed at the time the investigations of Piffl (1976), no data were reported; this is the section studied here.

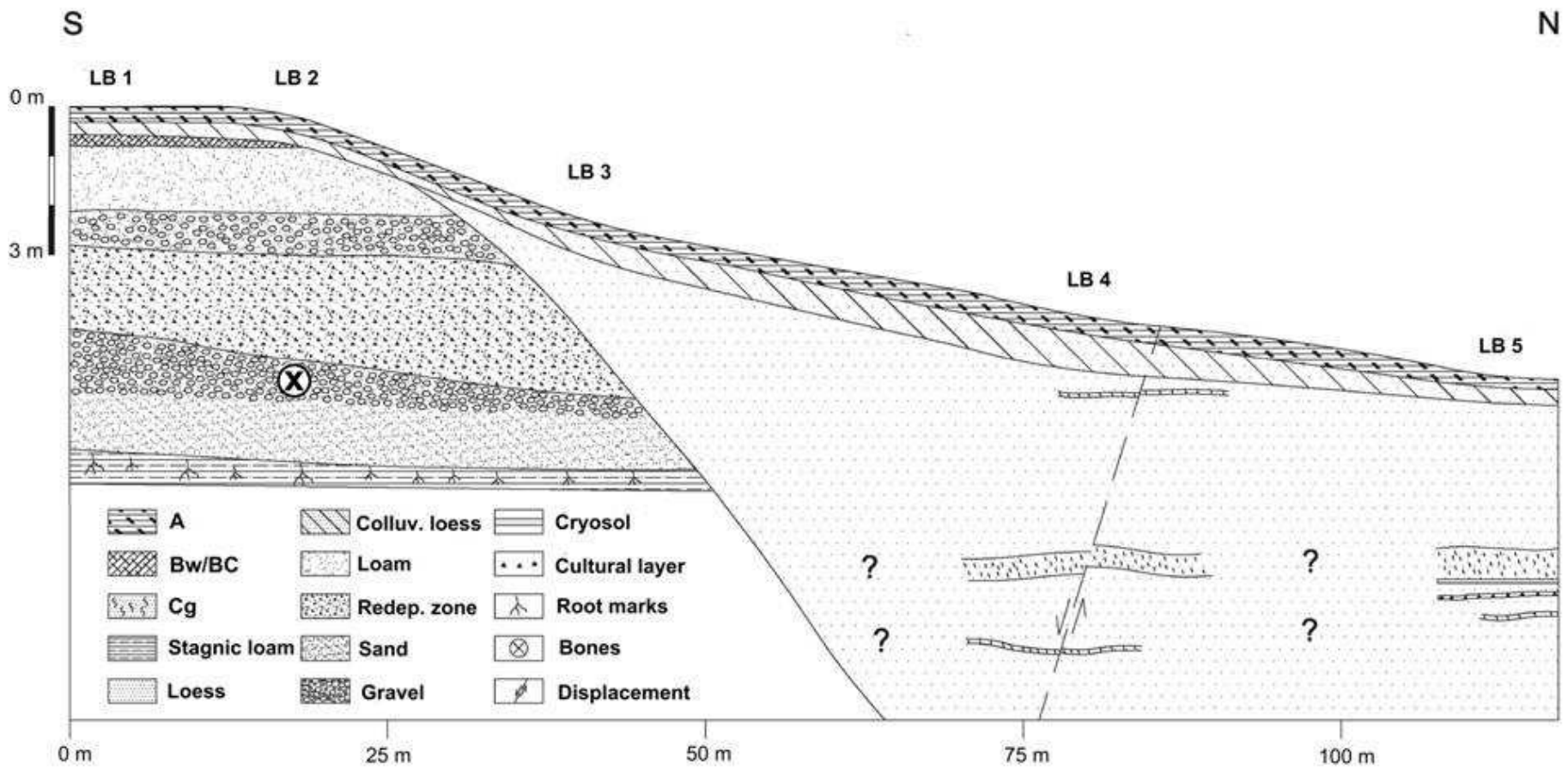

Fig. III.2: Sketch of the east-exposed wall and location of individual profiles. Profiles LB 1, LB 2 and LB 5 are presented in detail in this study because they are representative for the fluvial (LB 1+2) and aeolian (LB 5) deposition at this site. Transition from fluvial to aeolian deposition is reflected in profile LB 3. Luminescence sampling positions and ages are presented in Figs. III.3 and III.4.

III.1.3 Sampling and experimental details

Along the 120 m long east-exposed wall, a total of five profiles were excavated and described (Fig. III.2). Profile LB 1 is located in the southern corner of the sediment cliff where fluvial layers and reworked sediment can be found. These sedimentary units continue to profile LB 2, ~15 m away, and a transition between fluvial and aeolian deposition is found in profile LB 3. Forty metres to the north, the profile LB 4 is dominated by loess; the same is true for profile LB 5.

Profiles LB 1 and LB 5 are representative of the fluvial and aeolian sediment sequences exhibited in the brickyard and were hence investigated in detail (Figs. III.3 and III.4). Because large mammal bones and bone fragments were collected from a horizon (LB 2/8) of profile LB 2, this profile is also presented. To determine the deposition age of the sedimentary units under question, samples were taken for luminescence dating from two horizons of LB 2 and four horizons of LB 5.

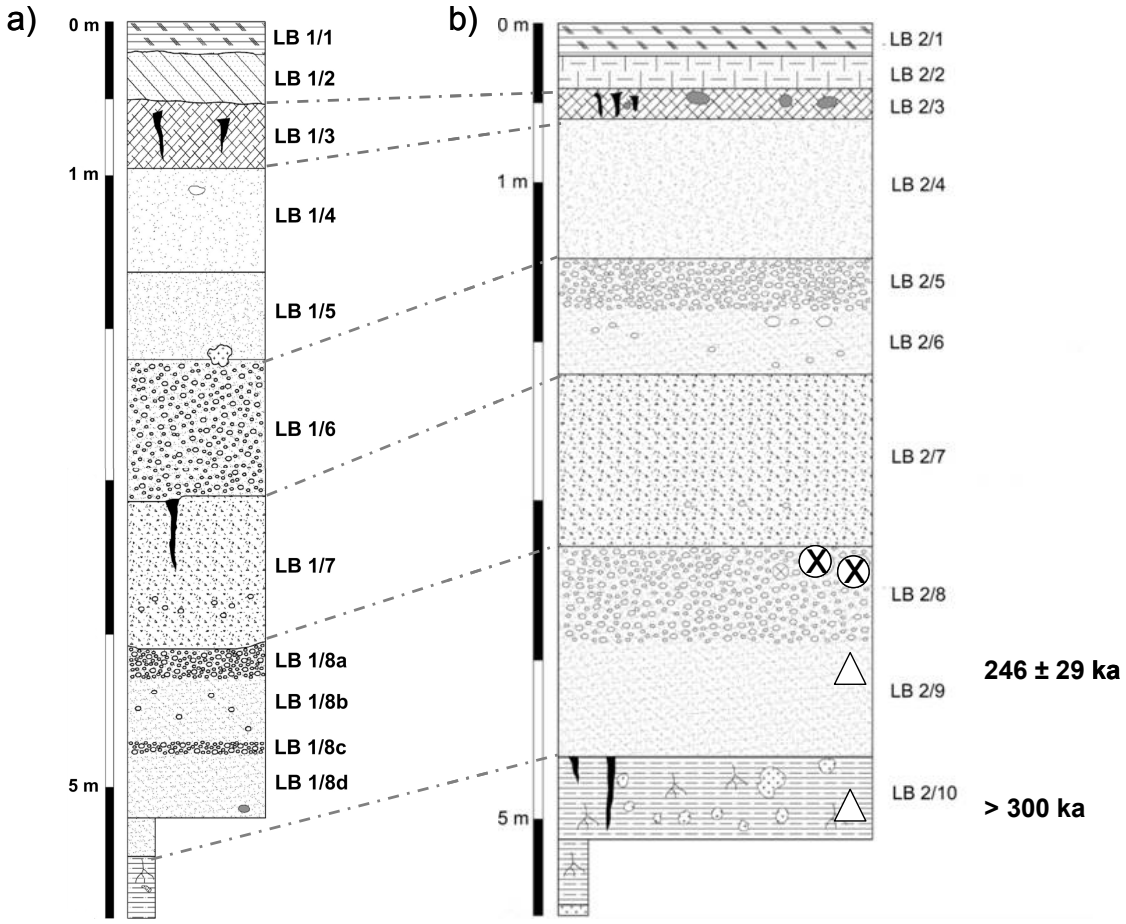

Fig. III. 3: Loggings of profiles LB 1 (a) and LB 2 (b). The individual horizons can be correlated (grey dashed lines). In b) the fading corrected post-IR IRSL ages are shown. Luminescence sampling locations (open triangles) and palaeontological finds (crossed circles) are indicated. For legend see Fig. III 2.

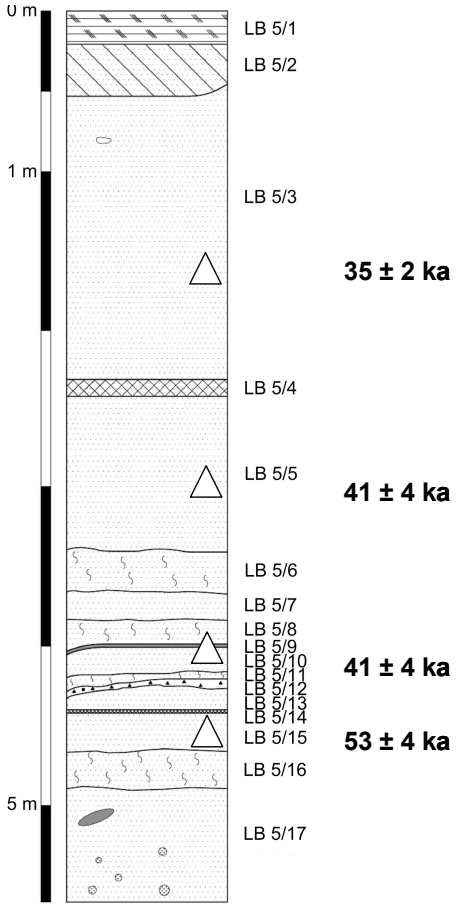

Fig. III. 4: Logging and fading corrected post-IR IRSL ages of profile LB 5. Luminescence sampling locations are indicated by open triangles. For legend see Fig. III.2.

III.1.3.1 Field survey and laboratory analyses

During the field survey, information on texture, bedding, carbonate content, colour and other pedogenetic properties was obtained for the individual horizons (Table III.1). Description and determination of soil horizons is based on the German Field Book for Soil Survey (AG Boden, 2005). The field description was adapted to the World Reference Base for soil resources (IUSS Working Group WRB, 2006).

Laboratory analyses on selected horizons (Tables III.2 and III.3) included grain size analysis and determination of the carbonate content. The grain size analysis is based on the Austrian norms ÖNORM L 1061/1 (2002) and ÖNORM L 1061/2 (2002) and comprises both wet-sieving and settling analysis. For the coarse grain fractions sieves with mesh-widths 2 mm (gravels), 630 µm (coarse sand), 200 µm (medium sized sand), and 63 µm (fine sand) were used, allowing also for collection of the material <63 µm. Depending on the maximum grain, size 100-250 g of dried sample material was suspended in water and sieved for 45

minutes in an automated Retsch AS200 basic sieving apparatus. The individual fractions were dried and weighed. To derive the coarse silt (20-63 μm), medium silt (6.3-20 μm), fine silt (2-6.3 μm), and clay (<2 μm) fractions, 25 ml of sodium pyrophosphate was added to ~10 g of material <63 μm. After six hours reaction time, de-ionized water was added to fill up the conical flasks, which were then placed in a rotating shaker to disperse for eight hours. To ensure no sand grains are present the solution was transferred through a 63 μm sieve into a 1000 ml cylinder, and this was then filled up precisely to 1000 ml. After the given settling time for each fraction (from Stokes' law) 20 ml of the suspension was extracted with a Köhn pipette, starting with the coarse silt fraction. After the extraction of a fraction, the cylinder was again made up to 1000 ml. The material in the extracted suspension was dried and weighed. The percentages of the fraction were derived by back-calculating the individual weights to the net weights.

The determination of the mineralogical carbonate content ($CaCO_3$, $CaMg[CO_3]_2$) is based on the Austrian norm ÖNORM L 1084 (2006). Ten ml of hydrochloric acid (HCl; 10 %) was added to 1 g of air-dried sample (<2 mm). The evolved carbon dioxide (CO_2) was volumetrically measured using a modified Scheibler apparatus. The mass-specific carbonate content ($CaCO_3$ in g/kg) was calculated with respect to air temperature and air pressure.

For mineralogical analyses bulk samples as well as the clay fractions (<2 μm) were analysed. The samples were studied by means of X-ray diffraction (XRD) using a Philips 1710 diffractometer with automatic divergent slit, 0.1° receiving slit, Cu LFF tube 45 kV, 40 mA, and a single-crystal graphit monochromator. The measuring time was 1s in step-scan mode and stepsize of 0.02°.

Sample preparation generally followed the methods described by Whittig (1965) and Tributh (1989). Dispersion of clay particles and destruction of organic matter was achieved by treatment with diluted hydrogen peroxide, and separation of clay fraction was carried out by centrifugation. The exchange complex of each sample (<2 μm) was saturated with Mg and K using chloride solutions by shaking. The preferential orientation of the clay minerals was obtained by suction through a porous ceramic plate, in a manner similar to that of Kinter and Diamond (1956). To avoid disturbance of the orientation during drying, the samples were equilibrated for 7 days over a saturated NH_4NO_3 solution. Afterwards expansion tests were made, using ethylenglycol, glycerol and DMSO, as well contraction tests by heating the samples up to 550°C. After each step the samples were X-rayed from 2-40°2θ.

The clay minerals were identified according to Thorez (1975), Brindley and Brown (1980), Moore and Reynolds (1997) and Wilson (1989). Semiquantitative estimations were carried out using the corrected intensities of characteristic X-ray peaks (Riedmüller 1978).

Semiquantitative mineral composition of the bulk samples was estimated using the method described by Schultz (1964).

Table III.1: Summary of field survey (including pedogenic details) for profiles LB 1, LB 2 and LB 5.

Horizon	Depth (cm)	Colour (dry)	Colour (wet)	Texture[1] (Fine earth)	Structure[2]	Carbonate[3]	Lower Boundary[4]	Other features[5]
LB 1/1	0-20	-	-	-	-	2	l	disturbed topsoil
LB 1/2	20-50	2.5Y 7/4	2.5Y 6/4	SiCL	cemented	3	l	
LB 1/3	50-90	10YR 5/6	10YR 4/6	SiCL	abk, sbk	1 (2)	l	
LB 1/4	90-160	10YR 6/6	10YR 6/6	SiCL	abk, sbk	2	l	
LB 1/5	160-220	10YR 7/4	10YR 6/6	SiCL	abk, sbk	3	l	
LB 1/6	220-310	10YR 6/6	10YR 5/6	SCL	sg	0	l	
LB 1/7	310-410	10YR 5/6	10YR 4/6	SCL	abk, sbk	0	l	
LB 1/8a	410-430	10YR 5/6	10YR 4/6	SL	sg	0	l	
LB 1/8b	430-465	10YR 6/6	10YR 5/6	-	sg	0	l	
LB 1/8c	465-480	10YR 6/8	10YR 4/6	-	sg	0	l	
LB 1/8d	480-540	10YR 6/8	10YR 4/6	-	sg	0	l	
LB 1/9	540-585	-	-	-	-	-	-	scp.
LB 2/1	0-20	-	-	-	-	2	-	disturbed topsoil
LB 2/2	20-40	10YR 8/1	10YR 8/3	-	cemented	3	l	cemented
LB 2/3	40-60	10YR 6/6	10YR 5/6	SCL	abk, sbk	2	l	sec. carb.; crotov.
LB 2/4	60-150	10YR 8/3	10YR 6/4	SiCL	abk, sbk	3	l	-
LB 2/5	150-180	10YR 6/6	10YR 5/6	S	sg	0	l	-
LB 2/6	180-220	10YR 6/6	10YR 5/6	S	sg	0	l	-
LB 2/7	220-330	10YR 5/6	10YR 4/6	SCL	abk, sbk	0	l	-
LB 2/8	330-390	10YR 6/6	10YR 5/6	S	sg	0	l	bone fragments
LB 2/9	390-460	10YR 7/6	10YR 5/6	S	sg	0	l	bone fragments
LB 2/10	460-555	10YR 5/6	10YR 5/6	SiCL	abk	0	-	sec. carb., Mn, scp
LB 2/11	555-560	-	-	-	-	0	-	-
LB 5/1	0-20	-	-	-	-	2	-	disturbed topsoil
LB 5/2	20-40	2.5Y 6/3	2.5Y 5/3	SiL	pl	3	l	sec. carb.
LB 5/3	40-230	2.5Y 7/3	2.5Y 5/4	SiL	abk, sbk	3	l	sec. carb.
LB 5/4	230-240	2.5Y 7/3	2.5Y 5/4	SiL	abk, sbk	3	l	sec. carb., iron mottles
LB 5/5	240-340	2.5Y 7/3	2.5Y 5/4	SiL	abk, sbk	3	w	sec. carb.
LB 5/6	340-365	2.5Y 7/2	2.5Y 6/3	SiL	pl	3	w	-
LB 5/7	365-380	2.5Y 7/3	2.5Y 5/4	SiL	abk, sbk	3	w	sec. carb.; Mn
LB 5/8	380-400	2.5Y 7/3	2.5Y 5/4	SiL	abk, sbk	2	l	sec. carb.
LB 5/9	400-402	2.5Y 7/2	2.5Y 6/3	-	-	2	l	ash band
LB 5/10	402-420	2.5Y 7/3	2.5Y 5/4	SiL	abk, sbk	3	w	sec. carb.; Mn
LB 5/11	420-428	2.5Y 7/2	2.5Y 5/3	SiL	pl	3	l	Mn
LB 5/12	428-435	2.5Y 6/3	2.5Y 4/3	SiL	-	2	l	charcoal; Mn
LB 5/13	435-440	2.5Y 7/3	2.5Y 5/3	SiL	abk, sbk	3	l	Mn
LB 5/14	440-443	2.5Y 7/3	2.5Y 5/4	SiL	-	3	l	-
LB 5/15	443-470	2.5Y 7/3	2.5Y 5/4	SiL	pl	3	w	Mn
LB 5/16	470-490	2.5Y 7/3	2.5Y 5/3	SiL	pl	3	w	sec. carb.; Mn
LB 5/17	490-560	2.5Y 6/4	2.5Y 6/4	SiL	abk, sbk	2	-	sec. carb.; Mn

[1] SiL = silt loam ; SiCL = silty clay loam; SCL = sandy clay loam; SL = Sandy loam; S = sand (field survey data)
[2] shape: gr = granular, abk = angular blocky, sbk = subangular blocky, pl = platy
[3] Carbonate reaction: 0 = non-calcareous, 1 = slightly calcareous, 2 = moderately calcareous, 3 = strongly/extremely calcareous
[4] c = clear, g = gradual; l = linear, w = wavy
[5] crotov. = crotovinas; sec. carb. = secondary carbonates; Mn = Manganese; scp = stagnic colour pattern

Table III. 2: Results of sedimentological analyses for selected horizons of profiles LB 1, LB 2 and LB 5.

Horizon	Clay [%]	Silt [%]				Sand [%]				Total fine-earth	Gravels [%]	$CaCO_3$
	<2 µm	2 - 6.3 µm	6.3 - 20 µm	20-63 µm	Total	63 - 200 µm	0.2 - 0.63 mm	0.63 - 2 mm	Total	[%]	> 2mm	[%]
LB 1/2	28.3	8.1	14.9	30.0	53.0	8.5	7.1	3.1	18.7	99.4	0.6	23.2
LB 1/3	36.0	6.4	13.6	24.9	44.9	8.9	7.0	3.4	19.3	99.2	0.8	8.7
LB 1/4	31.3	8.7	11.6	25.7	45.9	9.2	9.7	3.9	22.7	99.4	0.6	23.2
LB 1/5	32.3	5.3	12.4	22.6	40.2	11.7	10.1	5.8	27.6	98.7	1.3	9.1
LB 1/6	20.9	2.6	5.2	7.6	15.4	9.4	25.8	28.4	63.6	76.4	23.6	0.8
LB 1/7	27.2	3.1	8.3	12.3	23.7	12.2	25.8	11.3	49.2	99.3	0.7	0.8
LB 1/8b	11.0	1.3	1.6	3.0	6.0	11.8	44.8	26.4	83.0	78.8	21.2	21.2
LB 2/7	26.5	2.7	6.4	9.1	18.3	13.5	26.4	15.4	55.3	98.6	1.4	0.8
LB 2/10	30.5	3.0	10.9	16.3	30.2	15.1	16.6	7.6	39.2	98.9	1.1	1.0
LB 5/3	14.4	5.8	20.9	52.6	79.3	5.1	1.1	0.1	6.3	99.9	0.1	33.6
LB 5/4	14.5	5.2	19.3	53.3	77.8	6.9	0.7	0.1	7.7	99.9	0.1	30.3
LB 5/6	12.4	5.5	21.9	56.5	83.9	3.3	0.5	0.0	3.8	100.0	0.0	22.0
LB 5/12	23.2	7.6	18.8	40.6	67.0	7.1	2.5	0.2	9.8	99.7	0.3	22.0
LB 5/17	17.4	8.2	21.8	46.6	76.6	5.4	0.4	0.1	5.9	98.0	2.0	14.7

Table III.3: Results of mineralogical analyses for selected horizons of profiles LB 1, LB 2 and LB 5. xxx = high abundance, xx = medium abundance, x = low abundance, * = traces, / = not present. Empty field indicate that no analyses were conducted.

Horizon	Minerals								Clay minerals					
	Quartz	K-feldspar	Plagioclase	Mica	Calcite	Dolomite	Hornblende	Other Silicates	Smectite	Vermiculite (18 Å)	Illite	Kaolinite	Chlorite	mixed layers
LB 1/2	x	/	x	x	x	x	x	x	xxx	/	x	x	x	*
LB 1/3	x	x	x	x	x	x	/	x	xx	x	x	x	x	*
LB 1/4	x	x	x	x	x	x	/	x	xxx	/	x	x	x	*
LB 1/5	x	x	x	*	x	x	/	x	xxx	/	x	x	*	*
LB 1/6	x	xx	x	*	x	x	/	x	xx	x	x	xx	*	*
LB 1/7	x	x	x	*	x	*	/	x	x	xx	x	x	*	*
LB 1/8b	xx	xx	x	x	*	*	/	x	x	xx	x	xx	*	*
LB 2/7	x	x	x	x	x	x	/	x						
LB 2/10	xx	xx	x	*	x	*	/	x						
LB 5/3	x	x	x	x	x	xx	*	x	xxx	/	x	x	x	*
LB 5/4	xx	x	x	x	x	xx	*	x	xx	/	x	xx	x	*
LB 5/6	x	/	x	xx	x	xx	*	x	xxx	/	x	x	x	*
LB 5/9	x	*	x	x	x	x	*	x	xx	x	x	x	x	*
LB 5/12	x	/	x	x	x	x	*	x	xx	/	x	x	xx	*
LB 5/17	x	x	xx	xx	x	x	*	x	xxx	/	x	xx	x	*

III.1.3.2 Luminescence dating

III.1.3.2.1 Sample preparation and analytical facilities

Luminescence samples were taken by hammering metal tubes into the freshly cleaned profile; the tubes were sealed to prevent any light intrusion. Sample LB 2/9 was taken at a depth of 4.2 m below top ground surface, and sample LB 2/10 was taken at a depth of 5.0 m (profile LB 2, Fig. III.3b). In profile LB 5, five samples were taken from different loess layers (Fig. III.4; Table III.4). All luminescence sample codes are equivalent to the sedimentary units (Table III.1).

Due to the sensitivity to daylight, all samples for equivalent dose (D_e) determination were treated under subdued red/orange light in the laboratory. The outer ends (~1 cm) of the samples were exposed to daylight during sampling and were therefore discarded. The inner material was treated with hydrochloric acid (HCl) and hydrogen peroxide (H_2O_2) to remove carbonates and organic material, respectively. Between every treatment step the sediment was washed with distilled water. The fine silt fraction (4-11 μm) of the samples (except sample LB 2/9) was extracted by repeated settling and washing. Sample LB 2/9 was wet-sieved and the fraction 100-150 μm was then treated with HCl and H_2O_2. Potassium feldspar grains were separated from the other minerals using heavy liquids (ρ = 2.58 gm^{-3}). After drying, the fraction was etched with 10% hydrofluoric acid for 40 minutes and subsequently treated with 10% HCl. Finally, the sample was sieved again to ensure that no smaller fractions are present.

For the fine-grained fraction, aluminium discs (diameter 9 mm) were used for luminescence measurements. The sand-sized potassium feldspar grains (several hundred grains per disc) were mounted on stainless steel discs using silicone oil as an adhesive.

Luminescence measurements were made with automated Risø TL/OSL readers (DA-20; Thomsen et al., 2006) using calibrated $^{90}Sr/^{90}Y$ beta sources. The feldspar signal of the samples was stimulated with an array of infrared light diodes emitting at 870 nm, and the luminescence was detected in the blue-violet region through a Schott BG39/Corning 7-59 filter combination.

Samples for dosimetry measurements were taken from immediately around the luminescence samples. After drying and homogenizing, about 500 g of each sample was ground and ashed for 24 h at 450°C. About 200 g of this material was then cast in wax to prevent radon loss. The casts were stored for at least one month to ensure equilibrium between radon and its daughter nuclides before counting. The concentrations of ^{238}U, ^{232}Th and ^{40}K were determined by high-resolution gamma spectrometry. The radionuclide concentrations were converted to dose rates using the conversion factors of Olley et al. (1996). Contribution of the cosmic dose rate was calculated following Prescott and Hutton (1994). In addition to the external dose rate, the internal dose rate was calculated for the sand sized potassium feldspar of sample LB 2/9; this calculation is based on a potassium

concentration of 12.5 ± 0.5% (Huntley and Baril, 1997) and ^{87}Rb concentration of 400 ± 100 ppm (Huntley and Hancock, 2001). The absorbed beta dose fraction was taken from Mejdahl (1979). For all samples except LB 2/10 a water content of 15 ± 5% was used, allowing for changes in water content throughout time. Because horizon LB 2/10 shows stagnic properties which could be associated with water logging, a water content of 25 ± 5% was assumed. A mean a-value of 0.08 ± 0.01 was used for dose rate calculation of the polymineral fine-grains. A summary of the dose rates is given in Table III.4; all values are in the range expected from other studies in Lower Austria (Zöller et al., 1994; Thiel et al., 2010a, b).

III.1.3.2.2 Post-IR IRSL measurements and measurement performance

For our samples we used the single-aliquot regenerative (SAR) protocol presented by Buylaert et al. (2009), i.e. a preheat of 250°C (60 s), IR bleach at 50°C (100 s; hereafter referred to as IR_{50}) and subsequent IRSL measurement at 225°C (100 s; hereafter referred to as $pIRIR_{225}$). The response to a test dose was measured in the same manner (Blair et al., 2005), and an IR illumination at 290°C for 40 s was inserted at the end of each SAR measurement cycle to reduce the signal carry over from one measurement cycle to the next (based on Murray and Wintle, 2003) (Table III.5). The initial 2 s of the decay curve were used for De determination after subtracting a background from the last 60 s. Dose responses and decay curves for samples LB 2/9 (representing 'old' material) and LB 5/3 (representing 'young' material) are shown in Fig. III.5.

The performance of the measurement protocol was tested by means of recycling ratios, recuperation and dose recovery tests (Wintle and Murray, 2006). Recycling ratios close to 1.0 indicate that the luminescence signal following a particular laboratory dose given after repeated heating of the sample can be reproducibly measured. The recycling ratios (Table III.4) for IR_{50} vary between 0.96 ± 0.05 (n=6; sample LB 2/10) and 1.01 ± 0.03 (n=9; sample LB 5/5) and for $pIRIR_{225}$ between 0.95 ± 0.01 (n=18; sample LB 2/9) and 1.01 ± 0.02 (n=9; sample LB 5/10). Recuperation is below 5% for all samples and both signals. To test whether doses given in nature (i.e. before any heating) can be measured accurately, dose recovery tests were conducted; a measured to given dose ratio within 10% of unity indicates good measurement performance. Three natural aliquots per sample were bleached for 2 hours in a Hönle SOL2 solar simulator. After bleaching, the aliquots were given a beta dose similar to the measured De for that sample and the given dose was then measured in the usual manner. Dose recovery results for IR_{50} range from 0.99 ± 0.01 (n=3; sample LB 5/5) to 1.10 ± 0.07 (n=3; sample LB 2/10) and for $pIRIR_{225}$ from 1.00 ± 0.01 (n=3; sample LB 5/15) to 1.21 ± 0.11 (n=3; sample LB 2/10) (Table III.4). The results of these standard quality tests demonstrate the applicability of the measurement protocol.

Table III.4: Sampling depths, dose rates, measured to given dose ratios, equivalent doses (D_e), g_{2days}-values (fading rate), and fading uncorrected and fading corrected ages for both IR_{50} and $pIRR_{225}$ (correction model of Huntley and Lamothe, 2001). The fading corrected $pIRR_{225}$ ages are considered the most reliable age estimates.

Sample	Depth [m]	Dose rate [Gy/ka]	n	measured/given dose		D_e [Gy]		g_{2days}-value [%/decade]		uncorrected age [ka]		corrected age [ka]	
				IR_{50}	$pIRR_{225}$	IR_{50}	$pIRR_{225}$	IR_{50}	$pIRR_{225}$	IR_{50}	$pIRR_{225}$	IR_{50}	$pIRR_{225}$
LB 2/9	4.2	4.1 ± 0.1	18	1.08 ± 0.08	1.10 ± 0.16	> 950	784 ± 54	4.6 ± 0.5	2.6 ± 0.8	> 230	191 ± 14	> 230	246 ± 29
LB 2/10	5.0	4.1 ± 0.1	6	1.10 ± 0.07	1.21 ± 0.11	> 1000	> 1250	3.0 ± 0.9	2.1 ± 1.0	> 250	> 300	> 250	> 300
LB 5/3	1.6	2.8 ± 0.2	9	1.05 ± 0.08	1.07 ± 0.16	81 ± 5	93 ± 3	2.6 ± 0.6	0.6 ± 0.2	29 ± 2	33 ± 1	36 ± 4	35 ± 2
LB 5/5	3.0	2.9 ± 0.2	9	0.99 ± 0.01	1.03 ± 0.01	94 ± 7	99 ± 4	4.1 ± 0.8	2.0 ± 0.6	32 ± 3	34 ± 1	48 ± 7	41 ± 4
LB 5/10	4.1	3.2 ± 0.2	9	1.03 ± 0.03	1.03 ± 0.01	109 ± 5	123 ± 4	0.8 ± 0.5	0.9 ± 0.7	34 ± 2	38 ± 2	36 ± 3	41 ± 4
LB 5/15	4.6	2.8 ± 0.2	9	1.00 ± 0.03	1.00 ± 0.01	105 ± 2	127 ± 2	2.6 ± 0.4	1.7 ± 0.4	37 ± 1	45 ± 1	47 ± 4	53 ± 4

Table III.5 : Flowchart of the post-IR IRSL SAR protocol (Buylaert et al., 2009). For IR_{50} steps 3 and 7, and for $pIRIR_{225}$ steps 4 and 8 were used for equivalent dose determination.

Step	Treatment	Observed
1	Give dose, D_i	
2	Preheat, 250°C, 60 s	
3	IR stimulation, 100 s at 50°C	L_x
4	IR stimulation, 100 s at 225°C	$\mathbf{L_x}$
5	Give test dose, D_T	
6	Preheat, 250°C, 60 s	
7	IR stimulation, 100 s at 50°C	T_x
8	IR stimulation, 100 s at 225°C	$\mathbf{T_x}$
9	IR stimulation, 40 s at 290°C	
10	Return to 1	

Due to anomalous fading in feldspar, i.e. an signal decrease with time (Wintle, 1973; Spooner, 1994) we measured the laboratory fading rates as the IRSL signal decrease over time using artificially irradiated aliquots; this is expressed in terms of the percentage decrease of signal intensity per decade of time (the *g*-value; Aitken, 1985, Appendix F). After D_e measurement and a final IR illumination at 290°C for 40 s, the same aliquots were given a beta dose close to their natural doses and measured using the above SAR protocol. Varying storage times were inserted after irradiation and preheating (Auclair et al., 2003). The *g*-value was normalised to a measurement delay time of 2 days after irradiation (Huntley and Lamothe, 2001).

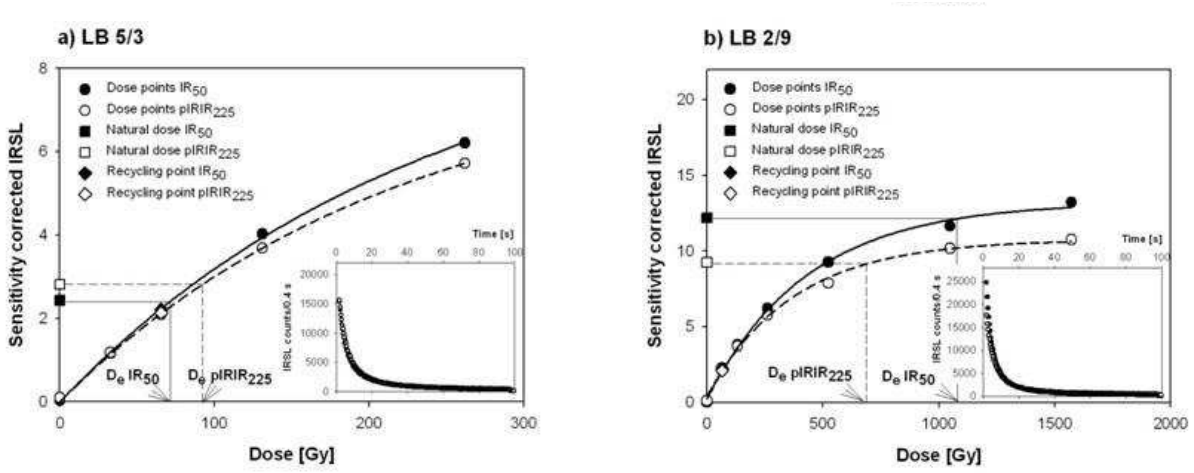

Fig. III. 5: Dose response curve for both IR_{50} and $pIRIR_{225}$ for a) one representative medium-sized aliquot of the sand-sized potassium feldspar grains (sample LB 2/9) and b) one representative aliquot of a polymineral sample (LB 5/3); the insets show the decay curves for both IRSL signals.

The $pIRIR_{225}$ equivalent doses (Table III.4) are associated with the lowest fading rates and are thus less dependent on the correction models; as a result the fading corrected $pIRIR_{225}$ ages are considered more reliable. Huntley and Lamothe (2001) argued against the application of their fading correction beyond ~20-50 ka, but Buylaert et al. (2010) showed that their correction can lead to accurate ages at least back to the Eemian (~125 ka, D_e values up to ~200 Gy). We therefore applied the correction model to our older samples, but cannot exclude that this results in an age underestimation.

III.1.3.3 Palaeontological excavations

The sampling concentrated on the in-situ find and other bone fragments across a distance of circa 1.5 meters in profile LB 2. Due to the incrustations and the hard sediment matrix several samples with a total weight of circa five kilograms were taken. No palaeontological remains were found in any other profile. The bones and bone fragments were prepared and described at the Department of Palaeontology, University of Vienna.

III.1.4 Results

III.1.4.1 Profile LB 1

In total, twelve horizons can be differentiated by means of sedimentological data and pedogenic features (Table III.1, Fig. III.3a). The uppermost horizon of profile LB 1 is a 20 cm thick loosely bedded disturbed topsoil; it is underlain by cemented loamy colluvial loess (LB 1/2) with (sub)angular structure. The matrix is strongly calcareous (23.2%; Table III.2), and it exhibits individual carbonate concretions of up to 1 cm in diameter. The lower boundary of LB 1/2 is linear. The fine earth is clearly dominated by silt (53.0%); the clay content is 28.3% and the sand content is 18.7% (Table III.2).

The 40 cm thick clayey loam of horizon LB 1/3 is characterised by a reddish-brownish hue and by even denser bedding compared to LB 1/2. The matrix has a significantly lower carbonate content (8.7%; Table III.2) which increases with depth. The entire horizon exhibits carbonate concretions, and can be interpreted as a buried Bw horizon. Its clay content yields 36.0%. The silt fraction is reduced compared to LB 1/2, but the sand fraction is similar (Table III.1). The main structure is (sub)angular, whereas the fine structure is crumbly. Root channels filled with dark-brown loamy material are found in this horizon. The lower boundary to LB 1/4 is linear.

The clayey loam of LB 1/4 (Table III.1) is 70 cm thick and densely bedded and has a significantly lighter colour. Compared to the overlying horizon, an increase in the sand fraction (22.7%) can be observed (Table III.2). The clay content is slightly reduced, whilst the silt fraction is similar to that of LB 1/3. The field survey indicated moderate carbonate content (Table III.1), which was then however measure to be 23.2% (Table III.2). Partially carbonate concretions can be found. At a depth of 1.1 m few poorly rounded quartz gravels were found. The lower boundary to the underlying horizon LB 1/5 is linear.

The more intensely coloured and densely bedded sandy loam of horizon LB 1/5 is 60 cm thick (Table III.1). The appearance is similar to that of LB 1/4; however, the sand content is higher (27.6%; Table III.2). The calcareous matrix of LB 1/5 is pale brown (dry) to brownish yellow (wet). Many carbonate concretions up to 10 cm in diameter are present. The boundary to horizon LB 1/6 is linear.

The 90 cm thick horizon LB 1/6 is composed of cemented coarse sand and fine gravels (Table III.2); the boundary of LB 1/5 and LB 1/6 is thus the transition from aeolian to fluvial components (Figs. III.2 and III.3). The fine earth makes up 76.4% of the material, which clearly indicates the great influence of gravels; the sand fraction (63.6%) is the dominating component of the fine earth. The sand and gravels are bedded in a loamy-sandy, non calcareous matrix (<1%; Table III.2), which has a brownish-yellow hue. All gravels, which are dominated by schist and gneiss, are poorly rounded and horizontally orientated. The lower boundary to LB 1/7 is wavy to linear (Table III.1).

Horizon LB 1/7 has a reddish matrix and is very densely bedded. The grain size distribution clearly shows the dominance of finer sand fractions compared to the overlying horizon (Table III.2); gravels are of no importance. The horizon is enriched in silt (25.8%) and clay (27.2%) compared to both the overlying and underlying layers. The matrix is a non calcareous (<1%; Table III.2) yellowish-brown loamy sand (Table III.1). Filled root marks can be found on the left hand site of the profile. Additionally a gravel layer made up of horizontally orientated gravels up to 1 cm in diameter is present. The lower boundary is slightly wavy to linear.

The lowermost exposed part of profile LB 1 is composed of sandy-gravelly, densely bedded non-calcareous sediments (LB 1/8a-d; Fig. III.3a). Four individual horizons can be differentiated based on the grain size distribution (Table III.2). LB 1/8a, which is 20 cm thick, is characterised by high gravel and sand content; these components are bedded in a (loamy) sandy matrix. The fine gravels are mostly poorly rounded schist and gneiss fragments. The matrix is yellowish-brown. The underlying sand layer (LB 1/8b) has a lighter hue. The fine earth of LB 1/8b is clearly dominated by the sand fraction (83.0%; Table III.2), with the medium sand being the most important component; the coarse sand fraction is also large. The clay fraction makes up 11.0% of the fine earth, and the silt is only of very minor importance. The fine earth sums up to 78.8% of the total; thus 21.2% of the material is composed of gravels. The matrix has a very low carbonate content of only 1.0%. In some parts of this horizon individual secondary carbonate precipitates were found.

Horizon LB 1/8c is again composed of coarser material (similar to LB 1/8a) exposed as a layer clearly dominated by gravels. Most of the fine to medium-sized gravels are quartz or gneiss and are bedded in a sandy matrix, which shows a brownish-yellow (dry) to yellowish brown (wet) colour. The lowermost horizon (LB 1/8d) of the exposed profile is a 60 cm thick sand layer. The colour is identical to the overlying horizon. Crotovina are present at a depth of 5 m.

At the base of the profile a hand-drilling was conducted up to 5.4 m (Fig. III.3a). It revealed loamy sediments with stagnic properties and roots marks.

Quartz can be found in all horizons throughout profile LB 1 (Table III.3), particularly in horizon LB 1/8b, where it is accompanied by an increase in the sand fraction (Table III.2). Micas are present in the upper part of the profile (LB 1/2-4). In the lower part only traces of mica are found (expect LB 1/8b) (Table III.3). Both potassium feldspars as well as plagioclase are present throughout the profile. An enrichment of potassium feldspar is found in LB 1/6 and LB 1/8b. In no other horizon than LB 1/2 hornblende is present.

The decrease of carbonate content with increasing depth (Table III.2) is reflected in the abundance of calcite and dolomite; both minerals show low abundance throughout the profile, but especially at the base only traces of them can be found.

The analysis of clay minerals (Table III.3) reveals a clear dominance of smectite, with shows high abundance in LB 1/2-5, and low abundance in LB 1/7 and LB 1/8b. In these two horizons larger quantities of swellable vermiculite (18 Å) are found compared to the other

horizons (Table III.3). Illite can be found in throughout the profile but the quantities are small. The same is true for kaolinite, which is enriched in LB 1/6 and LB 1/8b. In horizons LB 1/2-4, chlorite is of minor abundance; in the deeper horizons only traces of chlorite are found. Traces of mixed layer minerals are present throughout the profile.

III.1.4.2 Profile LB 2

In profile LB 2, ten horizons can be distinguished by means of sedimentological and pedogenic features (Table III.1; Fig. III.3b). The uppermost horizon of profile LB 2 is a 20 cm thick loose, disturbed topsoil with moderate carbonate content (LB 2/1); the lower boundary is linear. This horizon is underlain by a 20 cm thick strongly cemented, strong calcareous pale grey horizon (LB 2/2). It is characterised by carbonate concretions, which are up to 7 cm in diameter. The 20 cm thick horizon LB 2/3 is made up of moderately calcareous sandy clay loam and is loosely bedded. The material has a brownish hue and a (sub-)angular structure. The horizon is characterised by secondary carbonates in the form of pseudomycelia and carbonate concretions; crotovina are present especially in the upper part of the layer. Horizon LB 2/3 is equivalent to horizon LB 1/3 (Fig. III.3).

The underlying calcareous pale brown to pale yellowish brown horizon LB 2/4 is about 90 cm thick and corresponds to a silty clay loam with a (sub-)angular structure, and is thus the equivalent of horizon LB 1/4 (Fig. III.3). The lower boundary to LB 2/5, a 30 cm thick densely bedded fluvial layer, is linear. Fluvial gravels are horizontally embedded in a fine-sandy matrix and are poorly rounded. At the bottom the gravels and sands of LB 2/5 are replaced by interbedded strata of coarse sand and fine to coarse gravels (LB 2/6; Fig. III.6a). Horizons LB 2/5 and LB 2/6 correspond to LB 1/6 (Fig. III.3).

The fluvial layers are underlain by a 1.1 m thick, strongly hardened, yellowish brown sandy clay loam; this is a reworked layer with (sub-) angular structure (LB 2/7). This reworked horizon, the equivalent of LB 1/7, has very low carbonate content (0.8%) and contains poorly rounded gravels up to 5 cm in diameter. The clay content of the reworked layer is 26.5% (total of fine earth), whereas the silt yields 18.3%; the horizon is clearly dominated by sand (55.3%; Table III.2). Quartz, feldspars, mica, clay minerals, calcite and dolomite are present, but there is no clear dominance of any of these minerals (Table III.3).

Horizon LB 2/8 is composed of fluvial sandy-gravely deposits up to 60 cm thick. The gravels, mainly made up of quartzite and gneiss, are poorly rounded and horizontally embedded in a brownish-yellow sandy matrix. Bones were excavated at a depth of 3.3 to 3.5 m below ground surface. The bones are brittle to vitreous and show intense cracking through weathering/corrosion. Most of the bones are sintered and covered by siliceous crusts (Fig. III.6b).

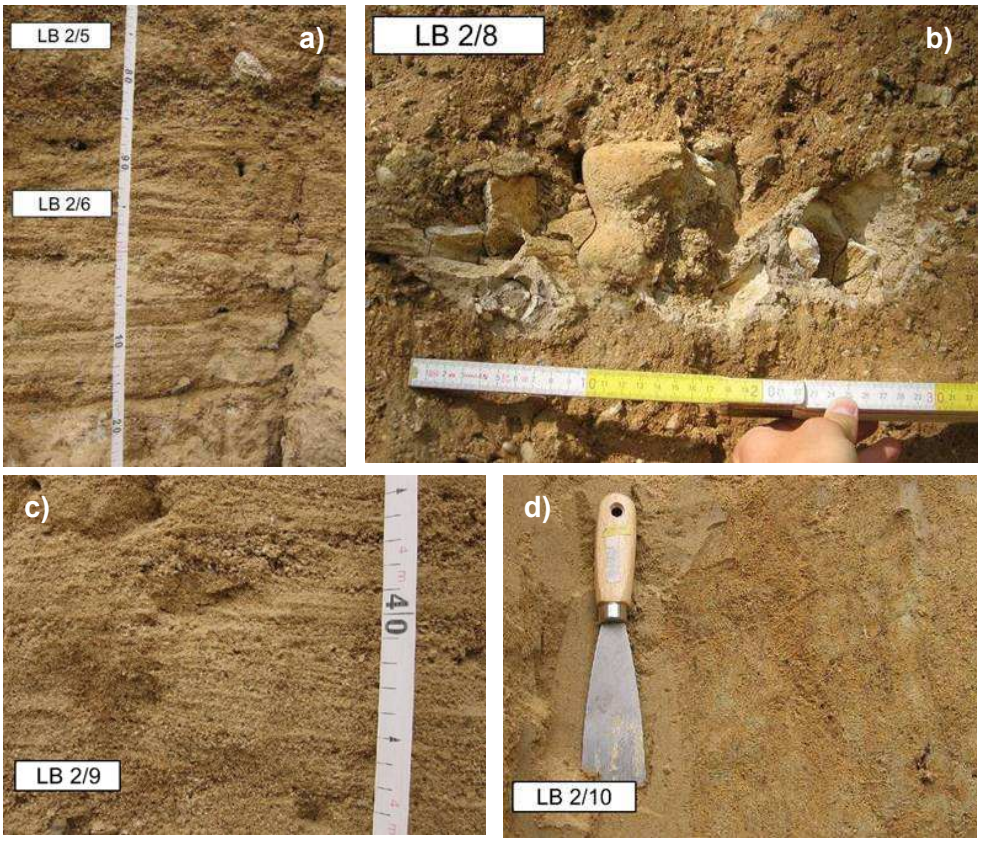

Fig. III.6: Selected features of profile LB 2. a) Gravels and sands of LB 2/5, which are underlain by interbedded strata (LB 2/6), b) Conglomeratic horizon with distal humerus (right) and ulna (left), parts of a left elbow joint in anatomical order, extended position, of a rhinocerotid (LB 2/8), c) interbedded strata of coarse and fine sands (LB 2/9) and d) densely bedded clayey loam with signs of deoxidisation (LB 2/10).

The bone-bed horizon LB 2/8 is underlain by 70 cm thick horizontally interbedded strata of coarse and fine sands, which contains small gravels (LB 2/9; Fig. III.6c). The sands, which were dated to 246 ± 29 ka (fading corrected $pIRIR_{225}$; Table 4), are yellow up to yellowish brown and characterised by low carbonate content. The fluvial sediments of LB 2/8 and LB 2/9 are equivalent to the basal horizons of profile LB 1 (LB 1/8a to LB 1/8d) (Fig. III.3).

The lowermost horizon LB 2/10 is 95 cm thick and shows signs of stagnic properties. The silty clay loam has an angular structure and is densely bedded. Compared to the overlying layers, LB 2/10 has higher silt content (30.2%) at the expense of the sand fractions, which sum up to 39.2% (fractions of fine earth; Table III.2). The mineralogical composition is more differentiated than for the fluvial layers: Clay minerals, plagioclase and calcite are of minor importance, whereas enrichment in quartz and potassium feldspar can be observed (Table III.3); mica and dolomite are negligible. The horizon is characterised by manganese precipitation and carbonate concretions up to 15 cm in diameter (Fig. III.6d). The total carbonate content of the matrix (excluding carbonate concretions) was 1.0%. The horizon is disturbed by several filled root marks. Luminescence dating gave an age of > 300 ka ($pIRIR_{225}$; Table III.4) for the loam of LB 2/10. This age is beyond the upper dating limit

(>1200 Gy; cf. Thiel et al., 2010a), and it has thus to be considered as an approximation of the depositional age. In any case, all dating results for this layer clearly point to an age > 250 ka (Table III.4).

In addition to the excavation of the profile, hand-coring was conducted for the deeper parts. The lower boundary of LB 2/10 was found at a depth of 5.6 m below top ground surface; it is made up of carbonate cement.

III.1.4.3 Preliminary analysis of the LB 2/8 faunal remains

During field work the initial signal of the faunal assemblage was the fragments of the articulated elbow joint of a rhinoceros (Fig. III.6b), but with a missing radius; this had apparently fallen out of the section onto the talus slope some time before. In the course of the preparation another anatomical unit, the hind extremity of a deer species and other identifiable specimens were discovered. The intense degree of fossilisation of the bones is indicated by their brittle and partly cracked appearance. A first taxonomic analysis of the faunal assemblage is based on 12 bones from at least three individuals of three species:

Stephanorhinus sp. can be determined from a fragmented left distal humerus and a fragmented proximal ulna (Fig. III.6b). A future detailed analysis will clarify if the specimens belong either to *S. hundsheimensis*, which is an Early to Middle Pleistocene element, or to the larger *S. kirchbergensis*, which is frequently attributed to forest-like biota or to S. hemitoechus, which is known as a steppe dweller. The last two species are considered Middle Pleistocene; but *S. hemitoechus* is expected to have lived also during the Eemian (e.g. Lacombat, 2009).

The presence of *Dama sp*. is evidenced by a maxillary fragment, a left proximal ulna and radius, parts of the right ankle joint including a distal tibia and the left distal tibia, most probably from the same individual. Due to the low tooth crown and the dimensions, the attribution to a fallow deer is clear; however, the identification of the species is hampered by the preservation condition. Limb bone morphology and dimension (Pfeiffer, 1999) allow us to assign the Langenlois fallow deer to the Middle Pleistocene *rhenana-clactoniana*-group. Pleistocene *Dama* records are restricted to interglacial periods and from forested to park palaeolandscapes; such areas are also preferred by the modern fallow deer.

Finally, a single metapodial sesamoid from *Alcine* sp. shows very close similarity to the recent moose *Alces alces* and excludes the *Megaloceros*-group. From the chronological distribution and frequency of finds in Central Europe of *Alces/Cervalces*, which is a genus living mainly in boreal to mixed forests and marshy habitats (e.g. Breda, 2005; Stefaniak, 2007) we hypothetically expect *A/C*.

A faunal assemblage including these three taxa has not been described elsewhere in the Eastern Alps and the surrounding foreland (Döppes and Rabeder, 1997). No clear

taxonomical determination is yet possible, and thus no other comparable Central European faunal assemblages can be referenced here.

III.1.4.4 Profile LB 5

The 5 m thick loess profile LB 5 can be subdivided into 17 horizons (Table III.1; Fig. III.4). The loess layers show very high carbonate contents, which decreases with depth. The disturbed topsoil (LB 5/1) of the loess profile is 20 cm thick, loosely bedded and moderately calcareous; the lower boundary is linear. Horizon LB 5/2 is 30 cm thick and is a loosely bedded colluvial layer, with a greyish hue. It has a laminated texture indicating layered deposition. In some parts of the horizon secondary carbonate in form of pseudo-mycelia can be found. The linear boundary to the underlying horizon LB 5/3 shows N-S inclination (Fig. III.4).

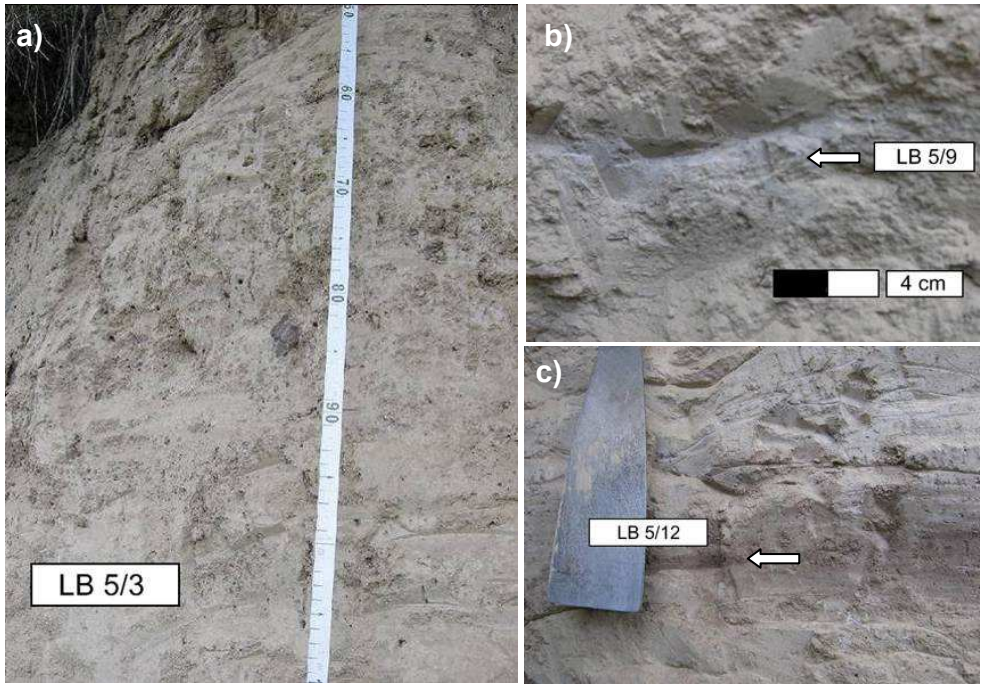

Fig. III.7: Selected features of profile LB 5. a) Compact loess of LB 5/3, b) 2 cm thin ash layer (LB 5/9), and c) 'cultural' layer (LB 5/12), in which charcoal pieces were found.

LB 5/3 is a 1.8 m densely bedded thick homogeneous loess layer (Fig. III.7a). Silt is the dominating fraction (79.3%), with only 14.4% clay and 6.3% sand (Table III.2). The loess of LB 5/3 has a (sub-)angular structure and contains pseudo-mycelia. These secondary carbonate structures are not found in the loess of horizon LB 5/4, which is about 10 cm thick and otherwise does not show any significant differences to LB 5/3 (Tables III.2 and III.3).

The loess (SiL; Table III.2) of the underlying horizon LB 5/5 is 1.0 m thick and noticeably homogenous; again secondary carbonates are present. The loess of LB 5/3 was dated to 35 ± 2 ka, and the loess of LB 5/5 to 41 ± 4 ka, respectively (fading corrected $pIRIR_{225}$; Table III.4).

Horizon LB 5/6 is 25 cm thick and characterised by dense bedding and lower carbonate content compared to the overlying horizons (Table III.1). An increase in the silt fraction (83.9 %) and corresponding decrease of the clay (12.4%) and sand (3.8%) was observed. This represents the lowest sand content found in the entire profile. The loess of LB 5/6 is grey and shows a platy structure. Both the upper and the lower boundary of this horizon are wavy. Due to the latter properties, this horizon can be interpreted as a Cryosol.

The underlying loess (LB 5/7) is 15 cm thick and very homogenous. Both pseudo-mycelia and manganese precipitates are present. The loess of horizon LB 5/8 is 20 cm thick and has a greyish hue. The carbonate content is lower than for the overlying loess layers. Both horizons are silty loams, with high silt contents (Tables III.2 and III.3).

LB 5/9 is a thin (2 cm) greyish ash layer (Fig. III.7b). It indicates either cultural activity or natural fire. No detailed investigations have been undertaken to address this question.

The homogenous loess of horizon LB 5/10 (SiL) is 18 cm thick and contains pseudo-mycelia and manganese precipitates. This layer was dated to 41 ± 4 ka (fading corrected $pIRIR_{225}$; Table III.4). The underlying 8 cm thick horizon LB 5/11 shows similar characteristics to horizon LB 5/6 and can be interpreted as a Cryosol.

Horizon LB 5/12 is composed of pale-brownish, 7 cm thick silty loam (Fig. III.7c), which shows no clear soil structure; the matrix has a carbonate content of 22.0%. Compared to the other horizons in profile LB 5, this horizon is characterised by a very distinct grain size distribution (Table III.2): The clay content is comparably enhanced (23.2%). The same is true for the sand fraction (9.8%), whereas the silt fraction is reduced to 67.0%. Most interestingly, the coarse silt fraction is only about 40.6 % and shows thus the lowest value in the profile. Charcoal remains are distributed throughout the horizon; however, they are not large enough for radiocarbon dating. It is possible that this layer is a cultural horizon, but no archaeological finds were recovered. The boundary to the underlying loess (LB 5/13) is irregular and shows a slight inclination (Fig. III.4).

The pale-yellowish loess of horizons LB 5/13 and 5/15 is interrupted by a 3 cm thick brownish layer (LB 5/14). Luminescence dating of LB 5/15 resulted in an age of 53 ± 4 ka (fading corrected $pIRIR_{225}$; Table III.4).

The greyish horizon LB 5/16 is 20 cm thick and has a weakly developed platy structure equivalent to LB 5/6 and LB 5/11. The boundaries to the overlying and underlying horizons are slightly wavy. The lowermost horizon is a 70 cm thick light yellowish-brown loess (LB 5/17), which has a lower carbonate content than the overlying loess layers. Several crotovina are present. Carbonate concretions up to 3 cm in diameter and small pebbles up to 0.5 cm in diameter are characteristic for this layer, which is reflected in the comparably higher content

(2%) of the fraction >2 mm. The loess of LB 5/17 is clearly dominated by silt (76.6%); clay (17.4%) and sand (5.9%) are of minor importance.

Mineralogical analyses revealed that quartz is present in all horizons that were analysed, but in small amounts (Table III.3). Only in horizon 5/4 quartz is enriched. Mica is present in all horizons. In the Cryosol LB 5/6 and the loess layer LB 5/17 mica is enriched. The feldspars are dominated by plagioclase, but the total amount of feldspars is in general low. Orthoclase is of minor importance, but shows comparably higher abundance in the upper horizons (LB 5/3 and LB 5/4) and in LB 5/17. The amount of calcite is low, but equally distributed throughout the profile, whereas dolomite is mainly present in the upper part (LB 5/3, LB 5/4, LB 5/6). The abundance of dolomite decreases with depth. Traces of hornblende can be found throughout the profile.

The clay minerals are dominated by smectite showing high abundance in LB 5/3, LB 5/6 and LB 5/17 (Table III.3) and moderate abundance in horizons LB 5/4, LB 5/9 and LB 5/12. Swellable vermiculite (18 Å vermiculite) is only present in horizon LB 5/9. Illite and chlorite were detected throughout the profile, but only in small quantities; LB 5/12 showed higher quantities of chlorite compared to all other horizons. Kaolinite is of minor importance with comparably higher values in horizons LB 5/4 and LB 5/17.

III.1.5 Discussion

The sediment succession at the east-exposed wall of the former brickyard in Langenlois clearly shows the transition from fluvial to aeolian deposition (Fig. III.2). The loamy deposits of LB 2/10 with its root marks and thick carbonate concretions display a former ground surface on which the fluvial gravels and sands (LB 1/8a-d, LB 2/9 and LB 2/8) were deposited. The degree of weathering, the low carbonate content and the enrichment in quartz and potassium feldspar (Table III.3) as well as by the palaeontological finds indicate sedimentation during the Middle Pleistocene. This is evidenced by the luminescence ages. For LB 2/9 it has to be noted that due to the restriction of the fading correction model of Huntley and Lamothe (2001) the derived luminescence age might be an age underestimate; it seems therefore appropriate to conclude that the sediments of LB 2/9 are > 250 ka. The post-IR IRSL age of > 300 ka for LB 2/10 clearly points to deposition of the material during or even before the Middle Pleistocene. The $pIRIR_{225}$ age of LB 2/10 is close to or even beyond the dating limit (Table III.4) (Thiel et al., 2010a, b); determination of an accurate age is not feasible. For the fluvial layers of the north exposed wall an age older than Brunhes Chron has been suggested (Piffl, 1976) but neither is a stratigraphical correlation possible, nor can the palaeomagnetic data considered to be reliable due to the low sampling density.

Because the gravels of LB 1/8a-d, LB 2/9 and LB 2/8 are poorly rounded, short distance transport has to be assumed, most likely by the nearby river Loisbach. The dominance of quartz, schist and gneiss which form the local geology (Wessely, 2006) underlines these

conclusions. The distinct grain size distributions of the interbedded strata (LB 1/8 and LB 2/9) point to normal fluvial dynamics whereas the fluvial sands of LB 2/8 seem to have been deposited during a flooding event; the latter is supported by the find of mammal bones at least partly in their original anatomical relationships. From a taphonomical point of view it is evident that sedimentation and deposition of carcasses of dead animals or their parts have taken place synchronously during very rapid channel sedimentation without significant relocation. The embedding of heavy dead animal bodies within badly sorted terrestrial gravels (as suggested by the *Dama* parts and by the rhinoceros fore arm) requires a very high sedimentation rate, and a short fluvial transport distance from the living area of the animals before disarticulation has to be assumed (Behrensmeyer, 2007). No human impact on the remains could be found. The assemblage speaks in favour of interglacial conditions, but the actual status of taxonomic research does not allow a closer attribution than Middle Pleistocene.

The reworked sediments (LB 1/7 and LB 2/7) depict another distinct dynamic landscape forming phase. The sedimentological and mineralogical data (Tables III.2 and III.3) indicate intensive weathering processes of this material, which was later reworked and is only recorded as soil sediment on top of the fluvial strata LB 1/8 and LB 2/8, respectively. The soil sediment has been affected by repeated fluvial deposition and was covered by gravels, sands and loams (LB 1/6 and LB 2/5-6). Because the sediment layers LB 1/6 and LB 2/5-6 show a similar degree of weathering compared to the underlying, luminescence dated layers, it is likely that the sands were deposited during the Middle Pleistocene, but no firm evidence from either luminescence dating or palaeontological finds is available. The reworked palaeosol is presumably older than the last interglacial. The less intensively weathered reworked loam (LB 1/4-5 and LB 2/4) might indicate an active landscape forming phase, i.e. glacial conditions. The overlying weak palaeosol (LB 1/3 and LB 2/3) can be interpreted as a residual of an interstadial soil, which was later eroded due to intensive landuse (LB 1/1-2 and LB 2/1-2).

Profile LB 5 contains aeolian sediments, as reflected by the grain size distribution (Table III.2). The transition from fluvial environment to aeolian sedimentation is reflected in profile LB 3 (Fig. III.2); the loess was deposited in a depression which was the result of a preceding erosional phase which cannot be constrained in time. In general, the loess layers of profile LB 5 are weakly weathered and have low clay content. This is indicative of a younger age despite the topographically lower position compared to profile LB 2. The fading corrected $pIRIR_{225}$ age indicates a prolonged deposition from ~55 ka (LB 5/15) to ~35 ka (LB 5/3) (Table III.4). No signs of intensive erosional processes could be found, and there are no indices for soil formation in this profile. However, the >5 m thick loess is differentiated by Cryosols (LB 5/6, LB 5/8, LB 5/16) indicating permafrost and associated retention of water. The boundaries of the Cryosols are wavy and the soil horizons are characterised by a platy frost structure. The overlying loess (LB 5/5) of the uppermost Cryosol (LB 5/6) was dated to 41 ± 4 ka (fading corrected $pIRIR_{225}$; Table III.4); other Cryosol complexes in Lower Austria have been dated

to ~25-40 ka (Haesaerts et al., 1996; Thiel et al., 2010a, b). It has to be noted that mineralogical analysis of the loess revealed that potassium feldspar is rare and that most samples are dominated by plagioclase. Only in a few studies the luminescence behaviour of plagioclase (e.g. Huntley and Lian, 2006; Tsukamoto et al., 2010) and the suitability of plagioclase for dating (e.g. Mejdahl, 1983; Krause et al., 1997; Barré and Lamothe, 2010; Tsukamoto et al., 2010) has been investigated. None of these studies involves post-IR IRSL signals and it is not clear how much plagioclase contributed to the post-IR IRSL signal. Despite this minor uncertainty, the Late Glacial depositional age of the loess in Langenlois is consistent with other studies from this area (Zöller et al., 1994; Thiel et al., 2010a, b).

It is interesting to note that, based on our data, permafrost was present during MIS 3, despite the warmer conditions compared to MIS 2, for which the formation of Crysols is well known from other sites (e.g. Bibus, 1989; Frechen, 1999). Furthermore, there is no evidence for the presence of the youngest MIS 3 palaeosol known as Lohner soil (acc. to Semmel, 1968), or Stillfried B (acc. to Fink, 1976). This fact is also known from the archaeological excavations of Krems-Wachtberg (Händel et al., 2008), Krems-Hundsteig (Neugebauer-Maresch, 2008) and Stratzing (Thiel et al., 2010a), and thus seems to be a typical situation found for the Last Glacial loess sequences in the western part of the Kremsfeld. In Upper Austrian loess sequences the equivalent of the Lohner soil is wide-spread (Terhorst 2010b). The absence of this soil formation might be due to erosion processes and/or specific climatic conditions, i.e. transition zone between dry and wet loess landscape (Brandtner, 1956) of the Kremsfeld during the Last Glacial. The relatively thick loess deposition in Langenlois during MIS 3 might also be due to the regional or even local palaeoclimatic conditions. Additionally, such thick loess deposition might have been selective due to palaeotopography (cf. Fig. III.2).

According to the field survey and post-IR IRSL dating results, the Upper Pleniglacial loess is absent in these profiles. The same observation was made for the profiles of Stratzing (Thiel et al., 2010a), Willendorf II (Haesaerts et al., 1996), Paudorf (Zöller et al., 1994; Thiel et al, 2010b) and Göttweig (Zöller et al, 1994; Thiel et al., 2010b). Thus the erosion of the last glacial maxiumum (LGM) loess seems to be, similar to the absence of MIS 3 soils, typical for this area. This has previously been found by Havliček et al. (1998), who stated that extensive Upper Pleistocene erosion causes an area-wide absence of loess from the last glacial maximum (LGM) at the south-eastern margin of the Bohemian Massif.

III.1.6 Conclusions

A detailed field survey and sedimentological analyses of the 120 m long east-exposed sediment wall in the brickyard of Langenlois have revealed a transition from fluvial to aeolian deposition. Mineralogical analyses of selected horizons have allowed a relative attribution of depositional ages: a high degree of weathering points to a much older age of the fluvial units compared to the loess. Palaeontological finds with a distinct interglacial assemblage from a

fluvial conglomeratic horizon and post-IR IRSL ages confirm the attribution to the Middle Pleistocene. The low degree of weathering found in the loess sequence indicates younger loess accumulation, most likely during the Last Glacial; this attribution was confirmed by post-IR IRSL dating. Middle Pleistocene sediments are found in a morphologically higher position than the younger aeolian deposits, which testifies Late Pleistocene superposition of the slopes. It remains unclear when the main erosion of the Middle Pleistocene sediments took place and whether loess was locally deposited prior to ~ 55 ka.

Our study is a further step towards unravelling the geomorphic and pedological processes that have formed the present day landscape in Lower Austria. These investigations give additional information on the stratigraphy of the study area. The Middle Pleistocene fluvial units indicate a flooding event which cannot be regionally correlated as yet. Further studies close to other ancient fluvial systems are needed to determine whether flooding occurred at a lager scale. As for other sites in Lower Austria and Europe, a (weak) soil formation during MIS 3 did not occur in Langenlois. This observation seems to be typical for the western part of the Kremsfeld. The same is true for erosion of the LGM loess. At this stage it is too early to draw final conclusions on why no or hardly any pedogenetics took place during MIS 3, and why the loess accumulated at such high rates. The latter seems to be a site specific phenomenon, which is most likely due to the morphological position.

Acknowledgements

This study was supported by the Leibniz Pakt Project 676 for Research and Innovation 2008-2010. We are indebted to Ingo Hofer, Robert Peticzka and Christa Herrmann (University of Vienna) for assistance during field and laboratory work and discussions on stratigraphy and sedimentology. We furthermore thank Reinhard Roetzel (Geological survey of Austria) for the introduction to the study area and several discussions during field work. We appreciate discussions on post-IR IRSL dating with Kristina Thomsen and Mayank Jain (National Laboratory for Sustainable Energy, Radiation Research Divison, Risø DTU). We are grateful to two anonymous reviewers for their constructive comments on an earlier version of the manuscript.

References

AG Boden, 2005. Bodenkundliche Kartieranleitung, 5th edition. Schweizerbart‟sche Verlagsbuchhandlung, Hannover.

Aitken, M. J., 1985. Thermoluminescence Dating. Academic Press, London, 359 pp.

Aitken, M. J., 1998. An Introduction to Optical Dating. The Dating of Quaternary Sediments by the Use of Photon-stimulated Luminescence. Oxford University Press, Oxford, 267 pp.

Auclair, M., Lamothe, M., Huot, S., 2003. Measurement of anomalous fading for feldspar IRSL using SAR. Radiation Measurement 37, 487-492.

Barré, M., Lamothe, M., 2010. Luminescence dating of archaeosediments: A comparision of K-feldspar and plagioclase IRSL ages. Quaternary Geochronology 5, 324-328.

Behrensmeyer, A. K., 2007. Bonebeds through geologic time. In: Rogers, R., Eberth, D., Fiorillo, T. (Eds.) Bonebeds: Genesis, Analysis, and Paleobiological Significance, 65-102. University of Chicago Press, Chicago.

Blair, M. W., Yukihara, E. G., McKeever, S. W. S., 2005. Experiences with single-aliquot OSL procedures using coarse-grain feldspars. Radiation Measurements 39, 361-374.

Bibus, E., 1989. Paläoböden im mittleren Neckarbecken unter besonderer Berücksichtigung von Lößstratigraphie und Paläoböden. Exkursionsführer 8. Tagung des Arbeitskreises Paläoböden der Deutschen Bodenkundlichen Gesellschaft, Heilbronn, pp.1-31.

Brandtner, F., 1956. Lößstratigraphie und paläolithische Kulturabfolge in Niederösterreich und in den angrenzenden Gebieten. Eiszeitalter und Gegenwart 7, 127-175.

Breda, M., 2005. The morphological distinction between the postcranial skeleton of Cervalces/Alces and Megaloceros giganteus and between the two Alceini genera from the Upper Pliocene-Holocene of Western Europe. Geobios 38, 151-170.

Brindley, G. W., Brown, G., 1980. Crystal Structures of Clay Minerals and their X-Ray Identification. Mineralogical Society, London, 495 pp.

Buylaert, J.-P., Murray, A. S., Thomsen, K. J., Jain, M., 2009. Testing the potential of an elevated temperature IRSL signal from K-feldspar. Radiation Measurements 44, 560-565.

Buylaert, J.-P., Huot, S., Murray, A. S., Van de haute, P., 2010. Infrared stimulated luminescence dating of an Eemian (MIS 5e) site in Denmark using K-feldspar. Boreas, doi: 10.1111/j.1502-3885.2010.00156.x.

Döppes, D., Rabeder, G., 1997. Pliozäne und pleistozäne Faunen Österreichs. Mitteilungen der Kommission für Quartärforschung der Österreichischen Akademie der Wissenschaften 10, 1-411.

Einwögerer, T., Friesinger, H., Händel, M., Neugebauer-Maresch, C., Simon, U., Teschler-Nicola, M., 2006. Upper Paleolithic infant burials. Nature 444, 285.

Fladerer, F. A., Havlíček, P., Roetzel, R., Salcher, T., Smolíková, L., Tuzar, J., 2005. Der Steppenwisentfund (Bison priscus) von Langenlois-Buriweg, Niederösterreich - Paläontologische und pleistozänstratigrafische Untersuchungen. Mitteilungen der Kommission für Quartärforschung 14. Österreichische Akademie der Wissenschaften. Wien.

Fink, J., 1956. Zur Korrelation der Terrassen 743 und Lösse in Österreich. Eiszeitalter und Gegenwart 7, 49-77.

Fink, J., 1976. Exkursion durch den österreichischen Teil des nördlichen Alpenvorlandes und den Donauraum zwischen Krems und Wiener Pforte. Erweiterter Führer zur Exkursion aus Anlass der 2. Tagung der IGCP-Projektgruppe „Quaternary Glaciations in the Northern Hemisphere". Mitteilungen der Kommission für Quartärforschung der Österreichischen Akademie der Wissenschaften 1, 1-113

Fink, J., 1978. Exkursion durch den österreichischen Teil des nördlichen Alpenvorlandes und den Donauraum zwischen Krems und Wiener Pforte. Ergänzungen zu Band 1. Mitteilungen der Kommission für Quartärforschung der Österreicher Akademie der Wissenschaften, Wien.

Frechen, M., 1999. Upper Pleistocene loess stratigraphy in Southern Germany. Quaternary Geochronology 18, 243-269.

Götzinger, G., 1936. Das Lößgebiet um Göttweig und Krems an der Donau. Führer für die Quartärexkursion in Österreich, 11 pp., Geologische Bundesanstalt Wien.

Haase, D., Fink, J., Haase, G., Ruske, R., Pécsi, M., Richter, H., Altermann, M., Jäger, K.-D., 2007. Loess in Europe - its spatial distribution based on a European Loess Map, scale 1:2,500,000. Quaternary Science Reviews 26, 1301-1312.

Haesaerts, P., Damblon, F., Bachner, M., Trnka, G., 1996. Revised stratigraphy and chronology of the Willendorf II sequence, Lower Austria. Archaeologia Austriaca 80, 25-42.

Händel, M., Simon, U., Einwögerer, T., Neugebauer-Maresch, C., 2008. Loess deposits and the conservation of the archaeological record - The Krems-Wachtberg example. Quaternary International 198, 46-50.

Haslinger, E., Heinrich, M., 2008. Der "Rote Aufschluss" 775 von Langenlois. Pedogenese und Mineralogie von Paläoboden-Sequenzen über Amphibolit. Abhandlungen der Geologischen Bundesanstalt Wien 62, 71-79.

Haslinger, E., Smoliková, Havliček, P., Roetzel, R., Heinrich, M., Holásek, O., Vachek, M., Ottner, F., 2009. Pedological and geochemical investigations at the "Red Outcrop" of Langenlois (Lower Austria). E&G Quaternary Science Journal 58(2), 135-147.

Havliček, P., Holásek, O, Smoliková, L., Roetzel, R., 1998. Zur Entwicklung der Quartärsedimente am Südostrand der Böhmischen Masse in Niederösterreich. Jahrbuch der Geologischen Bundesanstalt Wien, 141, 51-71.

Huntley, D. J., Baril, M. R., 1997. The K content of the K-feldspars being measured in optical dating or in thermoluminescence dating. Ancient TL 15, 11-13.

Huntley, D. J., Hancock, R. G. V., 2001. The Rb contents of K-feldspar grains being measured in optical dating. Ancient TL 19, 43-46.

Huntley, D. J., Lamothe, M., 2001. Ubiquity of anomalous fading in K-feldspars and the measurement and correction for it in optical dating. Canadian Journal of Earth Science 38, 1093-1106.

Huntley, D. J., Lian, O. B., 2006. Some observations on tunnelling of trapped electrons in feldspars and their implications for optical dating. Quaternary Science Reviews 25, 2503-2512.

IUSS Working Group WRB, 2006. World Reference Base for Soil Resources. World Soil Resources Reports 103. FAO, Rome.

Kinter, E. B., Diamond, S., 1956. A new Method for preparation and treatment of oriented aggregate specimens of soil clays for X-Ray diffraction analysis. Soil Sciences 81, 111-120.

Krause, W. E., Krbetschek, M. R., Stolz, W., 1997. Dating 808 of Quaternary lake sediments from the Schirmacher oasis (East Antarctica) by infra-red stimulated luminescence (IRSL) detected at the wavelength of 560 nm. Quaternary Science Reviews 16, 387-392.

Lacombat, F., 2009. Biochronologie et grands Mammifères au Pléistocène moyen et supérieur en Europe occidentale: l'apport des Rhinocerotidae (genre Stephanorhinus), Quaternaire 20, 429-435.

Mejdahl, V., 1979. Thermoluminescence dating: beta-dose attenuation in quartz grains. Archaeometry 21, 61-72.

Mejdahl, V., 1983. Feldspar inclusion dating of ceramics of burnt stones. PACT 9, 351-364.

Moore, D. M., Reynolds, R. C., 1997. X- Ray Diffraction and the Identification and Analysis of Clay Minerals. Oxford University Press, New York, 378 pp.

Murray, A. S., Wintle, A. G., 2003. The single aliquot regenerative dose protocol: potential for improvements in reliability. Radiation Measurements 37, 377-381.

Neugebauer-Maresch, C., (ed.), 2008. Krems-Hundssteig - Mammutjägerlager der Eiszeit. Ein Nutzungsareal paläolithischer Jäger- und Sammler(-innen) vor 41.000-27.000 Jahren. Mitteilungen der Prähistorischen Kommission der Österreichischen Akademie der Wissenschaften 67, 348 pp.

Noll, M., Leitner-Wild, E., Hille, P., 1994. Thermoluminescence dating of loess deposits at Paudorf, Austria. Quaternary Geochronology (Quaternary Science Reviews) 13, 473-476.

Olley, J., Murray, A. S., Roberts, R. G., 1996. The effects of disequilibria in the uranium and thorium decay chains on the burial dose rates in fluvial sediments. Quaternary Science Reviews 15, 751-760.

ÖNORM L 1061/1, 2002. Physikalische Bodenuntersuchungen. Bestimmung der Korngrößenverteilung des Mineralbodens. Teil 1: Grobboden. Österreichisches Normungsinstitut, Wien.

ÖNORM L 1061/2, 2002. Physikalische Bodenuntersuchungen. Bestimmung der Korngrößenverteilung des Mineralbodens. Teil 2: Feinboden. Österreichisches Normungsinstitut, Wien.

ÖNORM L 1084, 2006. Chemische Bodenuntersuchungen. Bestimmung von Karbonat. Österreichisches Normungsinstitut, Wien.

Pfeiffer, T. 1999. Die Stellung von Dama (Cervidae, Mammalia) im System plesiometacarpaler Hirsche des Pleistozäns. Courier Forschungsinstitut Senckenberg 211, 1-218.

Piffl, L., 1955. Exkursion von Krems bis Absberg. Verhandlungen der Geologischen Bundesanstalt, Sonderheft, 70-78.

Piffl, L., 1976. Stop 3/4: Ziegelwerk W Langenlois (Hammerer). In Fink, J. (ed.): Exkursion durch den österreichischen Teil des nördlichen Alpenvorlandes und den Donauraum zwischen Krems und Wiener Pforte. Erweiterter Führer zur Exkursion aus Anlass der 2. Tagung der IGCP-Projektgruppe „Quaternary Glaciations in the Northern Hemisphere". Mitteilungen der Kommission für Quartärforschung der Österreichischen Akademie der Wissenschaften 1, 113 pp.

Prescott, J. R., Hutton, J. T., 1994. Cosmic ray contributions to dose rates for luminescence and ESR dating: large depths and long-term variations. Radiation Measurements 23, 497-500.

Schultz, L. G., 1964. Quantitative Interpretation of Mineralogical Composition from X-Ray and Chemical Data of the Pierre Shales. Geological Survey Professional Paper, 391(C), 1-31.

Semmel, A., 1968. Studien über den Verlauf jungpleistozäner Formung in Hessen. Frankfurter geographische Hefte 45, 1-133.

Smolíková, L., 2003. Bericht 2002 über 875 Mikromorphologie, Typologie und Stratigraphie quartärer Böden vom Buriweg in Langenlois auf Blatt 38 Krems. Jahrbuch der Geologischen Bundesanstalt 143/3, 506-507.

Smolíková, L., Havlíček, P., 2007. Bericht 2005 und 2006 über mikromorphologische Untersuchungen von quartären Böden im Gebiet des unteren Kamptales auf den Blättern 21 Horn und 38 Krems. Jahrbuch der Geologischen Bundesanstalt 147/3-4, 682-683.

Spooner, N. A., 1994. The anomalous fading of infrared-stimulated luminescence from feldspars. Radiation Measurements 23, 625-632.

Stefaniak, K., 2007. Early and Middle Pleistocene elk (Alcinae Jerdon, 1874, Cervidae, Mammalia) from Poland. Acta Zoologica Cracoviensia 50A (1–2), 73-92.

Terhorst, B., Frechen, M., Reitner, J., 2002. Chronostratigraphische Ergebnisse aus Lößprofilen der Inn- und Traun-Hochterrassen in Oberösterreich. Zeitschrift für Geomorphologie N.F., Suppl.-Vol. 127, 213 - 232.

Terhorst, B., Solleiro-Rebolledo, E., Veit, H., 2010a. Preface: Quaternary landscape change and applied research fields. Geomorphology 122/3-4, 211-212.

Terhorst, B., Ottner, F., Holawe, F., 2010b. Pedostratigraphische, sedimentologische, mineralogische und statistische Untersuchungen an den Deckschichten des Profils Wels/Aschet (Oberösterreich). Mitteilungen der Kommission für Quartärforschung der österreichischen Akademie der Wissenschaften, in press.

Thiel, C., Buylaert, J.-P., Murray, A. S., Terhorst, B. Hofer, I., Tsukamoto, S., Frechen, M., 2010a. Luminescence dating of the Stratzing loess profile (Austria) - Testing the potential of an elevated temperature post-IR IRSL protocol. Quaternary International; doi:10.1016/j.quaint.2010.05.018.

Thiel, C., Buylaert, J.-P., Murray, A. S., Terhorst, B., Tsukamoto, S., Frechen, M., 2010b. Investigating the chronostratigraphy of prominent palaeosols in Lower Austria using post-IR IRSL dating. E&G Quaternary Science Journal, accepted.

Thomsen, K. J., Bøtter-Jensen, L., Denby, P. M., Moska,, P., Murray, A. S., 2006. Developments in luminescence measurement techniques. Radiation Measurements 41, 768-773.

Thorez, J.,1975. Phyllosilicates and clay minerals - a laboratory handbook for their x-ray diffraction analysis. Editions G. Lelotte, Liege, 579 pp.

Tributh, H., 1989. Notwendigkeit und Vorteil der Aufbereitung von Boden- und Lagerstättentonen. In: Tributh, H., Lagaly, G. (eds.). Identifizierung und Charakterisierung von Tonmineralen, p. 29-33, Gießen.

Tsukamoto, S., Duller, G. A. T., Wintle, A. G., Frechen, M., 2010. Optical dating of a Japanese marker tephra using plagioclase. Quaternary Geochronology 5, 274-278.

Wessely, G., 2006. Niederösterreich. Geologie der Österreichischen Bundesländer. Geologische Bundesanstalt, Wien.

Whittig, L. D., 1965. X-ray diffraction techniques for mineral identification and mineralogical identification. In: Black, C.A. (ed.). Methods of Soil Analysis, p. 671-698.

Wilson, M. J., 1987. A handbook of determinative methods in clay mineralogy. Blackie, Glasgow. London, 308 pp.

Wintle, A. G., 1973. Anomalous fading of thermoluminescence in minerals. Nature 245, 143-144.

Wintle, A. G., Murray, A. S., 2006. A review of quartz optically stimulated luminescence characteristics and their relevance in single-aliquot regeneration dating protocols. Radiation Measurements 41, 369-391.

ZAMG (Zentralanstalt für Meterologie und Geophysik), 2010. Klimadaten von Österreich 1971-2000. Station Langenlois (http://www.zamg.ac.at/fix/klima/oe71-00/klima2000/klimadaten_oesterreich_1971_frame1.htm).

Zöller, L., Oches, E. A., McCoy, W. D., 1994. Towards a revised chronostratigraphy of loess in Austria with respect to key sections in the Czech Republic and in Hungary. Quaternary Geochronology (Quaternary Science Reviews) 13, 465-472.

Zwittkovits, F., 1983. Klimatypen - Klimabereiche - Klimafacetten. Erläuterungen zur Klimatypenkarte von Österreich. Beiträge zur Regionalforschung 5, Österreichische Akademie der Wissenschaften, Wien.

III.2 Luminescence dating of the Stratzing loess profile (Austria) - Testing the potential of an elevated temperature post-IR IRSL protocol

Thiel, C.[1,2], Buylaert, J.-P.[2,3], Murray, A. S.[2], Terhorst, B.[4], Hofer, I.[5], Tsukamoto, S.[1], Frechen, M.[1]

[1] Leibniz Institute for Applied Geophysics, S3: Geochronology and Isotope Hydrology, Stilleweg 2, 30655 Hannover, Germany

[2] Nordic Laboratory for Luminescence Dating, Department of Earth Sciences, Aarhus University, Risø DTU, DK-4000 Roskilde, Denmark

[3] Radiation Research Division, Risø National Laboratory for Sustainable Energy, Technical University of Denmark, DK-4000 Roskilde, Denmark

[4] Institute of Geography, Department for Physical Geography, University of Würzburg, Germany

[5] Institute of Geography and Regional Research, University of Vienna, Austria

Quaternary International (2011) 234, 23-31 (http://dx.doi.org/10.1016/j.quaint.2010.05.018)

Abstract

Feldspar infrared stimulated luminescence (IRSL) signals saturate at ~2000 Gy, i.e. ~500-700 ka (assuming a dose rate of 3-4 Gy/ka, typical for loess) and it is therefore theoretically possible to date Middle Pleistocene loess. However, the accuracy of age estimates is hampered by anomalous fading, which leads to significant age underestimation. Fading corrections have been proposed but these corrections are reliant on inherent assumptions and in any case are inapplicable at large doses (as the growth curve approaches saturation). Recent studies have identified a post-IR IRSL signal that shows less fading and is thus less dependent on accurate fading corrections. This study builds upon these investigations and applies a post-IR IRSL SAR dating protocol to polymineral fine-grain samples of the loess/ palaeosol sequence in Stratzing, Lower Austria. After a preheat at 320°C (60 s) and an IR bleach at 50°C (200 s) IRSL was measured at 290°C for 200 s; the same set of conditions were used to measure the response to a test dose. Recycling ratios, recuperation and dose recovery tests show that this protocol is suitable for the loess under investigation, although finite residual doses of up to 20 Gy are observed. For the oldest samples, the natural signal is in, or close to, saturation, indicating that fading is negligible in nature. This observation is inconsistent with the measured laboratory fading rates of 1-1.5%/decade and needs further investigation.

Keywords: luminescence dating; post-IR IRSL; loess stratigraphy; Austria

III.2.1 Introduction

The loess stratigraphy of Austria has been studied for several decades (e.g. Götzinger, 1936; Fink, 1956, 1960, 1961, 1976, 1978; Pécsi and Richter, 1996; Terhorst, 2007). While detailed descriptions and sedimentological data exist for many loess/palaeosol sequences in Austria (Fink, 1976; Kohl, 1976; Neugebauer-Maresch, 1996; Haesaerts et al., 1996; Niederhuber, 1997; Terhorst, 2007) the correlation of these deposits with regional and global climatic events remains unclear due to a lack of reliable geochronological information. This is especially true for Middle Pleistocene (126-781 ka; Head et al., 2008) loess sequences because there is as yet no widely accepted instrumental dating method applicable to this age range.

Oches and McCoy (1995) attempted to correlate some Austrian loess deposits by means of amino acid racemisation, whereas Wallner et al. (1990) applied thermoluminescence (TL) to the type locality of Stillfried (Lower Austria). Noll et al. (1994) applied TL dating to loess deposits at Paudorf, one of the key sections in respect of stratigraphy and palaeopedology. The most detailed chronological work so far on Lower Austrian loess deposits has been conducted by Zöller et al. (1994) who revised the chronostratigraphy by means of TL dating.

In general, luminescence dating is the method of choice to date loess deposits because of the wide age range covered by this technique, from a few years to, theoretically, several hundred thousand years (Aitken, 1998). Luminescence dating techniques (TL and optically stimulated luminescence (OSL)), determine the time since the last exposure of mineral grains to sunlight, i.e. the deposition age (Aitken, 1998). As a result of exposure to natural ionising radiation electrons accumulate in meta-stable traps in the mineral crystal. In the laboratory, the grains are stimulated with light which frees the trapped charge and allows it to recombine. This recombination gives rise to a measurable luminescence signal. The amount of luminescence is related to the total radiation dose (palaeodose or equivalent dose, D_e) absorbed by a sample since its last exposure to daylight. It is important that any residual trapped charge population is reduced to a negligible value at the time of deposition. For loess, it can be confidently expected that any prior luminescence signal will have been removed by exposure to daylight during the long sub-aerial transport. Loess is also made up almost entirely of quartz and feldspar, both of which are suitable dosimeters for luminescence dating. For these reasons, loess was the first terrestrial deposit to which luminescence dating was systematically applied (Roberts, 2008).

The age range available using optically stimulated luminescence (OSL) of quartz from loess is usually limited by saturation of the dose response at ~200 Gy; this is equivalent to ~50-70 ka assuming a dose rate of between 3 and 4 Gy/ka (typical for loess, e.g. Frechen et al., 1997; Novothny et al., 2002; Buylaert et al., 2008; Roberts, 2008). In contrast, the age range available using feldspar infrared stimulated luminescence (IRSL) signals is hampered by anomalous fading (Wintle, 1973), despite a much higher saturation dose (~2000 Gy).

Anomalous fading is a result of quantum mechanical tunnelling (Visocekas, 1985), which causes a decrease of the IRSL signal with time faster than expected from thermal stability measurements. Hence, IRSL ages tend to underestimate. Corrections for this signal loss and the corresponding age underestimation have been proposed (Lamothe and Auclair, 1999; Huntley and Lamothe, 2001). However, these corrections are only applicable to the linear part of the growth curve, i.e. to young samples. Lamothe et al. (2003) and Kars et al. (2008) have proposed approaches which allowfor correction beyond the linear part of the growth curve and thus can be used for older material (>70 ka) (Auclair et al., 2007; Buylaert et al., 2007), but there has been little or no systematic testing of these procedures. Fading corrections have been applied to younger samples in various studies and these can give apparently accurate ages (Huntley and Lamothe, 2001; Novothny et al., 2010); nevertheless, such corrections can be large, and involve significant assumptions, including that the rate of fading observed on a laboratory timescale is relevant to geological time (e.g. Huntley and Lamothe, 2001; Lamothe et al., 2003). In some cases, even after fading correction, feldspar IRSL can underestimate when compared with independent age control (Wallinga et al., 2007). It would clearly be preferable to make use of a signal that shows less or no fading.

Thomsen et al. (2008) investigated laboratory fading rates of various feldspar luminescence signals and found among other observations that a post-IR IRSL signal (IR bleach at 50°C and subsequent IRSL measurement at 225°C, with detection in the blue part of the spectrum) faded more slowly than conventional IRSL measured at low stimulation temperature (usually 50°C, blue detection). During IR stimulation at 50°C electrons in unstable traps recombine with holes in nearby recombination centres. When stimulating with post-IR IRSL, any unstable traps are already empty, and recombination can only take place at distant recombination centres. Thus the post-IR IRSL signal is expected to be much more stable, i.e. it should fade less. The applicability of this post-IR IRSL signal to dating coarse-grain potassium feldspar has been tested by Buylaert et al. (2009); the observed fading rate was reduced by a factor of two, and the corrected ages agreed well with the expected values.

This study extends the investigation of an elevated temperature post-IR IRSL signal by making use of the observation of Murray et al. (2009) that the IR dosimetry trap lies above 320°C, and so preheat temperatures up to this temperature can be used; a temperature of 290°C for post-IR IR stimulation was chosen. Because of the systematic decrease of fading rates using higher stimulation temperatures observed by Thomsen et al. (2008), the expectation is that the fading rate will have decreased even more than that of the post-IR IRSL at 225°C. The laboratory behaviour of a protocol based on this signal is tested and used to date the Stratzing loess site in Lower Austria using polymineral fine grains (4-11 μm). The age estimates for this site are interpreted in conjunction with detailed stratigraphic investigations and contribute to a better understanding of Late to Middle Pleistocene loess stratigraphy in Austria.

III.2.2 Stratigraphy and sedimentology of the Stratzing loess/palaeosol sequence

The Stratzing loess/palaeosol sequence is situated at the eastern margin of the west-east elongated hill of the 'Galgenberg', which represents a characteristic landform in the loess of the Kremser Feld (Fig. III.8). The Galgenberg is 374 m asl., and the surface of the exposure is ~340 m a.s.l. In general, aeolian sedimentation took place in the lee of Tertiary or Quaternary terrace bodies during westerly winds. The sequence is on a slope with a slight northern inclination up to 16%, i.e. up to 25 cm over a distance of 1.5 m.

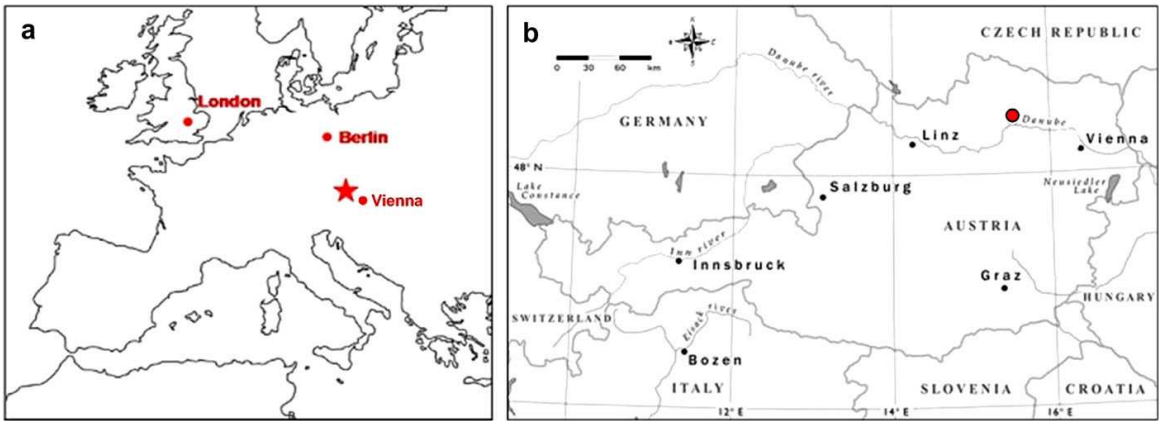

Fig. III.8: Map showing (a) the study area, Kremser Feld (red star) in Austria, and (b) the sampling location, Stratzing (red circle) (map redrawn from Damm and Terhorst, in press).

The loess/palaeosol sequence of Stratzing has been excavated to a depth of 7.5 m and is subdivided in 19 prominent horizons (Fig. III.9). The three uppermost horizons (ST 1 - ST 3) are disturbed by viticulture activities. Soil horizons were described in the field according to standard procedures of the German Field Book for Soil Survey (AD-HOC-AG Boden, 2005; see Table III.6). The results of the field survey were adapted to the World Reference Base for Soil Resources (IUSS Working Group WRB, 2006).

The whole sequence contains high carbonate concentrations with carbonate reactions varying between strongly and extremely calcareous; exceptions can be derived from Table III.6. The precipitation of secondary carbonates is common for all horizons. In general, the boundaries between the horizons are clear and not gradual (Table III.6). The colours described represent the matrix colours.

The undisturbed part of the sequence starts at a depth of 1.45 m with a Cryosol complex, formed by two different Cg horizons. The upper horizon (ST 4a) is a light yellowish brown silty loam. The matrix of the underlying Cg horizon (ST 4b) has a pale yellow colour and a weakly developed medium-sized platy structure. It contains very few angular rock fragments and shows moderate stagnic properties similar to the overlying horizon.

Layer ST 5 is pale yellow loess. Below the upper boundary flat and rounded gravels with an average length of 3 cm have accumulated as a stone line. Smaller angular rock fragments are

present throughout the horizon. The following horizons (ST 6 - ST 9) correspond to another Cryosol complex. Rock fragments have only a minor abundance or are completely absent. Layer ST 10 represents a horizon with archaeological finds (archaeological layer I) covering the loess layers ST 11, ST 12a and b. Horizon ST 13 corresponds to the second archaeological layer (II). The layer is recorded as a humic A horizon, a pale yellow silt loam. It is underlain by the loess layer ST 14, which includes small gravels.

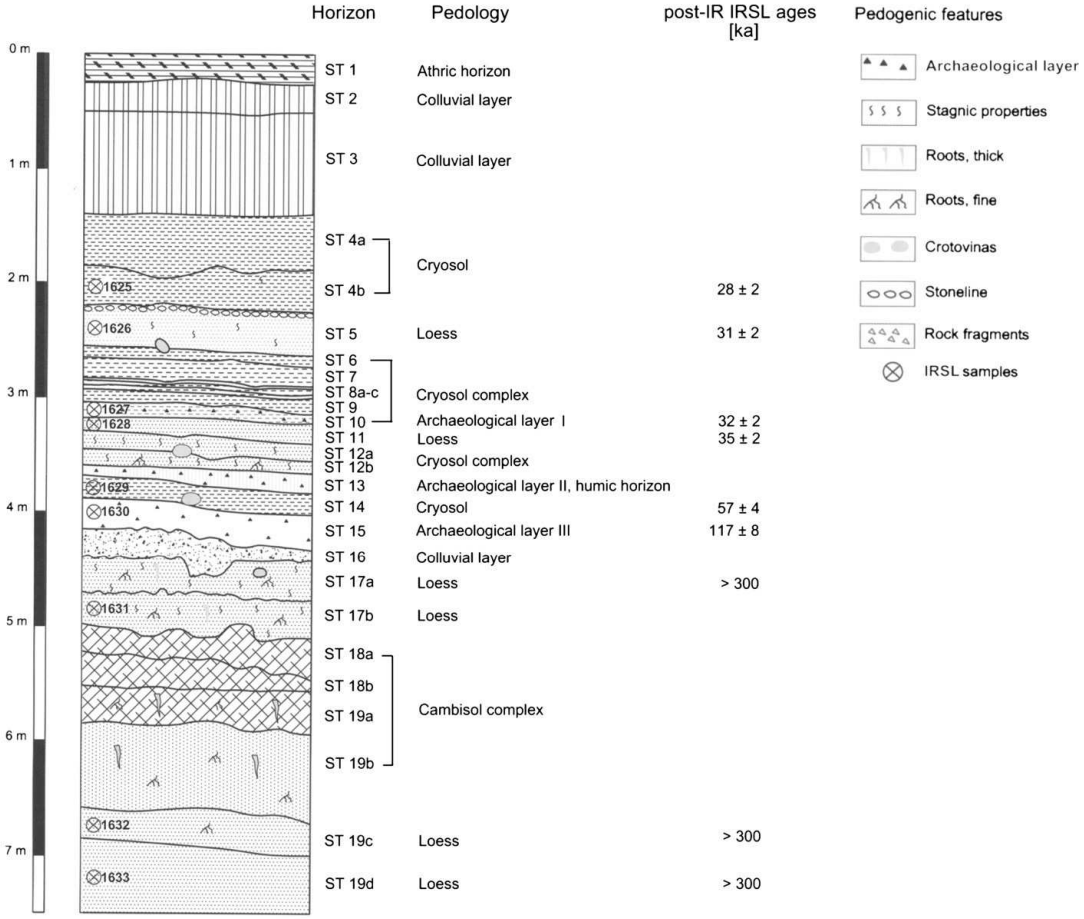

Fig. III.9: Log of the investigated loess/palaeosol sequence in Stratzing. The ages presented are based on post-IR IRSL at 290°C without subtraction of the residual. Further details on why this signal was chosen for age estimates see section III.2.4.3.

Below ST 14, the third archaeological layer (III) shows weak traces of initial pedogenesis and is classified as BC horizon (ST 15). The matrix of the underlying BC horizon (ST 16) is similar to that described above, although it is rich in rounded and angular small gravels, with diameters ranging from 0.5 to 4 cm. The loess of ST 17a and ST 17b is darker than in the overlying loess horizons; it shows light yellowish brown to yellowish brown colours. Former root channels can be traced throughout the horizon. Layers ST 18a to ST 19c form a well developed Cambisol complex. ST 18a and ST 18b correspond to two Bw horizons of yellowish brown colour. ST 18a is the only horizon where a weak clay illuviation in form of thin brownish clay cutans can be observed.

Table III.6: Pedologic description and Munsell colours of the Stratzing profile (ST 2 - 19d). The grey rows indicate archaeological layers.

No.	Horizon	Depth (cm)	Colour (dry)	Colour (wet)	Texture[1]	Structure[2]	Rock fragments[3]	Stagnic properties[4]	Carbonate[5]	Lower Boundary[6]	Other features
ST 2	Cu	30-50	10YR 6/4	10YR 6/6	Sil	1 m cr	1	-	3	c l	-
ST 3	Cu	50-145	10YR 6/4	10YR 6/4	Sil	1 m cr	2	-	3	c l	-
ST4a	Cg	145-188	10YR 6/4	2,5Y 6/4	Sil	1 f cr/gr	1	2	3	c w	-
St 4b	Cg	188-220	2.5Y 7/3	2,5Y 6/4	Sil	1 m p	v1	2	3	c w	Mn
ST 5	C	220-255	2,5Y 7/4		Sil	1 m p	S	1	3	c w	-
ST 6	Cg	255-265	2.5Y 7/3		Sil	3 m p	v1	3	3	c w	Mn, crot
ST 7	Cg	265-283	2.5Y 7/3		Sil	3 f p	v1	3	3	c w	Mn, crot
ST 8a	A	283-285	2,5Y 6/2		Sil	3 f p	-	2	3	c w	-
ST 8b	Cg	285 –289	2,5Y 6/3		Sil	1 m p	-	3	3	c w	Mn
ST 8c	Cg	289-293	2,5Y 6/4		Sil	3 f p	-	1	3	c w	-
ST 9	Cg	293-304	2.5Y 7/3		Sil	3 f p	-	1	3	c l	Mn, mol
ST 10	Cg	304-312	2.5Y 7/3		Sil	3 m p	-	3	3	c w	mol
ST 11	C	312-329	2,5Y 7/4		Sil	1 m p	-	-	3	c w	ch, mol
ST 12a	C	329-345	2,5Y 7/4		Sil	1 m p	-	1	3	c w	Mn, ch, crot
ST 12b	C(h)	345-354	2,5Y 7/4		Sil	1 gr	-	1	3	c l	Mn, ch, mol, humic
ST 13	A	354-368	2,5Y 7/4		Sil	2 gr	2	-	3	c w	ch
ST 14	Cg	368-388	2,5Y 7/4		Sil	1 m p	2	-	3	c l	ch, crot
ST 15	BC	388-415	10YR 6/4		Sil[1]	cr	-	1	3	c w	Mn
ST 16	BC	415-440	10YR 6/4		Sil[1]	cr	3	-	3	c w	
ST 17a	C	440-470	10YR 6/4		Sil[1]	1 f sbk	-	1	3	c w	Mn, roots, crot
ST 17b	C	470-498	10YR 5/6		Sil[1]	2 m p	-	-	1	c w	Mn, roots, mol
ST 18a	Bw	498-522	10YR 5/6		Sil[1]	2 c sbk/ 2 f gr	v1	-	1	g w	Mn, clay cutans, mol
ST 18b	Bw	522-552	10YR 5/6		Sil[1]	2 c sbk/ 2 f gr	-	-	2	c l	Mn, mol
ST 19a	BC	552-585	10YR 5/6		Sil[1]	2 c sbk/ 2 f gr	-	-	3	c w	roots
ST 19b	BCk	585-658	10YR 5/4		Sil[1]	1 m cr	-	-	3	c w	roots
ST 19c	Ck	658-685	2,5Y 6/6		Sil[1]	1 m cr	-	-	3	c l	roots
ST 19d	Ck	685-750	2,5Y 6/6		Sil[1]	1 c sbk/ 1 f gr	v1	1	3	-	Mn, roots

[1] Sil = silt loam (clay-poor), Sil[1] = silt loam (clay-rich)
[2] Grade: 1 = weak, 2 = moderate, 3 = strong; size: f = fine, m = medium, c = coarse; shape: gr = granular, abk = angular blocky, sbk = subangular blocky, cr = crumbly
[3] Abundance: v1 = very few, 1 = few, 2 = common, 3 = many; distribution: c= continuous, p = patchy, S = Stone line
[4] Grade: 1 = weak, 2 = moderate, 3 = strong
[5] Carbonate reaction: 0 = non-calcareous, 1 = slightly calcareous, 2 = moderately calcareous, 3 = strongly/extremely calcareous
[6] c = clear, g = gradual; w = wavy, l = linear
Mn = Manganese, mol = mollusc shells, ch = charcoals, crot = crotovinas, roots = pseudomorphic roots
Depth measures left hand side (Fig. III.9).

III.2.3 Sample preparation and analytical facilities

III.2.3.1 Sampling and preparation for equivalent dose measurements

Two metal tubes per sample were hammered into the freshly cleaned profile and immediately closed and sealed from light. The sample depths and numbers are shown in Table III.7 and Fig. III.9.

In the laboratory, all samples for equivalent dose (D_e) determination were treated under subdued red/orange light. After opening the tubes, the outer ends (~1 cm) of the samples which might have been exposed to sunlight during sampling were removed prior to subsequent chemical treatment with hydrochloric acid, sodium oxalate, and hydrogen peroxide. Between every treatment step the samples were washed with distilled water. The fine silt fraction (4-11 mm) of the loess was extracted by repeated settling and washing (Frechen et al., 1996).

The polymineral fine grains were mounted on aluminium discs from a suspension in acetone (2 mg/ml). Luminescence measurements were made with an automated Risø TL/OSL reader (DA-20; Thomsen et al., 2006) using a calibrated $^{90}Sr/^{90}Y$ beta source (~0.21 Gy/s). The feldspar signal of the polymineral samples was stimulated with infrared light diodes emitting at 870 nm, and the luminescence was detected in the blue-violet region through a Schott BG39/Corning 7-59 filter combination.

III.2.3.2 Dosimetry

Samples for dosimetry measurements were taken from immediately around the luminescence samples. After drying at ≤50°C, the samples were homogenised and 50 g of each sample was packed in N-type beakers, sealed and stored for at least one month (to ensure equilibrium between radon and its daughter nuclides) before counting. The concentrations of U, Th and K were determined by high resolution gamma-ray spectrometry, and the dose rates derived using the conversion factors of Adamiec and Aitken (1998). Calculation of the cosmic dose rate is based on Prescott and Hutton (1994). For all samples a water content of 15 ± 5% (Frechen et al.,1997) and a mean a-value of 0.08 ± 0.02 was assumed (Rees-Jones, 1995).

Table III.7: Dosimetry data for the samples.

Sample	Depth [m]	K [%]	U [ppm]	Th [ppm]	Dose rate [Gy/ka]
1625	1.85	1.4 ± 0.1	3.4 ± 0.2	10.9 ± 0.9	3.3 ± 0.2
1626	2.35	1.5 ± 0.1	3.3 ± 0.1	11.7 ± 0.8	3.4 ± 0.2
1627	3.05	1.6 ± 0.1	3.5 ± 0.2	11.5 ± 0.8	3.5 ± 0.2
1628	3.20	1.6 ± 0.1	3.6 ± 0.2	11.6 ± 0.8	3.5 ± 0.2
1629	3.80	1.4 ± 0.1	3.2 ± 0.1	10.4 ± 0.8	3.2 ± 0.2
1630	4.05	1.4 ± 0.1	3.1 ± 0.1	11.2 ± 0.9	3.3 ± 0.2
1631	4.85	1.9 ± 0.1	3.1 ± 0.1	14.3 ± 1.0	4.0 ± 0.3
1632	6.65	1.8 ± 0.1	3.1 ± 0.1	12.6 ± 0.9	3.8 ± 0.2
1633	7.10	1.7 ± 0.1	3.1 ± 0.2	12.9 ± 0.9	3.6 ± 0.3

A summary of the dose rates is given in Table III.7. They range from 3.2 ± 0.2 Gy/ka (sample 1629) to 4.0 ± 0.3 Gy/ka (sample 1631) and are typical of the dose rates found in European loess (Zöller et al., 1994; Frechen et al., 1997; Preusser and Fiebig, 2009; Novothny et al., 2009).

III.2.4 Luminescence measurements

III.2.4.1 Elevated temperature post-IR IRSL protocol

Conventionally, a stimulation temperature of 50°C is used during IRSL measurements when the single aliquot regenerative procedure (SAR; Murray and Wintle, 2000) is applied to potassium feldspar and polymineral fine grains extracts (e.g. Wallinga et al., 2000) and preheat temperatures between 180°C and 260°C are usually used (e.g. Buylaert et al., 2007; Roberts, 2008; Novothny et al., 2010). When measuring IRSL, it seems advisable to keep the stimulation temperature sufficiently below the preheat temperature to avoid a TL contribution contaminating the optically stimulated signal. To enable comparison with published data, Buylaert et al. (2009) used a preheat of 250°C for 60 s, and hence their post-IR IR stimulation temperature was chosen to be 225°C. Recently, Murray et al. (2009) showed for coarse-grain potassium feldspar that there is no systematic increase in equivalent dose for a preheat temperature range from 80°C up to 320°C (60 s duration), suggesting either that the range of traps contributing to IRSL in this temperature region are all geologically stable, or, more likely, that the dosimetry trap is not significantly eroded by preheating up to 320°C. If one adopts the more stringent preheat of 320°C for 60 s, this allows post-IR IR stimulation at significantly higher temperatures. Here, the use of stimulation at 290°C is investigated. The expectation is that the fading rate should be even smaller than for the stimulation temperature tested by Buylaert et al. (2009), because the higher stimulation temperature should allow charge in more distant trap/recombination centres to recombine. In this protocol, after a preheat of 320°C for 60 s the polymineral fine grains were bleached with IR diodes at 50°C for 200 s to recombine the near-neighbour trap/centre pairs and then the aliquot was held at 290°C while measuring the IRSL for 200 s. The latter signal is referred to in what follows as ‘post-IR IRSL’. The response to a test dose was measured in the same manner, and an IR illumination at 325°C for 100 s was inserted at the end of each SAR measurement cycle to reduce the effect of recuperation (based on Murray and Wintle, 2003). The measurement protocol is shown in Table III.8. The initial 2.4 s of the decay curve was integrated and used for D_e determination after subtracting a background from the last 100 s.

To compare the fading rates of the IRSL signal at 50°C and the post-IR IRSL signal at 290°C, the laboratory fading rate, i.e. the IRSL signal decrease over time measured using artificially irradiated aliquots, was measured. This is expressed in terms of the percentage decrease of signal intensity per decade of time (the *g*-value; Aitken, 1985). After D_e

measurement and a final IR illumination at 325°C for 100 s, the same aliquots (6-9 per sample, see Table III.9) were given a dose of ~200 Gy and measured using this SAR protocol; varying storage times (ranging from as short as experimentally possible ('prompt') to delays of ~15 h) were inserted immediately after irradiation and preheat, and before storage (Auclair et al., 2003).

Table III.8: Flowchart of the post-IR IRSL SAR protocol. For IRSL at 50°C steps 3 and 7, and for post-IR IRSL at 290°C steps 4 and 8 were used for equivalent dose determination.

Step	Treatment	Observed
1	Give dose, D_i	
2	Preheat, 320°C, 60 s	
3	IR stimulation, 200 s at 50°C	L_x
4	IR stimulation, 200 s at 290°C	$\mathbf{L_x}$
5	Give test dose, D_T	
6	Preheat, 320°C, 60 s	
7	IR stimulation, 200 s at 50°C	T_x
8	IR stimulation, 200 s at 290°C	$\mathbf{T_x}$
9	IR stimulation, 40 s at 325°C	
10	Return to 1	

III.2.4.2 Luminescence characteristics

The signal intensity of the post-IR IRSL signal at 290°C is much greater than that of the IRSL signal at 50°C (inset Fig. III.10) for all samples presented in this study. Thomsen et al. (2008) observed similar behaviour for the post-IR IRSL signal at 225°C. The dose response curves are indistinguishable for both the IRSL signal at 50°C and the post-IR IRSL signal at 290°C (Fig. III.10). This has also been observed by Buylaert et al. (2009) comparing the IRSL signal at 50°C with the post-IR IRSL signal at 225°C for coarse grained potassium feldspar. Recycling ratios for all samples and both signals vary between 0.97 ± 0.01 (n = 9) and 1.00 ± 0.01 (n = 9). Recuperation for the post-IR IRSL at 290°C is below 5% for all samples, with the lowermost and thus oldest sample (1633) yielding the smallest values of 0.82 ± 0.02% (n = 6). Samples 1625 to 1629 show recuperation of about 4%, whereas for sample 1630 it is only 1.31 ± 0.03% (n =9). The IRSL measurements at 50°C show slightly greater recuperation of 6-8% for samples 1625-1629, and 2.47 ± 0.06% (n = 9) for sample 1630. For the oldest samples (1631-1633) recuperation is reduced below 2%.

Table III.9: Equivalent doses, *g*-values, and ages for both the IRSL at 50°C and post-IR IRSL at 290°C. The uncorrected post-IR IRSL ages without subtraction of the residuals are considered the most reliable age estimates. For details see text.

Sample	Unit	no. of aliquots	D_e [Gy]		*g*-value [%/decade]		uncorrected age [ka]			corrected age [ka]		
			IRSL at 50°C	post-IR IRSL at 290°C	IRSL at 50°C	post-IR IRSL at 290°C	IRSL at 50°C	post-IR IRSL at 290°C	post-IR IRSL at 290°C - residual* subtracted	IRSL at 50°C	post-IR IRSL at 290°C	post-IR IRSL at 290°C - residual* subtracted
1625	ST 4b	9	60 ± 4	93 ± 6	2.8 ± 0.4	1.4 ± 0.1	18.1 ± 1.2	28 ± 2	22 ± 2	23 ± 2	32 ± 3	25 ± 3
1626	ST 5	9	71 ± 7	105 ± 7	2.1 ± 0.4	1.0 ± 0.3	21.1 ± 1.4	31 ± 2	25 ± 2	25 ± 3	34 ± 3	27 ± 3
1627	ST 10	9	74 ± 6	114 ± 6	2.1 ± 0.3	1.2 ± 0.1	21.1 ± 1.3	32 ± 2	27 ± 2	25 ± 3	36 ± 3	30 ± 3
1628	ST 11	9	81 ± 7	123 ± 9	3.6 ± 1.3	1.1 ± 0.3	23 ± 2	35 ± 2	29 ± 3	32 ± 6	39 ± 4	35 ± 4
1629	ST 14	9	108 ± 9	180 ± 11	1.4 ± 0.3	0.8 ± 0.2	34 ± 3	57 ± 4	50 ± 4	38 ± 4	60 ± 5	53 ± 5
1630	ST 15	9	185 ± 12	375 ± 23	2.1 ± 0.7	1.5 ± 0.1	58 ± 4	117 ± 8	111 ± 8	67 ± 8	129 ± 11	122 ± 11
1631	ST 17b	6	920 ± 65	>1450**	2.1 ± 0.2	1.3 ± 0.1	230 ± 19	>300**	>300**	277 ± 29	>300**	>300**
1632	ST 19c	6	758 ± 79	>1250**	2.1 ± 0.8	1.1 ± 0.8	199 ± 13	>300**	>300**	240 ± 34	>300**	>300**
1633	ST 19d	6	705 ± 58	>1250**	2.3 ± 0.1	1.2 ± 0.1	198 ± 18	>300**	>300**	241 ± 28	>300**	>300**

* Residual signal equivalent to 20 Gy subtracted.

** Samples are in saturation. Equivalent doses and ages given are minimum values according to $2*D_0$ (Wintle and Murray, 2006).

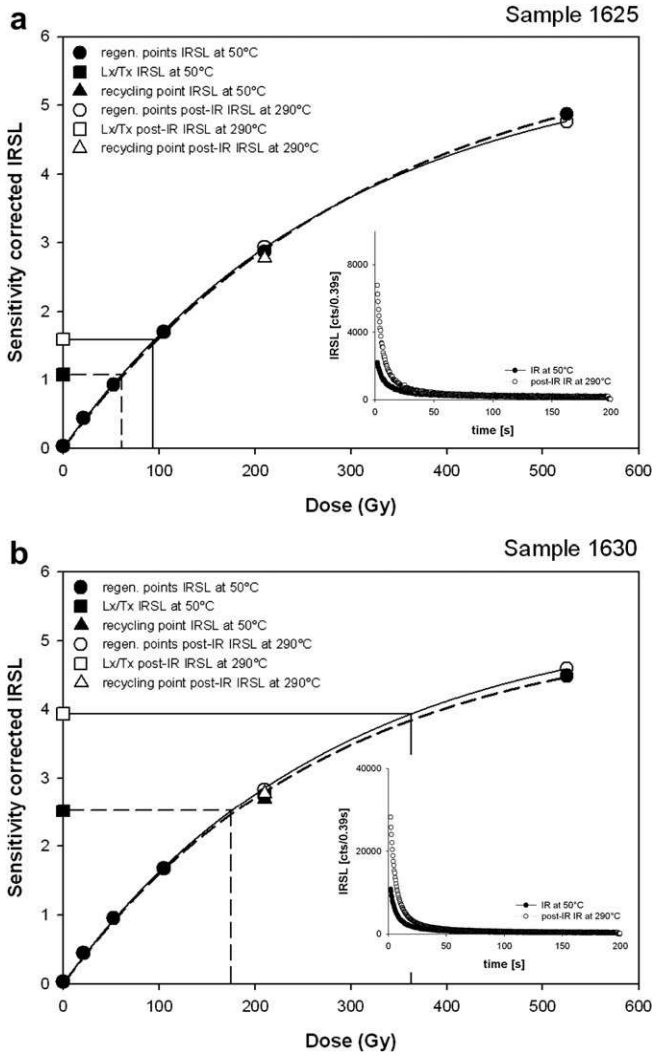

Fig. III.10: Dose response curves for both the IRSL signal at 50°C and the post-IR IRSL signal at 290°C for samples (a) 1625 (young sample; one representative aliquot) and (b) 1630 (moderately old sample; one representative aliquot). The natural sensitivity corrected IRSL for the post-IR IRSL signal at 290°C is in both cases larger than for the IRSL signal at 50°C. The insets show the decay curves of the natural for both signals.

Satisfactory recycling ratios demonstrate the ability of this measurement protocol to reproducibly measure the response to a laboratory dose given after the sample has been heated. However such behaviour does not necessarily suggest that doses given in nature (before any heating) can also be measured accurately. The applicability of the elevated temperature post-IR IRSL SAR protocol to dose measurement using these samples was tested by means of a dose recovery test (Wallinga et al., 2000). Three natural aliquots of samples 1625 and 1630 were bleached for 4 h in a Hönle SOL2 simulator at ~1.2 m from the light source to minimise any heating. The aliquots were then given a beta dose similar to the

measured D_e for that sample and the given dose measured in the usual manner. If the protocol is suitable, the measured to given dose ratio should be close to 1.0. After subtraction of the signal left after bleaching (typically 15-20 Gy, measured on separate aliquots) measured to given dose ratios of 0.97 ± 0.02 (n = 3; sample 1625) and 1.03 ± 0.03 (n = 3; sample 1630) were obtained. These ratios are indistinguishable from unity, and clearly demonstrate the applicability of the measurement protocol. Choi et al. (2009) showed for quartz that the results of dose recovery tests can depend on bleaching conditions. Therefore the same experiment was repeated on additional aliquots but using daylight bleaching (for a total of 24 h through a glass window) rather than a solar simulator. The measured residuals were indistinguishable from those after SOL2 bleaching. Measured to given dose ratios for post-IR IRSL were 0.97 ± 0.03 (n = 3; sample 1625) and 1.05 ± 0.02 (n = 3; sample 1630), confirming the suitability of the measurement protocol. The measured to given dose ratios for IRSL at 50°C without subtraction of the residual (~3 Gy) gave values of between 0.95 ± 0.0.2 (n = 3; sample 1625) and 0.98 ± 0.01 (n = 3; sample 1630), and are equally satisfactory. The IRSL at 50°C signal is known to be bleachable in nature (Buylaert et al. in prep); despite this the observed 3 Gy residual after laboratory bleaching is surprisingly large. It is difficult to decide on the relevance of these residual measurements to naturally bleached samples. In nature bleaching is likely to be episodic and to take place over much longer times than in the laboratory. One can test the size of any residual by measuring a luminescence age on material of independently known age, or by examining the dose in recently transported modern material (modern analogues). In this case comparison with age control is complicated by the uncertainty over fading correction (see below), and there is no modern analogue available at the site. At this stage, no conclusions can be drawn as to the relevance of the laboratory residual measurements to natural dose measurements.

III.2.4.3 Equivalent doses and fading

The elevated temperature post-IR IRSL protocol allows for a comparison of the equivalent doses (D_e) derived for the IRSL signal at 50°C and those from the post-IR IRSL signal, because measurements are made on the same aliquots (Table III.8).

All data are given with total uncertainties (systematic and random added in quadrature) at a 1 sigma confidence level. There is an increase of D_e values with depth for both signals, with the post-IR IRSL signal at 290°C resulting inmuch bigger doses than the IRSL signal at 50°C for all samples up to sample 1631. A summary of the D_e values is shown in Table III.9. On average, the ratio of the D_e values for the IRSL signal and the post-IR IRSL signal is about 1:1.5, except for sample 1630, where the D_e value for the post-IRIRSL signal is more than twice the IRSL signal. Post-IR IRSL residual doses may be larger than those from IR at 50°C (see above). Buylaert et al. (2009) have found that post-IR IRSL signals may bleach more slowly; this difference may suggest that sample 1630 was not as well bleached as the others.

The D_e values for the three lowermost samples (1631-1633) are poorly known because the natural signals are in or approaching saturation, indicating a very low fading rate in nature. However, because of anomalous fading, the natural IRSL signals at 50°C are all well below saturation, and interpolation onto the dose response curves to derive the D_e's are possible for all samples. For both signals, the equivalent doses of the lowermost samples are much larger (>700 Gy) than those of the six samples above.

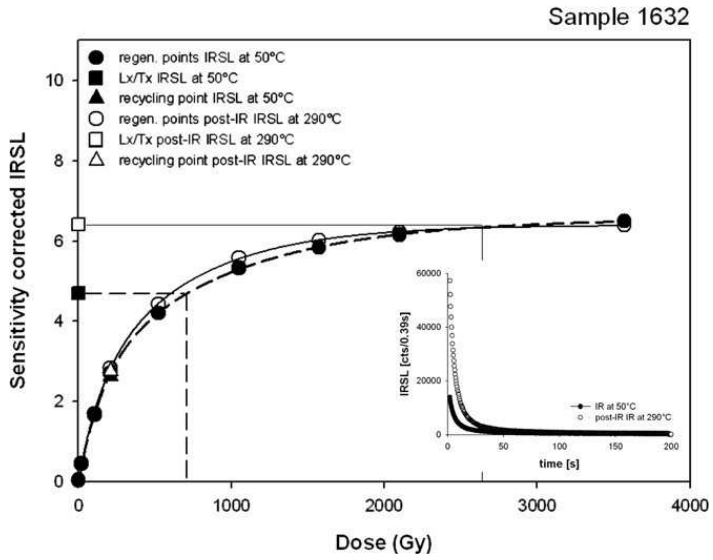

Fig. III.11: Dose response curves and natural decay curves (inset) for both the IRSL signal at 50°C and the post-IR IRSL signal at 290°C for sample 1632; in both cases the curves of one representative aliquot are shown. The natural signal for the post-IR IRSL signalat 290°C is in saturation.

A natural feldspar signal in saturation, as found for the natural post-IR IRSL signals of samples 1631-1633 (Fig. III.11), has not been reported before, and to support this exciting observation, the natural signal and dose response curve of an additional polymineral fine-grains extract from loess (sample 1664) below the Brunhes/Matuyama (B/M) boundary (~780 ka, expected natural dose >2700 Gy) was also measured. The sample was taken in the loess wall of the Krems shooting range ('Schießstätte'), because it is the only site near (~7 km) Stratzing where the magnetic characteristics of the B/M boundary have been measured (Fink and Kukla, 1977). The sample was to be expected in field saturation (i.e. the rate of storage of charge should equal the rate of charge loss through fading). Again, the natural of the post-IR IRSL signal at 290°C lies in the saturating part of the dose response curve (Fig. III.12; D_e > 1600 Gy) whereas the natural of the conventional IRSL signal at 50°C is approximately 70% of saturation (D_e ~650 Gy). These data suggest that, in nature, the post-IR IRSL signal at 290°C does not fade detectably on a time scale of >750 ka.

The greatest difference in IRSL and post-IR IRSL fading rates was measured for sample 1628, with *g*-values of 3.6 ± 1.3%/decade for the IRSL signal at 50°C and 1.1 ± 0.3%/decade for the post-IR IRSL signal; i.e. laboratory fading was reduced by a factor of three. However, the observation that the natural signal for the sample from below the B/M boundary (Fig. III.12) is in saturation suggests that the small fading rate of post-IR IRSL may be a laboratory artefact. To investigate the observed fading rates in more detail, the fading rate of fine-grained quartz extracted from Chinese loess from the Duanjiapo site was measured (see Sun et al., 2000; the quartz from Stratzing was too insensitive for this measurement, and Chinese loess is known to result in reliable ages; e.g. Lu et al., 2007). Quartz, unless originating from volcanic sources (Tsukamoto et al., 2007) is not thought to suffer from anomalous fading (Aitken, 1998). The measured fading rate was 1.3 ± 0.3%/decade (n = 3) which underlines the suggestion that low fading rates may be a laboratory artefact. It is in any case evident that the post-IR IRSL signal at 290°C does not seem to fade more than quartz.

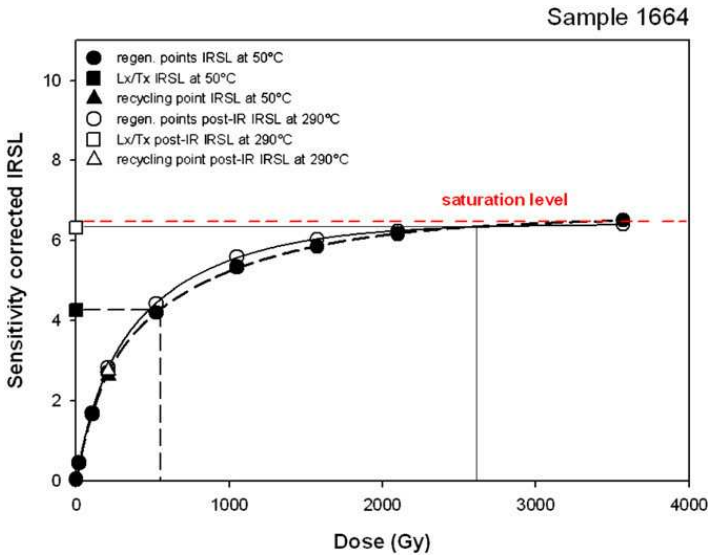

Fig. III.12: Dose response curves of one representative aliquot for both the IRSL signal at 50°C and the post-IR IRSL signal at 290°C for a sample below Brunhes/Matuyama boundary (1664; Krems shooting range, Fink and Kukla, 1977), which is expected to bein field saturation. The saturation level is indicated by the red dotted line.

III.2.5 Results and discussion of the age estimates

Uncorrected and fading-corrected ages for both the IRSL at 50°C and post-IR IRSL measurements are shown in Table III.9. The observation of a natural signal in saturation (Fig. III.12) implies that the most reliable age estimates result from the post-IR IRSL signal without any fading correction. From the bleaching experiments it appears that there is,

nevertheless, the possibility of residual doses of up to 20 Gy at the time of deposition. However, there is so far no firm evidence that the observed laboratory residuals apply in nature. Of course in older samples (i.e. >200 Gy, ~50-70 ka) such a residual would rapidly become unimportant, and the size of any fading correction would become more significant as the growth curve approaches saturation. Thus identifying whether post-IR IRSL ages should or should not be corrected for fading would become progressively more straightforward with older known age samples. Unfortunately such samples do not exist at this site. For these reasons, the uncorrected post-IR IRSL ages without subtraction of the residual were chosen as the preferred ages (see Fig. III.9). However, firm evidence to support this choice is not available.

The only possibility of examining the reliability of the dating results is given by radiocarbon ages (derived from charcoal; Neugebauer-Maresch, 1993, 1996) and TL ages derived by Zöller et al. (1994). It has to be noted that these age estimates partially originate from an adjacent loess/palaeosol sequence and that correlation of the sequences is based on the archaeological layers (Niederhuber, 1997). Whereas the outcrop in this study exhibits three archaeological horizons (ST 10, ST 13, and ST 15; Fig. III.9), the site presented in Zöller et al. (1994) shows only two find horizons, with the lower one being the main archaeological layer (Neugebauer-Maresch, 1993, 1996; Niederhuber, 1997). Thus some lateral variability is clearly present, and this must reduce the reliability of the age control. At the upper artefact horizon in this adjacent sequence (correlated to ST 10, i.e. sample 1627) Zöller et al. (1994) obtained an age of 26.2 ± 2.5 ka using polymineral finegrain TL dating. The same horizon gave a radiocarbon age of 31 ka (Neugebauer-Maresch, 1993). Unfortunately it is not evident whether the radiocarbon age was calibrated or not. If calibration needs to be applied it would result in an age of ~35 ka (estimated after Reimer et al., 2009). Neugebauer-Maresch (1996) presented two radiocarbon ages obtained from charcoal of 28, 210 ± 500 and 29,260 ± 460 BP for the upper find horizon; calibration results in ages ~32-34 ka. Zöller et al. (1994) concluded that their TL age was an underestimate and attributed this to reworking of this find horizon at the beginning of the Late Pleniglacial. An in situ hearth of the same horizon was polymineral TL dated to 30.2 ± 3.5 ka (Zöller et al., 1994); however, this age was discarded because of apparent disequilibrium in the ^{238}U decay chain. Taking all the radiocarbon dating results as the independent age control, the fading uncorrected post-IR IRSL age of 33 ± 2 ka for sample 1627 is consistent with the expected age (Table III.9). This gives some confidence that the uncorrected post-IR IRSL ages without residual subtraction are the most reliable age estimate of the IRSL ages presented here.

The uppermost samples were dated to 28 ± 2 ka (1625) and 31 ± 2 ka (1626), respectively. Together with sample 1627, which comes from an archaeological layer within a Cryosol (ST 10; Fig. III.9), the ages of the uppermost samples are in good agreement with age estimates obtained from other Cryosol complexes in Lower Austria (Haesaerts et al., 1996). Zöller et al. (1994) dated the loess above the archaeological horizons to 25.4 ± 2.5 ka using TL (their

sample STRATZ3); given the uncertainties in the degree of fading and in the size of the unbleachable residual of their signals, their TL age is considered to be in acceptable agreement with these results.

Sample 1629, from the loess layer (ST 14) above archaeological layer III (ST 15), gave a significantly older age (uncorrected post-IR IRSL 57 ± 4 ka) than the overlying samples. This sudden increase in age is surprising; however, this might originate from post-depositional mixing and corresponding summation of burial doses. The underlying archaeological layer III helps to provide some age control; the artefacts from this layer are attributed to the Upper Palaeolithic (40,000/35,000-10,000 years ago; Neugebauer-Maresch, 1993), which is supported by an uncalibrated radiocarbon age of >32.640 ± 330 BP (Neugebauer-Maresch, 1996). However, a non-finite radiocarbon age (i.e. >45 ka) for loess deposition cannot be excluded. At a nearby section, loess from this archaeological layer (ST 15 in the outcrop, with weak soil development) was dated by Zöller et al. (1994) to 46.4 ± 4.4 ka using fine-grain polymineral TL. The loess ages for both the IR and post-IR IRSL signals are much older, the latter resulting in an uncorrected age of 117 ± 8 ka (sample 1630). One possible explanation is that the parent material was deposited during Marine Isotope Stage (MIS) 5, shortly after the Eemian (MIS 5e). However, it is more likely that there has been post-depositional mixing. This is not only indicated by the distribution of the artefacts throughout the archaeological layer (Fig. III.9), but also by the greater discrepancy in D_e values of the two IRSL signals. For samples 1630 the ratio of the IRSL to post-IR IRSL is 1:2, whereas for all other samples it is only 1:1.5.

The lowermost three samples (1631-1633) gave much larger D_e values for all signals and thus much older ages. However, for such apparently old material (IRSL at 50°C >200 ka; post-IR IRSL at 290°C >300 ka), even the post-IR IRSL results must be interpreted as minimum ages, because of saturation of the dose response curve (see Fig. 4; others have interpreted such old ages as bounded estimates, Preusser and Fiebig, 2009). The argument is based on the suggestion of Wintle and Murray (2006) that it is not possible to obtain a reliable D_e value when the natural signal is more than 85% of the maximum achievable value (referred to as $2*D_0$). From the minimum ages of samples 1631 to 1633 it can be concluded that the well developed Cambisol complex (layers ST 18a to ST 19c) is ≥MIS 7, thus indicating a prolonged discontinuity in this loess/palaeosol sequence.

It is also interesting to investigate whether the IRSL signal at 50°C yields ages consistent with expectations after correction for fading. For the younger samples (1625-1628) the fading corrected IRSL ages are only in agreement with the post-IR IRSL ages when a residual of ~20 Gy is subtracted from the post-IR IRSL ages; the agreement is poor if a residual is not taken into account. It is also worth noting that for the four youngest samples there is good agreement of fading corrected IRSL ages and fading corrected post-IR IRSL ages with residual subtraction (Table III.9). Not surprisingly, for the older samples the IRSL ages clearly tend to underestimate. Previous studies (e.g. Wallinga et al., 2007) have observed that

the fading correction for the ages of the IRSL signal at 50°C is not sufficient, but the possibility that the post-IR IRSL ages are consistently overestimated to some degree cannot be ignored. However, the age control at ~32 ka indicates that this is unlikely to be a large effect.

III.2.6 Conclusions

Loess deposits in Austria lack a reliable chronostratigraphy because there are only a few geochronological studies, and there are no widely accepted dating methods applicable to sediments >45 ka. A post-IR IRSL dating approach at the Stratzing loess profile in Austria which should be applicable to such old material was tested. Detailed logging indicates 19 prominent layers, three of which are archaeological find horizons.

The applicability of the SAR protocol was tested by examining recycling ratios (all within 10%), recuperation (<5% for the post-IR IRSL), and measured to given dose ratios (all close to unity) in dose recovery experiments; these various indicators all suggest satisfactory performance.

For the first time in feldspar dating using luminescence, natural signals measured using post-IR IR at 290°C were observed to be in saturation on the laboratory growth curves of the oldest samples, including one which lay close to the B/M boundary at ~780 ka; this strongly suggests that there is no detectable fading of this signal in nature. However, laboratory measurements resulted in fading rates of 1-1.5%/decade for the post-IR IR signal from all samples. This discrepancy requires further investigation. Nevertheless, the fading uncorrected post-IR IRSL signal at 290°C yields the most reliable results. The applicability of this dating protocol to younger samples might be hampered by residual signals (residuals of 15-20 Gy were measured after laboratory bleaching). Unfortunately there is no modern or very young material available at this site, and so this conclusion could not be tested using natural residual signals. Such residuals would, of course, be of negligible significance for older samples. The fading uncorrected post-IR IRSL ages without residual subtraction were chosen as the best estimates for the loess/palaeosol sequence, although this choice requires further testing. Comparison with independent age control provided by radiocarbon ages (Neugebauer-Maresch, 1996) seems to confirm this choice.

The unexpectedly old age of 117 ± 8 ka (uncorrected) for layer ST 15 (sample 1630; archaeological layer III) needs further investigation. It is likely that there has been some post-depositional mixing, indicated by the distribution of artefacts throughout the archaeological layer. The age of the underlying Cambisol complex, of >300 ka (uncorrected age post-IR IRSL at 290°C) shows that the loess/palaeosol sequence at Stratzing is not a continuous record; the sequence includes at least one significant discontinuity. Unfortunately, more precise ages cannot be derived for the older part of the sequence because of saturation of the dose response curve for these samples.

The dating protocol tested here is a further step towards finding the most appropriate and reliable procedures to minimise fading and extend the age range using luminescence. The development of these methods is not only of special interest in areas such as Austria, where stratigraphical interpretations and correlations are made difficult by discontinuities in the loess/palaeosol sequences, but also of great importance for loess deposits all over the world as loess it one of the most important detailed terrestrial archives for environmental changes and landscape evolution.

Acknowledgements

This study was supported by the Leibniz Pakt Project for Research and Innovation 2008-2010. We thank Sonja Riemenschneider for support in the laboratory and Kristina Thomsen and Mayank Jain for fruitful discussions on post-IR IRSL dating. Sébastien Huot is thanked for the Excel macros which were used to calculate fading rates in a fast and elegant manner. We are grateful to two anonymous reviewers for their constructive comments.

References

Adamiec, G., Aitken, M. J., 1998. Dose-rate conversion factors: update. Ancient TL 16, 37-50.

AD-HOC-AG Boden, 2005. Bodenkundliche Kartieranleitung. In: Bundesanstalt für Geowissenschaften und Rohstoffe in Zusammenarbeit mit den Staatlichen Geologischen Diensten, fifth ed., Hannover, 438 pp.

Aitken, M. J., 1985. Thermoluminescence Dating. Academic Press, London, 359 pp.

Aitken, M. J., 1998. An Introduction to Optical Dating - The Dating of Quaternary Sediments by the Use of Photon-Stimulated Luminescence. Oxford University Press, Oxford, 267 pp.

Auclair, M., Lamothe, M., Huot, S., 2003. Measurement of anomalous fading for feldspar IRSL using SAR. Radiation Measurement 37, 487-492.

Auclair, M., Lamothe, M., Lagroix, F., Banerjee, S. K., 2007. Luminescence investigations of loess and tephra from Halfway House section, Central Alaska. Quaternary Geochronology 2, 34-38.

Buylaert, J.-P., Vandenberghe, D., Murray, A. S., Huot, S., De Corte, F., Van den haute, P., 2007. Luminescence dating of old (>70 ka) Chinese loess: a comparison of single aliquot OSL and IRSL techniques. Quaternary Geochronology 2, 9-14.

Buylaert, J.-P., Murray, A. S., Vandenberghe, D., Vriend, M., De Corte, F., Van den haute, P., 2008. Optical dating of Chinese loess using sand-sized quartz: Establishing a time frame for the Late Pleistocene climate changes in the western part of the Chinese Loess Plateau. Quaternary Geochronology 3, 99-113.

Buylaert, J.-P., Murray, A. S., Thomsen, K. J., Jain, M., 2009. Testing the potential of an elevated temperature IRSL signal from K-feldspar. Radiation Measurements 44, 560-565.

Choi, J. H., Murray, A. S., Cheong, C.-S., Hong, S. C., 2009. The dependence of dose recovery experiments on the bleaching of natural quartz OSL using different light sources. Radiation Measurements 44, 600-605.

Damm, B., Terhorst, B. A model of slope formation related to landslide activity in the Eastern Prealps, Austria. Geomorphology, in press, doi:10.1016/j.geomorph.2009.11.001.

Fink, J., 1956. Zur Korrelation der Terrassen und Lösse in Österreich. Eiszeitalter und Gegenwart 7, 49-77.

Fink, J., 1960. Leitlinien einer österreichischen Quartärstratigraphie. Mitteilungen der Geologischen Gesellschaft Wien 53, 249-266.

Fink, J., 1961. Die Gliederung des Jungpleistozäns in Österreich. Mitteilungen der Geologischen Gesellschaft Wien 54, 1-25.

Fink, J., 1976. Exkursion durch den österreichischen Teil des nördlichen Alpenvorlandes und den Donauraum zwischen Krems und Wiener Pforte. Erweiterter Führer zur Exkursion aus Anlass der 2. Tagung der IGCP-Projektgruppe “Quaternary Glaciations in the Northern Hemisphere. Mitteilungen der Kommission für Quartärforschung der Österreichischen Akademie der Wissenschaften 1, 113 pp.

Fink, J., 1978. Exkursion durch den österreichischen Teil des nördlichen Alpenvorlandes und den Donauraum zwischen Krems und Wiener Pforte. Ergänzung zu Band 1. Mitteilungen der Kommission für Quartärforschung der Österreichischen Akademie der Wissenschaften 2, 31 pp.

Fink, J., Kukla, J., 1977. Pleistocene climates in Central Europe: at least 17 interglacials after the Olduvai event. Quaternary Research 7, 363-371.

Frechen, M., Schweitzer, U., Zander, A., 1996. Improvements in sample preparation for the fine grain technique. Ancient TL 14, 15-17.

Frechen, M., Horváth, E., Gábris, G., 1997. Geochronology of Middle to upper Pleistocene loess sections in Hungary. Quaternary Research 48, 291-312.

Götzinger, G., 1936. Das Lößgebiet umGöttweig und Krems anderDonau.Führer für die Quartär-Exkursionen in Österreich. Geologische Bundesanstalt, Wien, pp. 1-11.

Haesaerts, P., Damblon, F., Bachner, M., Trnka, G., 1996. Revised stratigraphy and chronology of the Willendorf II sequence, Lower Austria. Archaeologia Austriaca 80, 25-42.

Head, M. J., Gibbard, P. L., Salvador, A., 2008. The Quaternary: its character and definition. Episodes 31, 234-238.

Huntley, D. J., Lamothe, M., 2001. Ubiquity of anomalous fading in K-feldspars and the measurement and correction for it in optical dating. Canadian Journal of Earth Science 38, 1093-1106.

IUSS Working Group WRB, 2006. World Reference Base for Soil Resources. World Soil Resources Reports 103. FAO, Rome.

Kars, R. H., Wallinga, J., Cohen, K. M., 2008. A new approach towards anomalous fading correction for feldspar IRSL dating e tests on samples in field saturation. Radiation Measurements 43, 786-790.

Kohl, H., 1976. Lehmgrube der Ziegelei Würzburger in Aschet bei Wels. Mitteilungen der Kommission für Quartärforschung der Österreichischen Akademie der Wissenschaften 1, 37-41.

Lamothe, M., Auclair, M., 1999. A solution to anomalous fading and age shortfalls in optical dating of feldspar minerals. Earth and Planetary Science Letters 171, 319-323.

Lamothe, M., Auclair, M., Hamzaoui, C., Huot, S., 2003. Towards a prediction of longterm anomalous fading of feldspar IRSL. Radiation Measurements 37, 493-498.

Lu, Y. C.,Wang, X. L., Wintle, A. G., 2007. A new OSL chronology for dust accumulation in the last 130,000 yr fort he Chinese loess Plateau. Quaternary Research 67, 152-160.

Murray, A. S., Wintle, A. G., 2000. Luminescence dating of quartz using an improved single-aliquot regenerative-dose protocol. Radiation Measurements 32, 57-73.

Murray, A. S., Wintle, A. G., 2003. The single aliquot regenerative dose protocol: potential for improvements in reliability. Radiation Measurements 37, 377-381.

Murray, A. S., Buylaert, J.-P., Thomsen, K. J., Jain, M., 2009. The effect of preheating on the IRSL signal from feldspar. Radiation Measurements 44, 554-559.

Neugebauer-Maresch, C., 1993. Zur altsteinzeitlichen Besiedlungsgeschichte des Galgenberges von Stratzing/Krems-Rehberg. Archäologie Österreichs 4, 10-19.

Neugebauer-Maresch, C., 1996. Zur Stratigraphie und Datierung der Aurignacienstation am Galgenberg. In: Svoboda, J. (Ed.), Paleolithic in the Middle Danube Region. Archeologicky ustav, Brno, p. 67.

Niederhuber, M., 1997. Stratzing/Krems-Rehberg. In: Döppes, D., Rabeder, G. (Eds.), Pliozäne und pleistozäne Faunen Österreichs. Österreichische Akademie der Wissenschaften, Wien, pp. 56-61.

Noll, M., Leitner-Wild, E., Hille, P., 1994. Thermoluminescence dating of loess deposits at Paudorf, Austria. Quaternary Geochronology (Quaternary Science Reviews) 13, 473-476.

Novothny, Á., Horváth, E., Frechen, M., 2002. The loess profile of Albertirsa, Hungary e Improvements in loess stratigraphy by luminescence dating. Quaternary International 95-96, 155-163.

Novothny, Á., Frechen, M., Horváth, E., Bradák, B., Oches, E. A., McCoy, W. D., Stevens, T., 2009. Luminescence and amino acid racemisation chronology of the loess-paleosol sequence at Süttő, Hungray. Quaternary International 198, 62-76.

Novothny, Á., Frechen, M., Horváth, E., Krbetschek, M., Tsukamoto, S., 2010. Infrared stimulated luminescence and radiofluorescence dating of aeolian sediments from Hungary. Quaternary Geochronology 5, 114-119.

Oches, E. A., McCoy, W. D., 1995. Amino acid geochronology applied to the correlation and dating of central European loess deposits. Quaternary Science Reviews 14, 767-782.

Pécsi, M., Richter, G., 1996. Löss Herkunft - Gliederung - Landschaften. Annals of Geomorphology 98, 391 pp.

Prescott, J. R., Hutton, J. T., 1994. Cosmic ray contributions to dose rates for luminescence and ESR dating: large depths and long-term variations. Radiation Measurements 23, 497-500.

Preusser, F., Fiebig, M., 2009. European Middle Pleistocene loess chronostratigraphy: some considerations based on evidence from the Wels site, Austria. Quaternary International 198, 37-45.

Rees-Jones, J., 1995. Optical dating of young sediments using fine-grain quartz. Ancient TL 13, 9-14.

Reimer, P. J., Baillie, M. G. L., Bard, E., Bayliss, A., Beck, J. W., Blackwell, P. G., Bronk Ramsey, C., Buck, C. E., Burr, G. S., Edwards, R. L., Friedrich, M., Grootes, P. M., Guilderson, T. P., Hajdas, I., Heaton, T. J., Hogg, A. G., Hughen, K. A., Kaiser, K. F., Kromer, B., McCormac, F. G., Manning, S. W., Reimer, R. W., Richards, D. A., Southon, J. R., Talamo, S., Turney, C. S. M., van der Plicht, J., Weyhenmeyer, C. E., 2009. IntCal09 and Marine09 radiocarbon age calibration curves, 0-50,000 Years cal BP. Radiocarbon 51, 1111-1115.

Roberts, H. M., 2008. The development and application of luminescence dating to loess deposits: a perspective on the past, present and future. Boreas 37, 483-507.

Sun, J., Kohfeld, K. E., Harrison, S. P., 2000. Records of aeolian dust deposition on the Chinese loess Plateau during the Late Quaternary. Technical Reports Max-Planck-Institute for Biogeochemistry 1, 318 pp.

Terhorst, B., 2007. Korrelationen von mittelpleistozänen Löss/Paläobodensequenzen in Oberösterreich mit der marinen Sauerstoffisotopenkurve. Quaternary Science Journal (Eiszeitalter und Gegenwart) 56, 172-185.

Thomsen, K. J., Bøtter-Jensen, L., Denby, P. M., Moska, P., Murray, A. S., 2006. Developments in luminescence measurement techniques. Radiation Measurements 41, 768-773.

Thomsen, K. J., Murray, A. S., Jain, M., Bøtter-Jensen, L., 2008. Laboratory fading rates of various luminescence signals from feldspar-rich sediment extracts. Radiation Measurements 43, 1474-1486.

Tsukamoto, S., Murray, A. S., Huot, S., Watanuki, T., Denby, P. M., Botter-Jensen, L., 2007. Luminescence property of volcanic quartz and the use of red isothermal TL for dating tephras. Radiation Measurements 42, 190-197.

Visocekas, R., 1985. Tunelling radiative recombination in laboradorite: its association with anomalous fading of thermoluminescence. Nuclear Tracks and Radiation Measurement 10, 521-529.

Wallinga, J., Murray, A. S., Wintle, A. G., 2000. The single aliquot regenerative-dose (SAR) protocol applied to coarse-grain feldspar. Radiation Measurements 32, 529-533.

Wallinga, J., Bos, A. J. J., Dorenbos, P., Murray, A. S., Schokker, J., 2007. A test for anomalous fading correction in IRSL dating. Quaternary Geochronology 2, 216-221.

Wallner, G., Wild, E., Aref-Azar, H., Hille, P., Schmidt,W. F. O., 1990. Dating of Austrian loess deposits. Radiation Protection Dosimetry 34, 69-72.

Wintle, A. G., 1973. Anomalous fading of thermoluminescence in minerals. Nature 245, 143-144.

Wintle, A. G., Murray, A. S., 2006. A review of quartz optically stimulated luminescence characteristics and their relevance in single-aliquot regeneration dating protocols. Radiation Measurements 41, 369-391.

Zöller, L., Oches, E. A., McCoy, W. D., 1994. Towards a revised chronostratigraphy of loess in Austria with respect to key sections in the Czech Republic and in Hungary. Quaternary Geochronology (Quaternary Science Reviews) 13, 465-472.

III.3 Investigating the chronostratigraphy of prominent palaeosols in Lower Austria using post-IR IRSL dating

Thiel, C.[1,2], Buylaert, J.-P.[2,3], Murray, A. S.[2], Terhorst, B.[4], Tsukamoto, S.[1], Frechen, M.[1], Tobias Sprafke[4]

[1] Leibniz Institute for Applied Geophysics, S3: Geochronology and Isotope Hydrology, Stilleweg 2, 30655 Hannover, Germany

[2] Nordic Laboratory for Luminescence Dating, Department of Earth Sciences, Aarhus University, Risø DTU, DK-4000 Roskilde, Denmark

[3] Radiation Research Division, Risø National Laboratory for Sustainable Energy, Technical University of Denmark, DK-4000 Roskilde, Denmark

[4] Institute of Geography, Department for Physical Geography, University of Würzburg, Germany

Quaternary Science Journal (E&G), in press

Abstract

The age of most Lower Austria loess deposits is unknown; this is especially true for Middle Pleistocene loess because there is no generally applicable dating method available. Recently it has been shown that infrared stimulated luminescence (IRSL) signals measured at elevated temperatures after an infrared (IR) stimulation are more stable than the standard IRSL signal measured at 50°C. These signals offer new opportunities to extend the datable age range by minimising or circumventing the undesirable anomalous fading correction. In this study we apply, for the first time, two post-IR IRSL single-aliquot regenerative (SAR) dating protocols to polymineral fine-grain samples from three loess/palaeosol sequences in Lower Austria. The luminescence characteristics and ages derived from these protocols are compared with the IRSL results obtained at 50°C. Recycling ratios, recuperation and dose recovery tests show that these protocols are applicable to the loess under investigation. Fading rates for the post-IR IRSL signals are significantly smaller than for the IRSL at 50°C; the differences in fading rates between post-IR IRSL at 225°C and post-IR IRSL at 290°C are less obvious. Significant fading corrections are needed for the ages derived from the IRSL signal at 50°C. From our study we conclude that the fading corrected post-IR IRSL at 225°C and the fading uncorrected post-IR IRSL at 290°C provide the best age estimates; we prefer the latter because no fading correction is apparently needed. Our data strongly suggest that the pedocomplex 'Paudorfer Bodenbildung' developed during marine isotope stage (MIS) 5, whereas the pedocomplex 'Göttweiger Verlehmungszone' is significantly older (≥ 350 ka) than has been suggested in former studies.

Keywords: post-IR IRSL; fading; loess; Middle Pleistocene; Lower Austria

III.3.1 Introduction

Loess/palaeosol sequences contain detailed archives of terrestrial palaeoenvironmental changes and landscape evolution. Unfortunately, most loess sequences lack a reliable absolute chronology and hence these changes are difficult to constrain in time. Especially for Middle Pleistocene loess deposits, geochronological information is scarce because there is, as yet, no generally applicable and reliable instrumental dating method which can be used for this age range.

Luminescence dating has proved to be a useful tool to date loess deposits (Roberts, 2008), not only because of the wide age range covered by this technique (from a few years to, theoretically, several hundred thousand years; Aitken, 1998) but also because of the long sub-aerial transport of the particles which make up loess; this is confidently expected to have bleached any luminescence signal prior to deposition. Loess is also made up almost entirely of quartz and feldspar, both of which are suitable dosimeters for luminescence dating. The main drawback in the optically stimulated luminescence (OSL) dating of quartz extracted from loess is the low saturation level of ~200 Gy; this is equivalent to ~50-70 ka assuming a dose rate of between 3 and 4 Gy/ka (typical for loess, e.g. Frechen et al., 1997; Novothny et al., 2002, 2009; Wang et al., 2006; Buylaert et al., 2007; Lai et al., 2010; Thiel et al., 2011a, b). In contrast, feldspar infrared stimulated luminescence (IRSL) signals have a much higher saturation dose (~1500-2000 Gy; equivalent to ~500-700 ka) but, on the other hand, most feldspars suffer from athermal signal loss, referred to as anomalous fading (Wintle, 1973; Spooner, 1994). Because of this phenomenon, IRSL ages tend to significantly underestimate the depositional age. Huntley and Lamothe (2001) have presented a model that can be used to correct the age underestimation, but these corrections are theoretically only applicable to the linear part of the growth curve, i.e. to young samples. Approaches which allow for correction beyond the linear region have been proposed by Lamothe et al. (2003) and Kars et al. (2008); in principle these models can be used for older material (in case of loess >50 ka), but there is little or no testing of these models available in the literature. Although fading corrections can give apparently accurate ages (Huntley and Lamothe, 2001; Buylaert et al., 2011) it seems more advisable to make use of IRSL signals that show less or no fading (Thiel et al., 2011a, submitted) because all correction models involve untestable assumptions, including that the fading rate observed on a laboratory timescale is relevant to geological time. In addition, there are examples where feldspar IRSL ages underestimate when compared with independent age control, even after fading correction (e.g. Wallinga et al., 2007).

Recent developments in luminescence dating offer the potential to circumvent the problem of anomalous fading, and thus to extend the reliable dating range to the Middle Pleistocene (126 to 781 ka; Head et al., 2008). The post-IR IRSL signal (IR stimulation at 50°C and subsequent IRSL measurement at 225°C, blue detection; Thomsen et al., 2008) seems to have great potential; in the laboratory, this signal fades more slowly than conventional IRSL

measured at 50°C. Buylaert et al. (2009) tested the applicability of this post-IR IRSL signal to dating sand-sized potassium feldspar grains; the fading rate of the post-IR IRSL signal was two times smaller than the one of the IRSL signal measured at 50°C. Thiel et al. (2011a) used a preheat of 320°C (60 s), IR stimulation at 50°C (200 s) and subsequent post-IR IR stimulation at 290°C (200 s) for polymineral fine grains (4-11 μm). They measured the natural signal and dose response curve of a sample from below the Brunhes/Matuyama boundary (~780 ka, expected natural dose >2700 Gy), and found the natural signal in saturation on the laboratory regenerated growth curve; from that they concluded that for their samples they were unable to detect any evidence for anomalous fading in the field using post-IR IRSL at 290°C.

Even though post-IR IRSL dating in its different forms has now been applied in several studies (Buylaert et al., 2009; Thiel et al., 2010, 2011a, submitted; Reimann et al., 2011) no study has compared the performance of the two different post-IR IRSL dating protocols now in use. In this paper we compare the ages derived from the IR signal at 50°C and two post-IR IRSL signals (post-IR IR stimulation at 225°C, Buylaert et al., 2009; post-IR IR stimulation at 290°C, Thiel et al., 2011a) for three loess/palaeosol sequences in Lower Austria: i) Joching, ii) Paudorf, and iii) Göttweig. These sites have a long scientific history, starting with the investigations of Bayer (1927) and Götzinger (1936). Nevertheless the ages of the pedocomplexes 'Paudorfer Bodenbildung' and 'Göttweiger Verlehmungszone' are still controversial (Fink, 1976; Noll et al., 1994; Zöller et al., 1994; Smolíková et al., 1994) due to discontinuities as the result of intensive erosional phases (cf. Havliček et al., 1998), and illustrate the need for a more reliable numerical dating method. We first demonstrate that our measurement protocols are applicable to these samples, by examining recuperation, recycling ratios and the ability of these protocols to measure a known dose given in the laboratory. Subsequently the luminescence characteristics, the equivalent doses and laboratory fading rates for the various signals are compared and the derived ages (corrected and uncorrected) are discussed in terms of their reliability. Finally, the most reliable set of IRSL ages is used to unravel the chronostratigraphy of the prominent palaeosols in Lower Austria.

III.3.2 Site descriptions and sampling

The loess/palaeosol sequences investigated in this study are located in the Kremser Feld in Lower Austria (Fig. III.13); this region is covered by up to 30 m of loess deposits. Three sites exhibiting the prominent palaeosols 'Paudorfer Bodenbildung' and 'Göttweiger Verlehmungszone' were investigated; samples for luminescence dating were taken by hammering metal tubes into the freshly cleaned profile. Samples for dosimetry measurements (~1000 g) were taken from immediately around the luminescence samples.

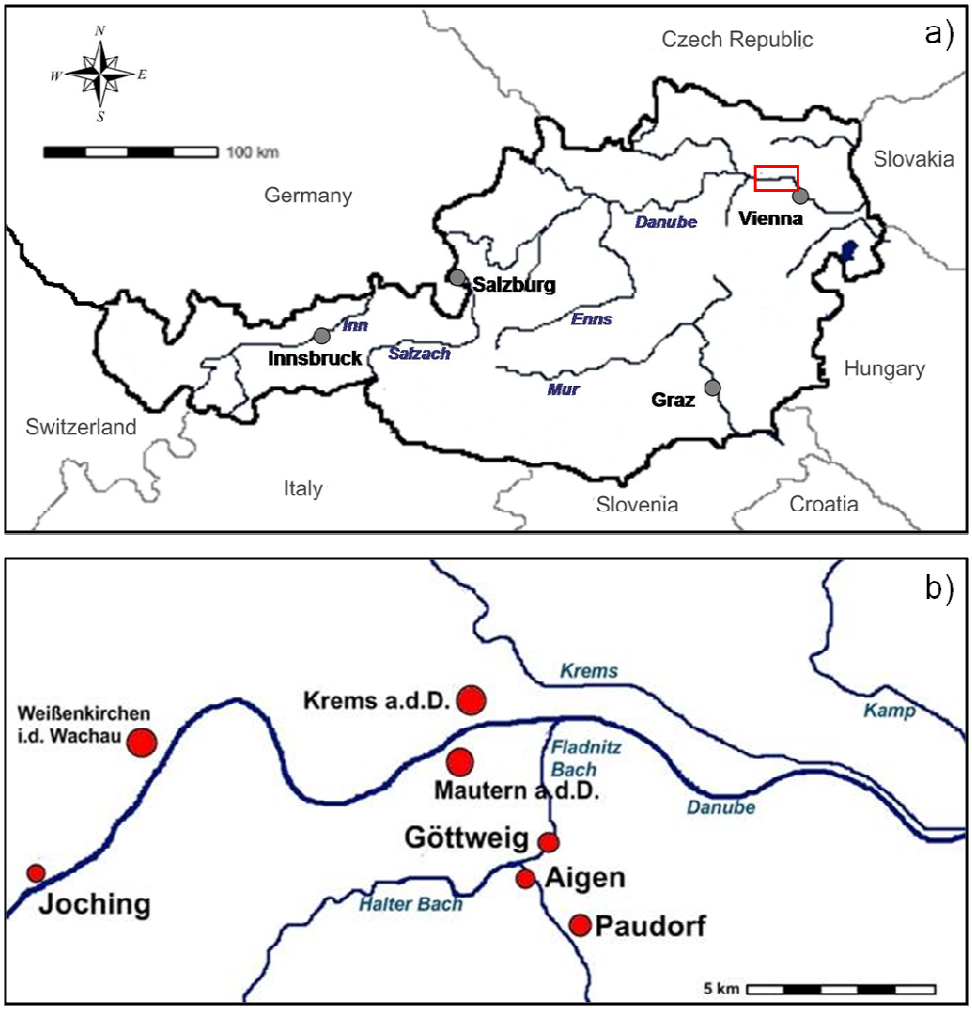

Fig. III.13: Maps of the study area. a) Austria; the red rectangle is framing the investigated sites b) enlargement of the study area showing the locations of the loess/palaeosol sequences of Göttweig (Furth and Aigen), Paudorf, and Joching.

III.3.2.1 Joching

The village of Joching is located on the left bank of the Danube (Fig. III.13) and is the furthest upstream of our sites. The loess/palaeosol sequence has a total thickness of about 10 m, with at least two distinct palaeosols (Fig. III.14). Below silty yellowish-brown loess (unit J1) a zone of Cryosol horizons (unit J2) is underlain by stratified loamy pellet sands ('Bröckelsande'; unit J3) of up to 4 m thickness. These sands cover a palaeosol horizon with interstadial intensity (J4). About 1.0 m of silty yellowish-brown loess rich in secondary carbonates and with few mollusc fragments (unit J5) is exposed below this soil. The loess is underlain by a pedocomplex (units J6-8) which intensity implies interglacial conditions. Loess (unit J9) is exposed below this pedocomplex.

At this site three luminescence samples were taken (Fig. III.14). Sample 1398 was taken from the loess unit J1 1.3 m below top ground surface. The 'Bröckelsand' (unit J3) was sampled (sample 1399) 0.2 m below the Cryosol complex (unit J2), and sample 1400 was taken in the loess unit J9 0.7 m below the pedocomplex, i.e. ~ 8.3 m below top ground surface.

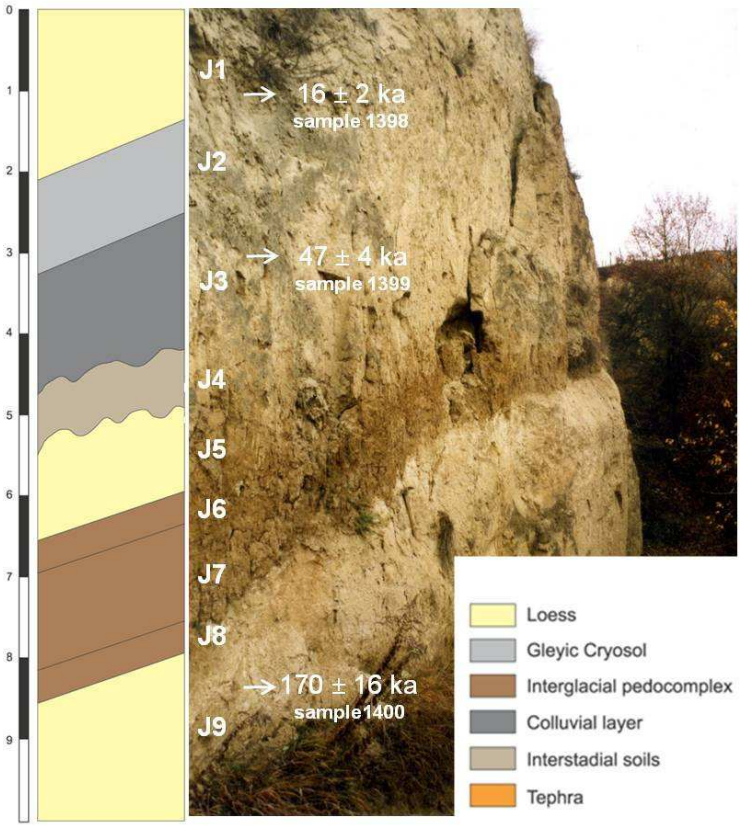

Fig. III.14: Photograph and simplified sketch of the loess/palaeosol sequences at Joching. The luminescence ages presented are uncorrected post-IR IRSL ages at 290°C. For details on the material composition, sampling depths and dating see text.

III.3.2.2 Paudorf

The village of Paudorf is located on a right bank tributary of the Danube. The loess/palaeosol sequence is exposed in a former brickyard and is the type locality of the 'Paudorfer Bodenbildung' *sensu* Götzinger (1936). The outcrop, last described by Fink (1976) and thermoluminescence (TL) dated by Zöller et al. (1994) and Noll et al. (1994), is about 9.5 m thick (Fig. III.15). At least two well-developed pedocomplexes are preserved at this site; the uppermost soil complex is the prominent 'Paudorfer Bodenbildung' (Fig. III.15).

The luminescence sampling points are shown in Figure III.15; two adjacent profiles were sampled (Paudorf I and II). The uppermost sample 1404 was taken in loess (unit PI-2) 0.3 m

above the 'Paudorfer Bodenbildung' (unit PI-3), which is here developed as a reddish-brown, clay-rich palaeosol with crotovina. The loess unit PI-4 below the 'Paudorfer Bodenbildung', was sampled 2.9 m below top ground surface (sample 1403).

In profile Paudorf II, the 4 m thick loess (PII-3) was sampled below the 'Paudorfer Bodenbildung' at a depth of 4.2 m (sample 1402); because of induration, this sample had to be taken as a block. The loess deposit is underlain by alternating Cryosol and loess horizons (PII-4 to PII-7). In its lower parts a weak brownish palaeosol is exposed (PII-8). A loess layer (PII-9) bracketing the weak palaeosol and the basal pedocomplex (PII-10), originally correlated with the 'Göttweiger Verlehmungszone' (Götzinger, 1936), was sampled at a depth of 7.8 m (sample 1401).

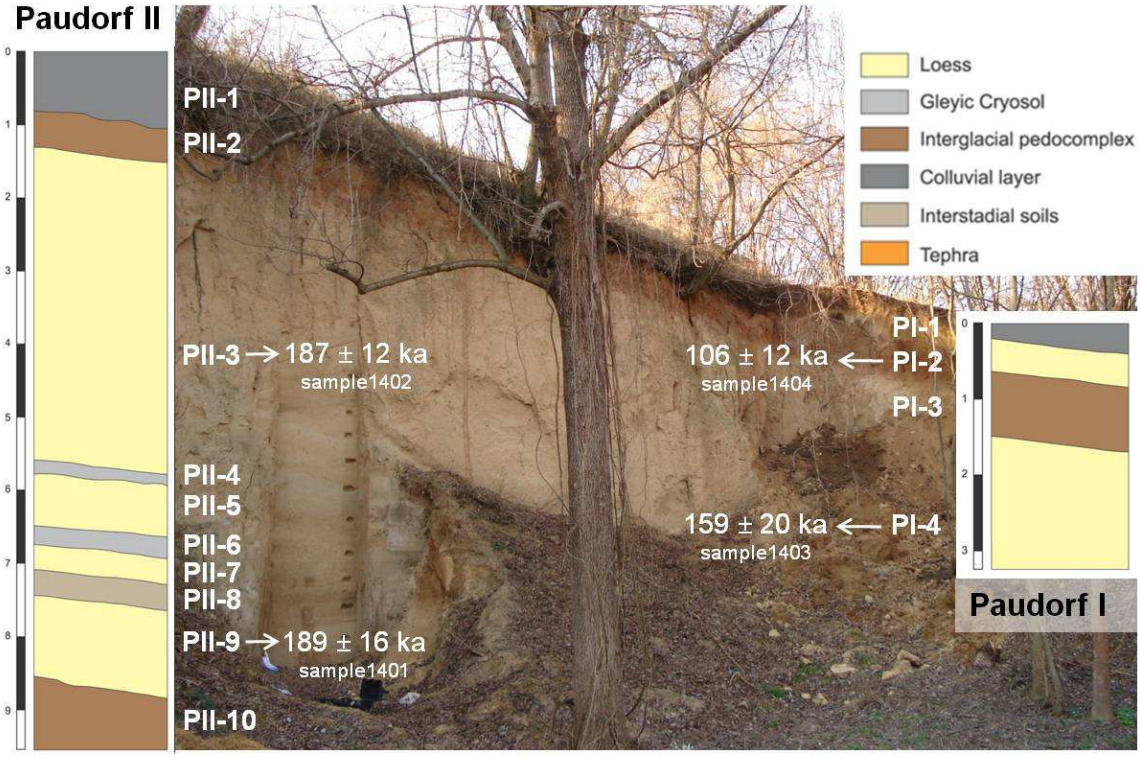

Fig. III.15: Photograph and simplified sketches of the loess/palaeosol sequence at Paudorf. The presented ages are based on post-IR IRSL dating at 290°C (except sample 1403, for which corrected post-IR IRSL at 225°C was used). For details on the material composition, sampling depths and dating see text.

III.3.2.3 Göttweig

Two different sections were investigated near the monastery of Göttweig, just north of the loess sequence at Paudorf (Fig. III.16). Section I (Fig. III.16a) is the classical site of the 'Göttweiger Verlehmungszone' *sensu* Bayer (1927) and Götzinger (1936), located near the town of Furth in a hollow way. The pedocomplex 'Göttweiger Verlehmungszone' (unit GI-4) and the overlying up to 6 m thick loess is exposed horizontally over several hundred meter

and lies on a Danube terrace; the correlation with other terraces is unclear. A continuous thin layer (unit GI-2) can be identified in the loess package; preliminary magnetic analysis suggest that this layer is a tephra (pers. comm. U. Hambach), whose origin and age is unfortunately unclear.

The luminescence sampling points at Section I are shown in Figure III.16a. Sample 1406 comes from silty loess (unit GI-1) 0.6 m above the tephra (unit GI-2), and sample 1405 was taken in sandy-silty yellowish-brown loess (unit GI-3) 0.3 m below the tephra. Another sample (1407; not shown in Fig. III.16) was taken 300 m upslope 30 cm below reworked loess which includes pebbles and sandy layers; the position of this sample with respect to the other samples is not unambiguously established but the sampling point definitely lies above the tephra layer.

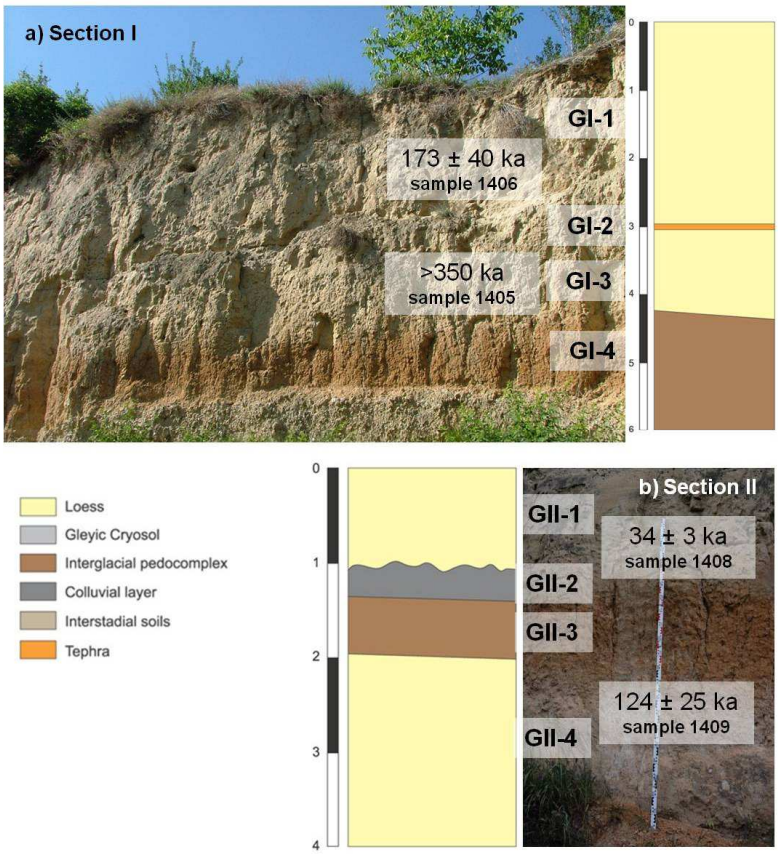

Fig. III.16: Photographs and simplified sketches of the loess/palaeosol sequences at Göttweig. a) Section I: type locality of the 'Göttweiger Verlehmungszone' (Göttweig-Furth), b) Section II (Göttweig-Aigen), with 'Paudorfer Bodenbildung' (Fink, 1976). Sample 1407 was taken 300 m upslope from Section I and is not shown in the figure. All ages are derived by post-IR IRSL dating at 290°C. For details on the material composition, sampling depths and dating see text.

Section II is located in the hollow way near the village of Aigen (between Göttweig and Paudorf), where a pedocomplex correlated with the 'Paudorfer Bodenbildung' is exposed (Fink, 1976; Fig. III.16b). However the pedocomplex (unit GII-3) is eroded at this site, deduced from the lack of an A horizon and a package of 30 cm thick reworked loess (unit GII-2) covering the soil. The fine-silty yellowish-brown loess (unit GII-1) was sampled 0.7 m

below top ground surface and 0.6 m above the 'Paudorfer Bodenbildung' (sample 1408); due to induration the sample had to be taken as a block. Sample 1409 was taken in carbonate rich silty loess (unit GII-4) 0.6 m below the 'Paudorfer Bodenbildung' (i.e. 2.5 m below top ground surface).

III.3.3 Sample preparation and analytical facilities

In the laboratory, all samples for equivalent dose (D_e) determination were treated under subdued red light. The outer ends (~1 cm) of the samples might have been exposed to daylight during sampling; these were discarded and the remaining sample treated with hydrochloric acid, sodium oxalate, and hydrogen peroxide. Between each treatment step the sediment was washed with distilled water. Special attention was paid to samples 1402 and 1408 (taken as blocks); all surfaces were scraped off to a depth of >1 cm before chemical treatment. The fine-silt fraction (4-11 μm) of the samples was extracted by repeated settling and washing (Frechen et al., 1996). The polymineral fine-grains were then deposited on aluminium discs (diameter 9.7 mm) from a suspension in acetone (2 mg/ml). Luminescence measurements were made with automated Risø TL/OSL readers (DA-15 and DA-20, respectively; Bøtter-Jensen et al., 2003; Thomsen et al., 2006) fitted with calibrated $^{90}Sr/^{90}Y$ beta sources calibrated using fine-grained quartz on aluminium discs. The feldspar signal of the polymineral samples was stimulated with infrared light diodes emitting at 870 nm, and the luminescence was detected in the blue-violet region (325-450 nm) through a Schott BG39/Corning 7-59 filter combination.

III.3.4 Dosimetry

The concentrations of U, Th and K were determined by high-resolution gamma-ray spectrometry equipped with a high-purity germanium detector. 700 g of each sample of dried material was homogenised and packed in Marinelli beakers, sealed and stored for at least one month to ensure equilibrium between radon and its daughter nuclides before counting. Details about the procedures for dosimetry measurements at the Leibniz Institute for Applied Geophysics (LIAG) laboratory in Hannover are given by Kunz et al. (2010).

The dose rates were derived using the conversion factors of Adamiec & Aitken (1998). For all samples a water content of 15 ± 5% was used (Frechen et al., 1997) to allow for possible changes in water content throughout time, and a mean a-value of 0.08 ± 0.02 was assumed (Rees-Jones, 1995). Calculation of the cosmic dose rate is based on Prescott and Hutton (1994).

The dosimetry data are summarised in Table III.10. The total dose rates range from 2.1 ± 0.1 Gy/ka to 3.8 ± 0.2 Gy/ka. The rather low dose rate of 2.1 ± 0.1 Gy/ka for samples 1400 and 1409 originate in the relatively low Th (~7 ppm) and K (<1%) contents. Nevertheless, all

dose rates are within the range expected for European loess (Zöller et al., 1994; Frechen et al., 1997; Novothny et al., 2002, 2009; Thiel et al, 2011a, 2011b).

Table III.10: Summary of dosimetry data. A water content of 15 ± 5% was estimated for all samples.

Sample	K [%]	U [ppm]	Th [ppm]	Cosmic dose rate [Gy/ka]	Total dose rate [Gy/ka]
1398	1.2 ± 0.1	3.0 ± 0.1	10.6 ± 0.3	0.18 ± 0.02	3.1 ± 0.1
1399	1.7 ± 0.1	3.2 ± 0.2	11.5 ± 0.4	0.14 ± 0.02	3.5 ± 0.2
1400	0.8 ± 0.1	2.3 ± 0.1	7.3 ± 0.3	0.08 ± 0.01	2.1 ± 0.1
1401	2.2 ± 0.1	2.8 ± 0.2	11.4 ± 0.4	0.13 ± 0.01	3.8 ± 0.2
1402	1.4 ± 0.1	2.5 ± 0.1	9.4 ± 0.3	0.15 ± 0.02	2.9 ± 0.1
1403	1.5 ± 0.1	2.5 ± 0.1	9.9 ± 0.3	0.17 ± 0.02	3.0 ± 0.1
1404	1.6 ± 0.1	2.8 ± 0.1	10.9 ± 0.4	0.20 ± 0.02	3.3 ± 0.1
1405	1.6 ± 0.1	2.9 ± 0.1	11.0 ± 0.4	0.09 ± 0.01	3.2 ± 0.2
1406	1.4 ± 0.1	2.8 ± 0.1	9.8 ± 0.3	0.10 ± 0.01	2.9 ± 0.1
1407	1.5 ± 0.1	2.9 ± 0.1	12.9 ± 0.3	0.11 ± 0.01	3.4 ± 0.2
1408	1.3 ± 0.1	2.9 ± 0.1	10.1 ± 0.3	0.20 ± 0.02	3.0 ± 0.3
1409	0.9 ± 0.2	2.2 ± 0.1	6.9 ± 0.2	0.16 ± 0.02	2.1 ± 0.1

III.3.5 Post-IR IRSL dating

Since Thomsen et al. (2008) first identified reduced laboratory fading rates from various feldspar signals, several studies have tested or made use of elevated temperature post-IR IRSL signals (e.g. Buylaert et al., 2009; Thiel et al., 2010, 2011a, b; Reimann et al., 2011).

Buylaert et al. (2009) used a preheat of 250°C for 60 s (used in many studies in the past), and their post-IR IR stimulation temperature was chosen to be 225°C. Because Murray et al. (2009) showed for sand-sized grains of potassium feldspar that there is no systematic increase in equivalent dose measured at 50°C for preheat temperatures ranging from 80°C up to 320°C (60 s duration), Thiel et al. (2011a) adopted a more stringent preheat of 320°C for 60 s to date their polymineral fine-grains with a post-IR IRSL protocol. This allowed them to use post-IR IR stimulation at significantly higher temperatures. They chose to investigate the use of stimulation at 290°C and observed the natural signal of a polymineral fine grain extract from below the Brunhes/Matuyama boundary (~780 ka, i.e. ~2700 Gy) in saturation on a laboratory growth curve. Based on these observations, they concluded that there is no detectable anomalous fading in nature of the post-IR IRSL signal at 290°C, even though they were able to measure a finite laboratory fading rate of ~1-1.5%/decade. Thiel et al. (submitted) have since compared ages obtained using the same post-IR IRSL at 290°C protocol with independent age control based on both fission track and radiocarbon dating as well as quartz OSL at two loess sites in Japan (Watanuki et al., 2005) and obtained very consistent results back to ~600 ka. Again they observed a low fading rate in the laboratory (1.1 ± 0.2%/decade; n=15) but argued that no fading correction was necessary.

In the following sections we compare the results obtained using the post-IR IRSL protocol described by Buylaert et al. (2009) (post-IR IRSL at 225°C) with those of Thiel et al. (2011a)

(post-IR IRSL at 290°C) (Table III.11). For comparison the results of the IRSL signal at 50°C (measured as part of the post-IR IRSL at 225°C protocol) are also discussed.

Table III.11: Flowcharts of the applied post-IR IRSL SAR protocols (Buylaert et al., 2009; Thiel et al., 2011a). For IRSL at 50°C steps 3 and 7 of protocol a) were used for equivalent dose determination.

a)			b)		
Step	Treatment	Observed	Step	Treatment	Observed
1	Give dose, D_i		1	Give dose, D_i	
2	Preheat, 250°C, 60 s		2	Preheat, 320°C, 60 s	
3	IR stimulation, 100 s at 50°C		3	IR stimulation, 200 s at 50°C	
4	IR stimulation, 100 s at 225°C	L_x	4	IR stimulation, 200 s at 290°C	L_x
5	Give test dose, D_T		5	Give test dose, D_T	
6	Preheat, 250°C, 60 s		6	Preheat, 320°C, 60 s	
7	IR stimulation, 100 s at 50°C		7	IR stimulation, 200 s at 50°C	
8	IR stimulation, 100 s at 225°C	T_x	8	IR stimulation, 200 s at 290°C	T_x
9	IR stimulation, 40 s at 290°C		9	IR stimulation, 100 s at 325°C	
10	Return to 1		10	Return to 1	

III.3.5.1 Post-IR IRSL measurements at 225°C

For these post-IR IRSL measurements we used the same temperature and stimulation conditions as Buylaert et al. (2009). After a preheat of 250°C for 60 s, we bleached the polymineral fine-grains (six aliquots per sample) with IR diodes at 50°C for 100 s to recombine the near-neighbour trap/centre pairs which fade most rapidly (discussed in e.g. Poolton et al., 2002; Thomsen et., 2008, 2011), and then held the aliquot at 225°C while measuring the IRSL for 100 s. The response to a test dose (~70 Gy) was measured in the same manner (Table III.11), and an IR illumination at 290°C for 40 s was inserted at the end of each SAR measurement cycle to reduce the effect of any recuperation (based on Murray and Wintle, 2003). The initial 2.4 s of the decay curve were used for D_e determination after subtracting a background from the last 60 s.

The laboratory fading rate was measured on three aliquots per sample as the IRSL signal decreased over time using artificially irradiated aliquots; this is expressed in terms of the percentage decrease of signal intensity per decade of time (the *g*-value; Aitken, 1985, Appendix F). After a final IR illumination at 290°C for 40 s, the same aliquots as for equivalent dose measurements were given doses of ~50 Gy ('young samples') and ~200 Gy ('old samples'), respectively, to monitor anomalous fading using the SAR protocol outlined in Table 2. The storage times after irradiation and preheating (Auclair et al., 2003) varied from as brief as experimentally possible ('prompt') to delays of up to ~10 hours. The *g*-values,

calculated using Equation 4 of Huntley and Lamothe (2001), were normalised to a measurement time delay of 2 days after irradiation.

The dose response curves and the post-IR IRSL decay curves of samples 1399 (a 'young' sample) and 1407 (an 'old' sample) are shown in Figure III.17; they are representative of all the other samples presented in this study. The sensitivity-corrected natural of the post-IR IRSL signal of sample 1399 lies on the relatively linear part of the dose response curve, whereas the natural post-IR IRSL signal of sample 1407 (Fig. III.17b) clearly lies beyond the linear region, which thus reduces the accuracy of the Huntley and Lamothe (2001) fading correction.

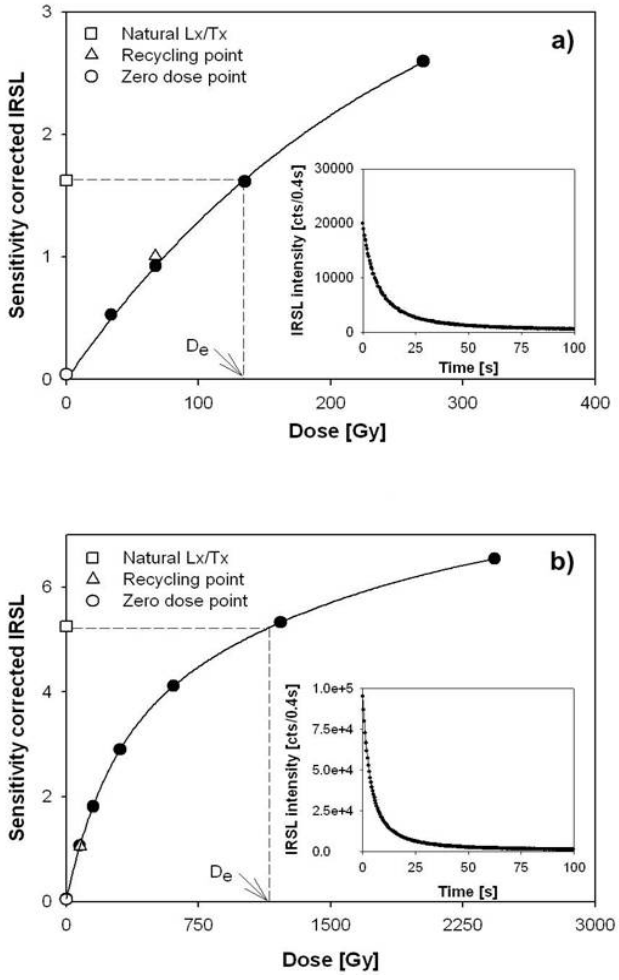

Fig. III. 17: Dose response and natural decay curves for the post-IR IRSL measurements at 225°C. a) Dose response curve for sample 1399, representative of younger samples. The inset shows the post-IR IRSL intensity against time (100 s). b) Dose response curve for sample 1407, representative of older samples. The natural sensitivity corrected post-IR IRSL signal (L_x/T_x) is beyond the linear part of the curve. The inset shows the post-IR IRSL intensity against time (100 s).

Table III.12: Recycling ratios, equivalent doses (D_e), fading rates, and fading uncorrected and fading corrected ages for the three (post-IR) IRSL signals. For all samples six aliquots were measured for D_e determination. The fading uncorrected ages for the post-IR IRSL signal at 290°C (in bold) are considered the most reliable (apart from sample 1403 for which the corrected age of post-IR IRSL at 225°C is considered the most reliable estimate). For details see text.

Location	Sample	Signal	Recycling ratio	D_e [Gy]	Fading rate [%/decade]	Fading uncorrected age [ka]	Fading corrected age [ka]
Joching	1398	IR at 50°C*	1.03 ± 0.02	15 ± 2	8.0 ± 0.5	5 ± 1	10 ± 1
		pIRIR at 225°C	1.02 ± 0.01	33 ± 3	2.8 ± 0.2	11 ± 1	13 ± 1
		pIRIR at 290°C	1.02 ± 0.01	50 ± 5	1.3 ± 0.5	**16 ± 2**	18 ± 2
	1399	IR at 50°C*	1.07 ± 0.07	140 ± 15	4.3 ± 0.5	40 ± 4	58 ± 8
		pIRIR at 225°C	1.05 ± 0.02	148 ± 11	1.8 ± 0.1	42 ± 2	49 ± 4
		pIRIR at 290°C	0.99 ± 0.01	163 ± 10	0.9 ± 0.5	**47 ± 4**	50 ± 5
	1400	IR at 50°C*	1.01 ± 0.02	329 ± 34	9.9 ± 0.5	157 ± 17	679 ± 74
		pIRIR at 225°C	1.00 ± 0.01	337 ± 32	2.7 ± 0.2	160 ± 17	201 ± 19
		pIRIR at 290°C	1.00 ± 0.01	356 ± 32	1.0 ± 0.3	**170 ± 16**	183 ± 19
Paudorf	1401	IR at 50°C*	1.02 ± 0.02	474 ± 37	1.0 ± 0.7	126 ± 10	135 ± 12
		pIRIR at 225°C	0.99 ± 0.01	596 ± 20	1.2 ± 0.2	158 ± 6	172 ± 15
		pIRIR at 290°C	1.00 ± 0.01	714 ± 58	1.1 ± 0.2	**189 ± 16**	204 ± 20
	1402	IR at 50°C*	1.03 ± 0.01	344 ± 15	2.2 ± 0.6	119 ± 6	141 ± 13
		pIRIR at 225°C	1.00 ± 0.01	427 ± 44	0.6 ± 0.6	147 ± 16	154 ± 20
		pIRIR at 290°C	0.99 ± 0.01	538 ± 34	0.7 ± 0.5	**187 ± 12**	195 ± 20
	1403	IR at 50°C*	1.01 ± 0.04	353 ± 19	4.3 ± 0.6	118 ± 7	172 ± 19
		pIRIR at 225°C	1.00 ± 0.01	414 ± 44	1.8 ± 0.1	138 ± 15	**159 ± 20**
		pIRIR at 290°C	0.98 ± 0.01	897 ± 97	0.7 ± 0.3	299 ± 33	315 ± 41
	1404	IR at 50°C*	1.03 ± 0.03	234 ± 20	3.7 ± 0.6	71 ± 6	97 ± 12
		pIRIR at 225°C	1.01 ± 0.01	225 ± 19	1.5 ± 0.2	68 ± 6	77 ± 9
		pIRIR at 290°C	1.01 ± 0.01	351 ± 40	1.5 ± 0.4	**106 ± 12**	120 ± 16
Göttweig	1405	IR at 50°C*	0.99 ± 0.01	728 ± 51	3.4 ± 0.3	228 ± 17	304 ± 30
		pIRIR at 225°C	0.99 ± 0.01	1295 ± 83	4.3 ± 0.5	>300	>300
		pIRIR at 290°C	0.99 ± 0.01	1845 ± 483	0.8 ± 0.4	**>350**	>350
	1406	IR at 50°C*	1.04 ± 0.02	440 ± 47	4.6 ± 0.6	152 ± 16	230 ± 34
		pIRIR at 225°C	1.00 ± 0.00	537 ± 30	2.3 ± 0.3	185 ± 12	233 ± 19
		pIRIR at 290°C	1.00 ± 0.01	503 ± 115	1.2 ± 0.3	**173 ± 40**	190 ± 46
	1407	IR at 50°C*	1.00 ± 0.01	847 ± 125	3.2 ± 0.3	243 ± 38	327 ± 53
		pIRIR at 225°C	0.98 ± 0.01	1149 ± 96	2.9 ± 0.5	>280	>280
		pIRIR at 290°C	1.00 ± 0.01	1265 ± 78	0.9 ± 0.3	**>300**	>300
	1408	IR at 50°C*	0.99 ± 0.05	75 ± 6	3.3 ± 0.4	25 ± 2	33 ± 4
		pIRIR at 225°C	1.00 ± 0.01	83 ± 6	2.0 ± 0.5	28 ± 2	32 ± 3
		pIRIR at 290°C	1.00 ± 0.01	101 ± 8	0.9 ± 0.4	**34 ± 3**	36 ± 4
	1409	IR at 50°C*	1.00 ± 0.01	244 ± 16	3.1 ± 0.3	116 ± 8	151 ± 13
		pIRIR at 225°C	1.00 ± 0.01	294 ± 23	1.3 ± 0.4	140 ± 13	155 ± 15
		pIRIR at 290°C	0.99 ± 0.01	263 ± 53	0.7 ± 0.3	**124 ± 25**	132 ± 30

* The equivalent doses of the IRSL signal at 50°C are derived from the same measurement cycle as the post-IR IRSL (225°C) results, i.e. preheat of 250°C. The same applies to the measured fading rates.

The ability of a measurement protocol to reproducibly measure the response to a laboratory dose given after repeated heating of the sample is represented by the recycling ratio, which ought to yield values indistinguishable from unity. The recycling ratios for the samples vary

between 0.99 ± 0.01 (n=6; sample 1407) and 1.05 ± 0.02 (n=5; sample 1399) (Table III.12 and Fig. III.18a). Recuperation is well below 5% of the natural signal for all except the uppermost sample of the Joching profile (sample 1398), which shows a recuperation of 8.8 ± 0.5% (n=6) (Fig. III.18b).

Satisfactory recycling ratios do not necessarily mean that doses given before any heating can also be measured accurately (which is the closest we can come to reproducing natural conditions). We therefore carried out a dose recovery test. Three natural aliquots of samples 1399 (Joching), 1401 (Paudorf) and 1405 (Göttweig) were bleached for 4 hours in a Hönle SOL2 simulator (sample to lamp distance ~1.2 m to avoid heating of the aliquots). The aliquots were then given a beta dose similar to the measured D_e for each sample and the given dose was measured in the usual manner. The results of the dose recovery test are shown in Figure III.19a.

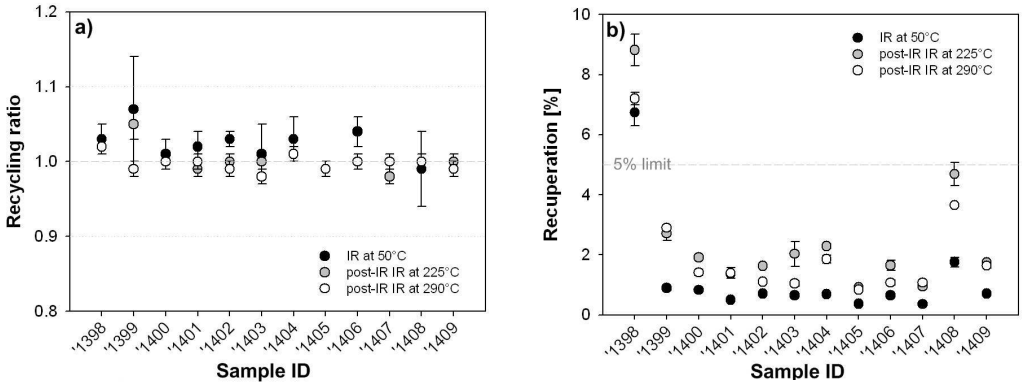

Fig. III.18: Recycling ratios and recuperation. a) For all signals and samples the recycling ratios are within 10% of unity. b) Recuperation [% of natural signal] for all signals and samples. Sample 1398 shows recuperation >5% for all (post-IR) IRSL signals, whereas for all other samples it is well below 5%; for IRSL at 50°C it is below 2%.

For all samples, measured/given doses are within 10% of unity. Because of the residual signals (and hence doses) observed for the post-IR IRSL signal at 225°C in other studies (Thomsen et al. 2008; Buylaert et al., 2009) we measured the residual signal after bleaching on separate aliquots of the same samples (three per sample). These residual signals were equivalent to a dose of 4.7 ± 0.5 Gy (n=9). After subtraction of these residual doses the measured/given dose ratios vary between 0.97 ± 0.01 (n=3; sample 1404) and 1.02 ± 0.04 (n=3; sample 1399). Both the measured to given ratios before and after residual subtraction are very close to unity (Fig. III.19), demonstrating the accuracy of the measurement protocol when measuring an artificial beta dose given prior to any heating.

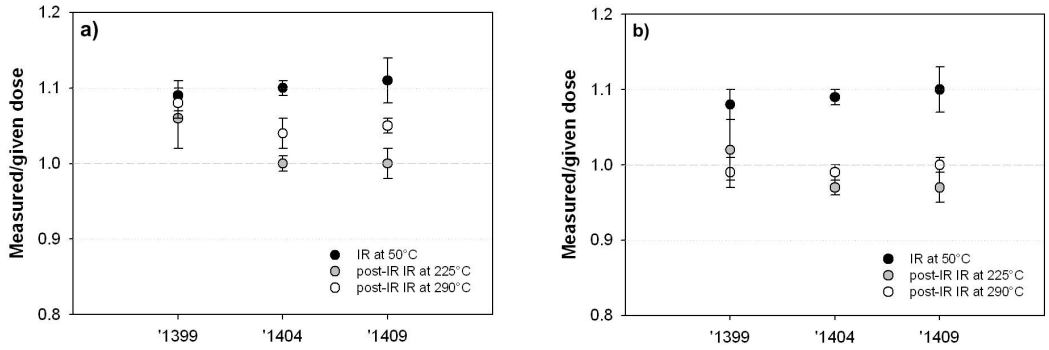

Fig. III.19: Results of dose recovery tests a) without residual subtraction, b) with residual subtraction. The residual signal is 1.5 ± 0.2 Gy (n=9) for the IRSL measurements at 50°C, 4.7 ± 0.5 Gy (n=9) for the post-IR IRSL measurements at 225°C, and 13 ± 2 Gy (n=9) for the post-IR IRSL measurements at 290°C. For details about the bleaching conditions and residual measurements see text.

III.3.5.2 Post-IR IRSL measurements at 290°C

Following Thiel et al. (2011a), after preheating the samples (six aliquots per sample) at 320°C for 60 s we bleached the polymineral fine-grains with IR diodes at 50°C for 200 s and subsequently measured the IRSL at 290°C for 200 s. The response to a test dose was measured in the same manner, and an IR illumination at 325°C for 100 s was inserted at the end of each SAR measurement (Table III.11). The light sum of the initial 2.4 s of the post-IR IRSL signal was used for D_e determination, less a background derived from the last 100 s. The fading rates on three aliquots per sample were measured in exactly the same way as for the IR at 225°C signal but using the preheating and stimulation conditions of the post-IR IRSL at 290°C protocol.

The dose response curves and the post-IR IRSL signals at 290°C of two samples (1399 and 1407) are shown in Figure III.20. Whereas the natural post-IR IRSL signal of sample 1399 lies in the linear region of the dose response curve, the natural post-IR IRSL signal of sample 1407 is well above and is approaching saturation. Recycling ratios are very close to unity for all samples (Table III.12 and Fig. III.18a), and recuperation varies between 0.91 ± 0.06% (n=6; sample 1405) and 7.2 ± 0.2% (n=6; sample 1398) (Fig. III.18b); except for sample 1398 recuperation is well below 5% of the natural (the acceptance threshold for quartz OSL suggested by Murray and Wintle, 2003).

Bleaching for dose recovery tests and residual determination was conducted in the same manner as for the post-IR IRSL measurements at 225°C. After giving a beta dose close to the natural the dose was measured using the settings described above. Without subtraction of the residual signals (13 ± 2 Gy; n=9), measured to given dose ratios vary between 1.04 ± 0.02 (n=3; sample 1404) and 1.08 ± 0.02 (n=3; sample 1399; Fig. III.19a); after subtraction of the

residual signals the ratios are 0.99 ± 0.02 (n=3; sample 1404) and 1.00 ± 0.01 (n=3; sample 1407; Fig. III.19b).

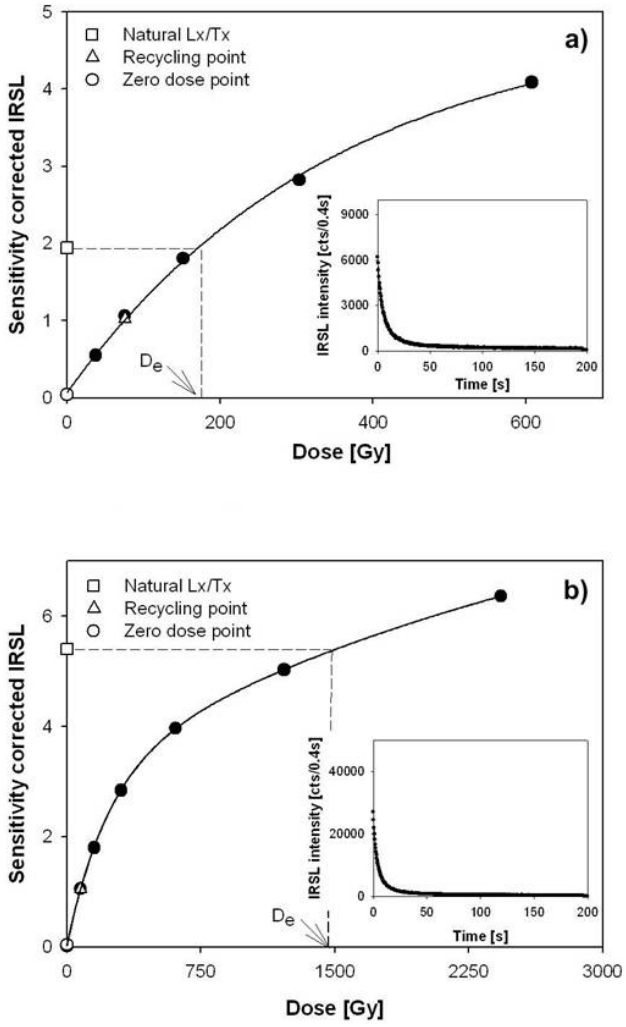

Fig. III.20: Dose response and natural decay curves for the post-IR IRSL measurements at 290°C. a) Dose response curve for sample 1399, representative of younger samples. The natural L_x/T_x lies in the linear part of the curve. b) Dose response curve for sample 1407, representative of older samples. The natural L_x/T_x approaches saturation. The insets show the IRSL intensity against time (200 s).

III.3.5.3 IRSL measurements at 50°C

The luminescence characteristics and SAR performance for IRSL at 50°C presented here are part of the post-IR IRSL measurements at 225°C. Thus, the data originates from the same aliquots measured in the post-IR IRSL protocol but the decay curves of the IRSL at 50°C stimulations are used for all calculations (Table III.11). For D_e determination the initial 2.4 s of the decay curve were used after subtracting a background from the last 60 s.

The dose response curves for samples 1399 and 1407 are shown in Figure III.21. Recycling ratios for all samples are all within 10% of unity (Table III.12 and Fig. III.18a), and recuperation varies between 0.4 ± 0.02% (n=6; sample 1407) and 6.7 ± 0.4% (n=6; sample 1398). The high recuperated signal of sample 1398 is unusual compared to the other values, which are all below 2% (Fig. III.18b).

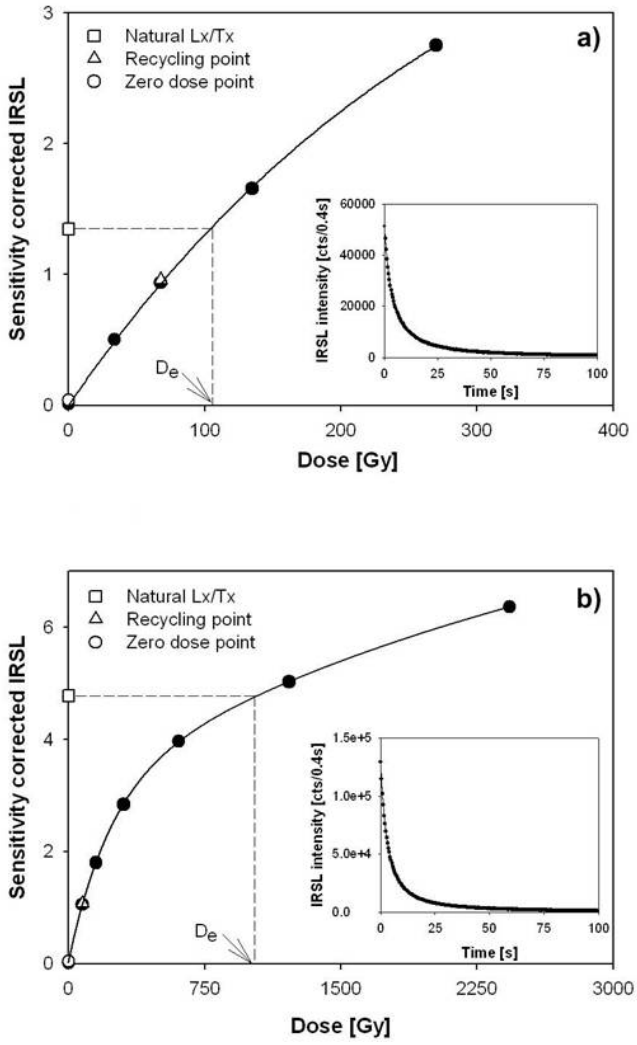

Fig. III.21: Dose response and natural decay curves for the IRSL measurements at 50°C as part of the post-IR IRSL measurements at 225°C, i.e. the same aliquots are used. a) Dose response curve for sample 1399, representative of younger samples. The natural L_x/T_x lies in the linear part of the curve. b) Dose response curve for sample 1407, representative of older samples. The natural L_x/T_x is beyond the linear part of the curve, nevertheless nowhere near saturation. The insets show the IRSL intensity against time (100 s).

The residual signals are equivalent to 1.5 ± 0.2 Gy (n=9). Without subtraction of the residual signals the measured to given dose ratios vary between 1.09 ± 0.02 (n=3; sample 1399) and 1.11 ± 0.04 (n=3; sample 1409; Fig. III.19a), whereas after subtraction the ratios lie between 1.08 ± 0.02 (n=3; sample 1399) and 1.10 ± 0.04 (n=3; sample 1409; Fig. III.19b). Although the results are within 10% of unity there does seem to be a systematic tendency to overestimate the given dose. Nevertheless, we consider these results acceptable, because they are within the 10% range.

III.3.6 Comparison of the fading rates and ages derived from the different signals

The laboratory fading rates for all samples and signals are listed in Table III.12 and plotted in Fig. III.22. The mean fading rate for IRSL at 50°C is 3.3 ± 0.4%/decade (excluding the two outliers 1398 and 1400), 2.1 ± 0.3%/decade for post-IR IRSL at 225°C, and 1.0 ± 0.4%/decade for post-IR IRSL at 290°C, confirming that post-IR IR stimulation at higher temperatures reduces fading (Thomsen et al., 2008).

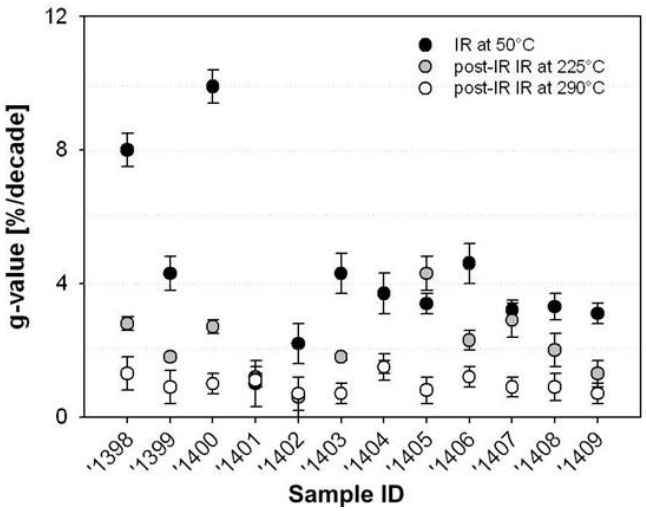

Fig. III.22: Comparison of laboratory fading rates [%/decade] for all samples using the different (post-IR) IRSL signals. Lowest fading rates are observed for the post-IR IRSL measurements at 290°C. For details about laboratory fading measurements see text.

The fading rates for the IRSL measurements at 50°C vary between 1.0 ± 0.7%/decade (sample 1401) and 9.9 ± 0.5%/decade (sample 1400) and are much higher than for the post-IR IRSL measurements, with the exception of sample 1401; the latter has a fading rate comparable to those of the post-IR IRSL signals (Fig. III.22). If this sample indeed does not fade significantly, then the various (uncorrected) D_e values should be similar, and ages should be indistinguishable. This, however, is not observed; the D_e values for the post-IR IRSL signals are significantly higher than for the IRSL measurement at 50°C and as a result the

ages do not agree (Table III.12 and Fig. III.23). Unexpectedly, for sample 1405 the laboratory fading rate of the IRSL signal at 50°C is slightly lower (3.4 ± 0.3%/decade) than that of the post-IR IRSL signal at 225°C (4.3 ± 0.5%/decade); the post-IR IRSL at 290°C fading rate is much lower (0.8 ± 0.4%/decade) than for both the other signals. Given the fact that our aliquots are made up of many hundreds of thousands of grains, which ought to result homogeneous luminescence behaviour, the variability observed in the fading rates, especially for the IR at 50°C signal, is surprising and difficult to explain; although it could originate from e.g. a change in source area, it seems more likely that it reflects some unknown laboratory source of variability.

Thiel et al. (2011a) measured fading rates of 1-1.5%/decade using the post-IR IRSL signal measured at 290°C for their polymineral fine-grain samples; they argued that because the natural signals from these samples were in saturation on a laboratory growth curve, it was unlikely that the natural signal had faded significantly. In addition, they also measured a fading rate of ~1%/decade for fine-grained quartz dominated by a fast OSL component; it seems clear that at the very least their post-IR IRSL signal did not fade any more than the blue-stimulated OSL signals from quartz. It may be that fading rates below 1%/decade are not meaningful, and in fact reflect systematic errors in laboratory fading measurements.

We have confirmed that for the higher temperature signals smaller fading rates are obtained and as a consequence it is expected that the fading uncorrected ages of the IRSL signal at 50°C ought to be younger than for any post-IR IRSL measurement. If fading measurements and fading corrections are applicable (Huntley and Lamothe, 2001), and if post-IR IRSL at 290°C does not show significant anomalous fading as suggested by Thiel et al. (2011a, submitted), fading corrected IRSL ages at 50°C and fading corrected post-IR IRSL ages at 225°C should be indistinguishable from fading uncorrected ages for the post-IR IRSL at 290°C, at least over the dose range for which the Huntley and Lamothe (2001) correction may be applicable in practice (~200 Gy; Buylaert et al., 2011). The fading uncorrected and fading corrected ages are listed in Table III.12 and shown in Figure III.23. We assume that the post-IR IRSL at 290°C gives the most accurate age estimates because there is evidence that these signals do not fade in nature (Thiel et al., 2011a, submitted); this can also be concluded from sample 1405, which is in or close to saturation, since laboratory saturation in feldspar is only possible when fading is negligible.

As expected, the fading uncorrected ages of the IRSL signal at 50°C (showing the largest fading rates) underestimates compared to the post-IRSL at 290°C (Fig. III.23a); the age underestimation is most evident for the older samples. On the other hand, uncorrected post-IR IRSL at 225°C ages only slightly underestimate compared to post-IR IRSL at 290°C (Fig. III.23b). The measured post-IR IRSL at 225°C laboratory fading rates (0.6 to 4.3%/decade; Table III.23), at least when >1%/decade, are probably significant, and it seems clear that the post-IR IRSL at 225°C needs fading correction. A similar observation was made by Buylaert et al. (2009) for their Eemian samples (see supplementary table in Buylaert et al., 2009). The

fading corrected ages for post-IR IRSL at 225°C are plotted against corrected ages for post-IR IRSL at 290°C in Figure III.23c, and against uncorrected ages for post-IR IRSL at 290°C in Figure 11d. It is recognised that the correction model is theoretically not applicable at higher doses, but such qualifications become of second order importance when the correction is so small. The fading correction for post-IR IRSL at 290°C is, on average, < 10% of the age and so Figures III.23c and III.23d are very similar. In both figures the agreement between the ages derived from the two signals is satisfactory with one exception (sample 1403), for which either post-IR IRSL at 225°C underestimates, or post-IR IRSL at 290°C overestimates.

The agreement between the fading corrected ages for IRSL at 50°C with the fading uncorrected (or corrected) ages for post-IR IRSL at 290°C is slightly poorer, especially for the older samples (> 100 ka; Fig. III.23e). Sample 1400, which has a fading rate of 9.9 ± 0.5%/decade resulted in a significantly overestimated age after correction of 679 ± 74 ka (Table III.12). This sample is well outside the applicable range of the Huntley and Lamothe (2001) correction model, but this should result in an underestimation, not overestimation; however, it is most likely that the fading rate for this sample is overestimated. A depositional age of >600 ka for this sample is unlikely not only from a stratigraphical point of view but also when compared with the post-IR IRSL age estimates. The overestimation is consistent with the observations of Reimann et al. (2011) using Holocene coastal sediments (to which the correction model is definitely applicable); they show that fading correction of the IRSL signal at 50°C for *g*-values >6 %/decade overestimates their depositional ages for which independent age control is available.

In most post-IR IRSL dating studies (e.g. Buylaert et al., 2009; Thiel et al., 2011a, 2011b; Reimann et al., 2011) it has been observed that a significant residual post-IR IRSL signal is present after daylight or solar simulator bleaching in the laboratory. Thomsen et al. (2008) showed in a bleaching experiment that there is no obvious difference in signal resetting between the IRSL at 50°C signal and the post-IR IRSL signal at 225°C. Nevertheless, using the same post-IR IRSL signal, Buylaert et al. (2009) found apparent residuals of up to 2 Gy for modern samples while residuals measured using IR at 50°C were ~0.5 Gy; either the two signals bleach to different degrees, or there are differences in thermal transfer. In contrast, Thiel et al. (2011a) measured laboratory residuals equivalent to 15-20 Gy for the post-IR IRSL signal at 290°C. For their samples it was difficult to decide on the relevance of these residual measurements to naturally bleached samples because there were no modern analogues available at their site. Again, some or all of the residual doses may have arisen through thermal transfer following the higher preheat temperature of 320°C. Thus it remains unclear to what degree the post-IR IRSL signals bleach more slowly than the IR at 50°C for these samples, or whether the differences are a result of the different preheat temperatures used (i.e. thermal transfer).

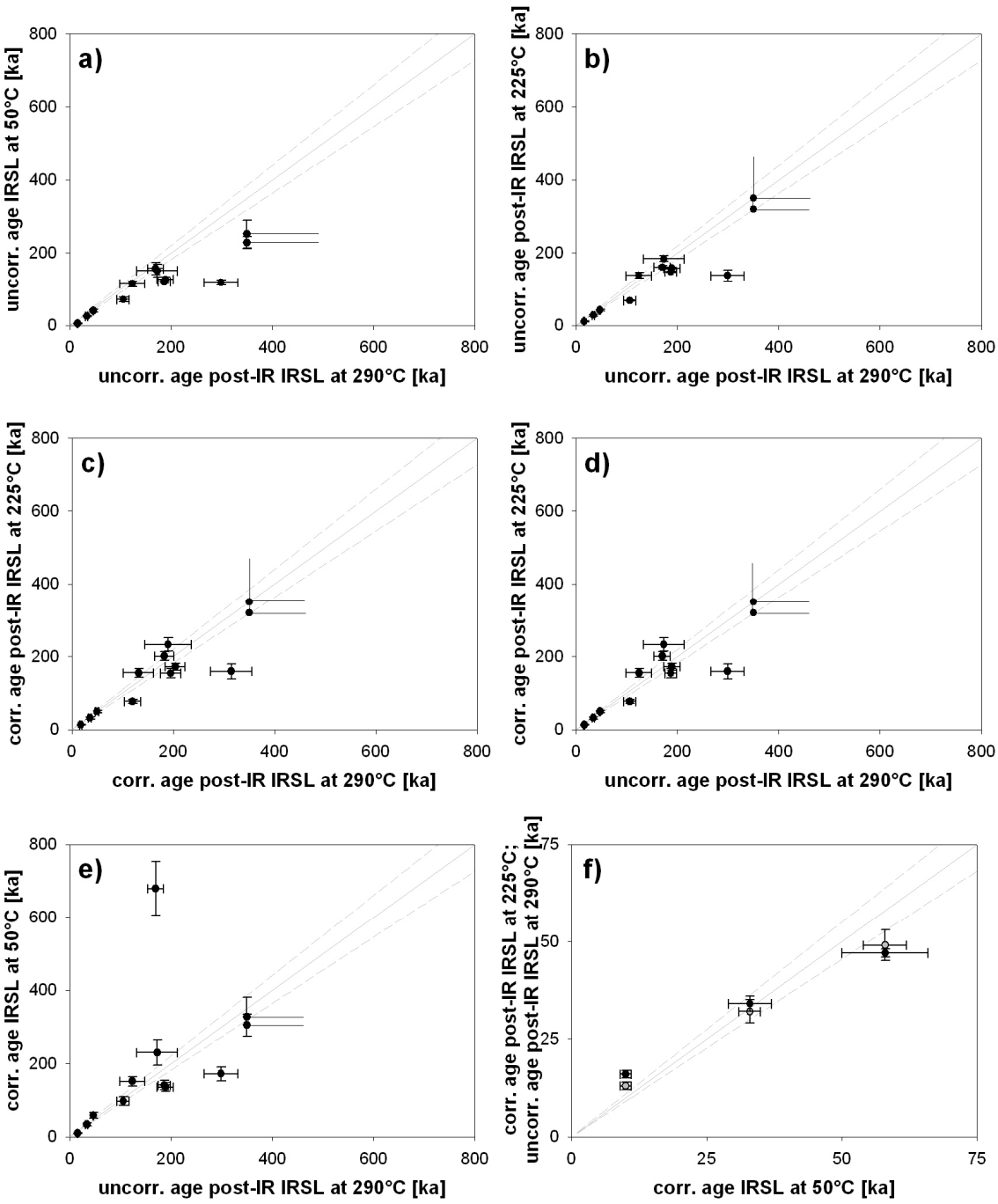

Fig. III.23: Comparison of ages for all samples using the different (post-IR) IRSL signals. The ages shown are without subtraction of the residuals. a) Fading uncorrected ages for IRSL at 50°C against fading uncorrected ages for post-IR IRSL at 290°C, b) fading uncorrected ages for post-IR IRSL at 225°C against fading uncorrected ages for post-IR IRSL at 290°C, c) fading corrected ages for post-IR IRSL at 225°C against fading corrected ages for post-IR IRSL at 290°C, d) fading corrected ages for post-IR IRSL at 290°C against fading uncorrected ages for post-IR IRSL at 290°C, e) fading corrected ages for IRSL at 50°C against fading uncorrected ages for post-IR IRSL at 290°C, and f) young (<70 ka) fading corrected ages for post-IR IRSL at 225°C (grey circles) and fading uncorrected ages for post-IR IRSL at 290°C (black circles) against corrected ages for IRSL at 50°C, to show the relative bleachability of the post-IR IRSL signals. Minimum ages are shown with open error bars. Solid line is a 1:1 line, and dashed lines represent ±10%.

None of the ages presented here have had a residual dose subtracted. From laboratory bleaching experiments, apparent residuals can vary between 1.5 ± 0.2 Gy (n=9) for IRSL at 50°C and 13 ± 2 Gy (n=9) for post-IR IRSL at 290°C. It is difficult to decide on the relevance of these residual measurements to naturally bleached samples (cf. Thiel et al., 2011a). In nature bleaching is likely to be episodic and take place over much longer times than is typical for laboratory bleaching experiments. One can test the size of any residual by determining the luminescence age on material of independently known young age, or by examining the dose in recently transported modern material (modern analogues). Unfortunately, there are no modern analogues available at our sites. To test the bleachability of the different IRSL signals the ages of the younger (<70 ka) samples are compared (Fig. III.23f). The IRSL at 50°C ages are taken as reference because there is good evidence in the literature that the signal can be bleached to very low levels (e.g. Huntley and Clague, 1996) and in this age range the fading correction is generally expected to yield accurate results (Huntley and Lamothe, 2001; Buylaert et al., 2011). For the youngest sample (sample 1398; IRSL at 50°C D_e: 15 ± 2 Gy), which might be expected to be significantly affected by residual doses, the post-IR IRSL ages are slightly older than the corrected IRSL age at 50°C. However, for this sample the corrected IRSL age at 50°C of 10 ± 1 ka seems, from a geological point of view too young, since there was no loess deposition in Lower Austria during the Holocene. The post-IR IRSL ages are thus closer to the expected age. This gives confidence that the post-IR IRSL signals are bleachable in nature, and as a result we do not subtract any residual from any of our ages. Nevertheless this assumption needs further testing using modern analogues and/or very young samples.

In summary, for young samples, for which the fading correction of the 225°C signal is likely to be accurate, both the fading corrected ages for post-IR IRSL at 225°C and the fading uncorrected ages for post-IR IRSL at 290°C seem to yield comparable results. For older samples any fading correction is likely to be increasingly inaccurate, and we favour the age estimates from the post-IR IRSL at 290°C, which apparently do not require significant fading correction (Thiel et al., 2011a, submitted). The following discussion on the chronological framework of the palaeosols is hence based on this IRSL signal unless otherwise stated.

III.3.7 Chronostratigraphy of the palaeosols

In Joching the loess unit J1 above the Cryosol complex (sample 1398) was dated to 16 ± 2 ka, whereas the ‘Bröckelsand’ (sample 1399) was dated to 47 ± 3 ka. This allows for formation of the Cryosol complex sometime between ~45 ka and ~20 ka. Cryosols in Lower Austria were described at Stratzing and luminescence dated to ~27-33 ka (Thiel et al., 2011a). This is in agreement with Haesearts et al. (1996), who have presented several radiocarbon ages (charcoal) from various sites in Lower Austria pointing to formation of the Cryosols between 27 and 39 ka. The loess unit J9 underlying the pedocomplex (sample 1400) was

dated to 170 ± 16 ka (MIS 6); it is therefore likely that the pedocomplex (unit J6-J8) developed during MIS 5; however, an unequivocal attribution to a sub-stage is not possible. Because the pedocomplex is composed of three horizons, it is possible that it comprises the entire MIS 5 with its sub-stages. The pedocomplex in Joching might thus be correlated with the 'Paudorfer Bodenbildung' (unit PI-3; Fig. III.14), which at its type locality in Paudorf developed during MIS 5. This is shown by the age of the loess unit PI-2 above the 'Paudorfer Bodenbildung' of 106 ± 12 ka (sample 1404), whereas the loess below (unit PI-4) gives an age of 159 ± 20 ka (post-IR IRSL at 225°C; sample 1403). Here, it has to be noted that the age of 299 ± 33 ka derived from post-IR IRSL at 290°C seems to be an overestimate; this is likely because the ratio of D_e's obtained (post-IR IRSL at 290°C/post-IR IRSL at 225°C) is for all samples <1.5, whereas for sample 1403 it is 2.1. Hence, for sample 1403, the fading corrected post-IR IRSL at 225°C age of 159 ± 20 (Table 3) seems the most reliable result and is, within errors, in agreement with the age of sample 1402 (unit PII-3), which also originates from below the 'Paudorfer Bodenbildung' (Fig. III.14) and was dated to 187 ± 12 ka. The individual soils of the 'Paudorfer Bodenbildung' might thus have formed during sub-stages of MIS 5. Originally the formation of the soil was attributed to a Würmian interstadial by Götzinger (1936); at that time it was not recognised as being a pedocomplex. Ložek (1976) revised the attribution of Götzinger (1936), because an interglacial mollusc fauna was found in the lowermost part of the 'Paudorfer Bodenbildung', i.e. the lower part of this pedocomplex developed most likely during MIS 5e. This is in agreement with our dating results and with the TL results of Zöller et al. (1994), who state that their age of 103 ± 11 ka below the 'Paudorfer Bodenbildung' at its type locality should be regarded as a minimum age. The attribution of the 'Paudorfer Bodenbildung' to MIS 3 as suggested by Noll et al. (1994) can clearly be dismissed.

At profile Paudorf II, the BC horizon, i.e. the weakly developed palaeosol (unit PII-8, Fig. III.14) is younger than 189 ± 16 ka (sample 1401); a correlation with other soils in this area remains unclear and needs further investigations. For the underlying pedocomplex (unit PII-10), which has been correlated with the 'Göttweiger Verlehmungszone', it can only be concluded that it has to be older than 189 ± 16 ka. Hence further investigations are needed to address the question whether this soil is equivalent to the 'Göttweiger Verlehmungszone', which is dated to >350 ka (sample 1405; minimum age based on $2*D_0$ for post-IR IRSL at 290°C; Wintle and Murray, 2006) at its type locality in Göttweig/Furth (Fig. III15a). Originally the 'Göttweiger Verlehmungszone' (unit GI-4) was attributed to MIS 5e (Götzinger, 1936), but Zöller et al. (1994) observed natural TL signals from above and below the 'Göttweiger Verlehmungszone' close to saturation and concluded that their ages of ~200 ka have to be interpreted as minimum ages. Furthermore, the alle/Ile ratio of *Pupilla* shells taken from loess immediately above the 'Göttweiger Verlehmungszone' soil is too high to be from penultimate glacial loess (Zöller et al., 1994). Smolíková (1994) suggest that this pedocomplex is perhaps of Holsteinian age, which at present is correlated with MIS 11. Our

minimum age is consistent with these findings. This age model is also supported by the dating of the loess sample 1407 above the tephra, 300 m upslope of Section I, which yielded ≥300 ka; the loess sample 1406 above the tephra was dated to 173 ± 40 ka, clearly showing a hiatus in the sequence. It has to be noted that the tephra, if found in other sequences, might be a useful Middle Pleistocene marker, dated to ≥300 ka.

At Section II (Göttweig/Aigen; Fig. III.15b) the loess unit GII-1 above the reworked loess (unit GII-2) and the pedocomplex (unit GII-3) is dated to 34 ± 3 ka (sample 1408) , and is thus in good agreement with Zöller et al.'s (1994) TL results of 28 ± 3 ka. They dated the loess below the pedocomplex to 107 ± 10 ka (regenerative dose method) and 119 ± 13 ka (additive dose method) and concluded that the soil formation lasted about 90 ka. Even though we have obtained a very similar age of 124 ± 25 ka for the loess from below the soil (sample 1409), we argue that there is certainly some break in the sedimentary record, rather than a long pedogenetic phase, because the pedocomplex is clearly eroded (indicated by the lack of an A horizon and a covering of reworked loess). Nevertheless, the age suggests that the pedocomplex exposed in Göttweig/Aigen corresponds with the 'Paudorfer Bodenbildung' at its type locality (Götzinger, 1936).

III.3.8 Conclusions

We have used two recently suggested post-IR IRSL dating protocols (Buylaert et al., 2009; Thiel et al., 2011a) to compare ages and so unravel the chronostratigraphy of prominent palaeosols in Lower Austria. In addition, we have compared the fading rates and ages derived from post-IR IRSL dating with IRSL at 50°C (measured as part of the post-IR IRSL measurements at 225°C).

The samples behave satisfactorily in the two post-IR IRSL SAR protocols, i.e. recycling ratios and dose recoveries are close to unity and recuperation is well below 5 % for most of the samples. The lowest laboratory fading rates are observed using the post-IR IRSL signal at 290°C, followed by post-IR IRSL at 225°C, and fading rates for IR at 50°C tend to be the highest. The fading rates of the post-IR IRSL at 290°C are in most cases below 1 %/decade, and based on the observations of Thiel et al. (2011a) we conclude that fading for this signal is probably negligible over geological time and so we do not attempt any fading correction of this signal. Good agreement between the ages derived from the post-IR IRSL signals and those from IRSL at 50°C on young samples shows that the post-IR IRSL signals are bleachable. Nevertheless it remains unclear whether the residual dose observed following laboratory bleaching, or some part of it, needs to be subtracted from the D_e. The fading corrected ages for post-IR IRSL at 225°C are in generally good agreement with the uncorrected ages for post-IR IRSL at 290°C. Both post-IR IRSL signals could be used for dating; we prefer the post-IR IRSL at 290°C because no fading correction seems to be needed, and so there are no dose/age limitations imposed by the use of a correction model. However,

one 290°C age appeared significantly overestimated in the stratigraphical context, which has to be a matter of future investigations.

We assign the 'Paudorfer Bodenbildung' at its type locality in Paudorf to MIS 5. It is furthermore very likely that the pedocomplex in Göttweig/Aigen developed during the same time and can hence be correlated with the 'Paudorfer Bodenbildung'. The same is true for the pedocomplex exposed in Joching. The absolute age of the 'Göttweiger Verlehmungszone' remains unclear due to saturation of the sample above this soil; the saturation implies an age >350 ka for the 'Göttweiger Verlehmungszone'. The discontinuities in sedimentation observed at these sites are hence significant. It has to be noted that sampling at higher resolution is needed to draw final conclusions on the extent of the discontinuities. The correlation of Lower Austrian loess deposits and their interleaved palaeosols thus remains problematic. Advances in absolute dating techniques such as post-IR IRSL dating are of importance to address the many remaining open questions on loess stratigraphy in the future.

Acknowledgements

This study was supported by the Leibniz Pakt Project for Research and Innovation 2008-2010. We are indebted to Bodo Damm for assistance during field work and to Sonja Riemenschneider for support in the laboratory. We thank Kristina Thomsen and Mayank Jain for fruitful discussions on post-IR IRSL dating. Sébastien Huot is thanked for the Excel macros which were used to calculate fading rates in a fast and elegant manner.

References

Adamiec, G., Aitken, M. J., 1998. Dose-rate conversion factors: update. Ancient TL 16, 37-50.

Aitken, M. J., 1985. Thermoluminescence Dating. Academic Press, London, 369 pp.

Aitken, M. J., 1998. An Introduction to Optical Dating. The Dating of Quaternary Sediments by the Use of Photon-stimulated Luminescence. Oxford University Press, 267 pp.

Auclair, M., Lamothe, M., Huot, S., 2003. Measurement of anomalous fading for feldspar IRSL using SAR. Radiation Measurement 37, 487-492.

Bayer, J., 1927. Der Mensch im Eiszeitalter, I. und II. Teil. Deutike, Wien.

Bøtter-Jensen, L., Andersen, C. E., Duller, G. A. T., Murray, A. S., 2003. Developments in radiation, stimulation and observation facilities in luminescence measurements. Radiation Measurements 37, 535-541.

Buylaert, J. P., Vandenberghe, D., Murray, A. S., Huot, S., De Corte, F., Van den Haute, P., 2007. Luminescence dating of old (>70 ka) Chinese loess: A comparison of single aliquot OSL and IRSL ages. Quaternary Geochronology 2, 9-14.

Buylaert, J. P., Murray, A. S., Thomsen, K. J., Jain, M., 2009. Testing the potential of an elevated temperature IRSL signal from K-feldspar. Radiation Measurements 44, 560-565.

Buylaert, J. P., Huot, S., Murray, A. S., Van den haute, P., in press. Infrared stimulated luminescence dating of an Eemian (MIS 5e) site in Denmark using K-feldspar. Boreas, doi: 10.1111/j.1502-3885.2010.00156.x.

Duller, G. A. T., Wintle, A. G., 1991. On infrared stimulated luminescence at elevated temperatures. Nuclear Tracks and Radiation Measurements 18, 379-384.

Fink, J., 1976. Exkursion durch den österreichischen Teil des nördlichen Alpenvorlandes und den Donauraum zwischen Krems und Wiener Pforte. Erweiterter Führer zur Exkursion aus Anlass der 2. Tagung der IGCP-Projektgruppe „Quaternary Glaciations in the Northern Hemisphere. Mitteilungen der Kommission für Quartärforschung der Österreichischen Akademie der Wissenschaften 1, 113 pp.

Frechen, M., Horváth, E., Gábris, G., 1997. Geochronology of Middle to Upper Pleistocene Loess Sections in Hungary. Quaternary Research 48, 291-312.

Frechen, M., Schweitzer, U., Zander, A., 1996. Improvements in sample preparation for the fine grain technique. Ancient TL 14, 15-17.

Götzinger, G., 1936. Das Lößgebiet um Göttweig und Krems an der Donau. Führer für die Quartär-Exkursionen in Österreich 1, 1-11.

Haesaerts, P., Damblon, F., Bachner, M., Trnka, G., 1996. Revised stratigraphy and chronology of the Willendorf II sequence, Lower Austria. Archaeologia Austriaca 80, 25-42.

Havliček, P., Holásek, O., Smolíková, L., Roetzel, R., 1998. Zur Entwicklung der Quartärsedimente am Südostrand der Böhmischen Masse in Niederösterreich. Jahrbuch der Geologischen Bundesanstalt 141, 51-72.

Head, M. J., Gibbard, P. L., Salvador, A., 2008. The Quaternary: its character and definition. Episodes 31, 234-238.

Huntley, D. J., Clague, J. J., 1996. Optical dating of tsunami-laid sands. Quaternary Research 46, 127-140.

Huntley, D. J., Lamothe, M., 2001. Ubiquity of anomalous fading in K-feldspars and the measurement and correction for it in optical dating. Canadian Journal of Earth Science 38, 1093-1106.

Kars, R. H., Wallinga, J., Cohen, K. M., 2008. A new approach towards anomalous fading correction for feldspar IRSL dating - tests on samples in field saturation. Radiation Measurements 43, 786-790.

Kunz, A., Frechen, M., Ramesh, R., Urban, B., 2010. Revealing the coastal event-history of the Andaman Islands (Bay of Bengal) during the Holocene using radiocarbon and OSL dating. International Journal of Earth Science (Geologische Rundschau). doi: 10.1007/ s00531-009-0507-4.

Lai, Z. P., Zhang, W. G., Chen, X., Jia, Y. L., Liu, X. J., Fan, Q. S., Long, H., in press. OSL chronology of loess deposits in East China and its implications for East Asian monsoon history. Quaternary Geochronology, doi:10.1016/j.quageo.2009.02.006.

Lamothe, M., Auclair, M., 1999. A solution to anomalous fading and age shortfalls in optical dating of feldspar minerals. Earth and Planetary Science Letters 171, 319-323.

Lamothe, M., Auclair, M., Hamzaoui, C., Huot, S., 2003. Towards a prediction of long-term anomalous fading of feldspar IRSL. Radiation Measurements 37, 493-498.

Ložek, V., 1976. Stop 8a/3: Hohlweg Aigen, Malakologie. In: Fink, J. (ed.). Exkursion durch den österreichischen Teil des nördlichen Alpenvorlandes und den Donauraum zwischen Krems und Wiener Pforte. Erweiterter Führer zur Exkursion aus Anlass der 2. Tagung der IGCP-Projektgruppe „Quaternary Glaciations in the Northern Hemisphere. Mitteilungen der Kommission für Quartärforschung der Österreichischen Akademie der Wissenschaften 1, 72-75.

Murray, A. S., Wintle, A. G., 2000. Luminescence dating of quartz using an improved single aliquot regenerative-dose protocol. Radiation Measurements 32, 57-73.

Murray, A. S., Wintle, A. G., 2003. The single aliquot regenerative dose protocol: potential for improvements in reliability. Radiation Measurements 37, 377-381.

Murray, A. S., Buylaert, J. P., Thomsen, K. J., Jain, M., 2009. The Effect of Preheating on the IRSL Signal from Feldspar. Radiation Measurements 44, 554-559.

Noll, M., Leitner-Wild, E., Hille, P., 1994. Thermoluminescence dating of loess deposits at Paudorf, Austria. Quaternary Geochronology (Quaternary Science Reviews) 13, 473-476.

Novothny, Á., Horváth, E., Frechen, M., 2002. The loess profile of Albertirsa, Hungary - Improvements in loess stratigraphy by luminescence dating. Quaternary International 95-96, 155-163.

Novothny, Á., Frechen, M., Horváth, E., Bradák, B., Oches, E. A., McCoy, W. D., Stevens, T., 2009. Luminescence and amino acid racemisation chronology of the loess-paleosol sequence at Süttő, Hungary. Quaternary International 198, 62-76.

Novothny, Á., Frechen, M., Horváth, E., Krbetschek, M., Tsukamoto, S., 2010. Infrared stimulated luminescence and radiofluorescence dating of aeolian sediments from Hungary. Quaternary Geochronology 5, 114-119.

Poolton, N. R. J., Ozanyan, K. B., Wallinga, J., Murray, A. S., Bøtter-Jensen, L., 2002. Electrons in feldspar II: a consideration of the influence of conduction band-tail states on luminescence processes. Physics and Chemistry Minerals 29, 217-225.

Prescott, J. R., Hutton, J. T., 1994. Cosmic ray contributions to dose rates for luminescence and ESR dating: large depths and long-term variations. Radiation Measurements 23, 497-500.

Rees-Jones, J., 1995. Optical dating of young sediments using fine-grain quartz. Ancient TL 13, 9-14.

Reimann, T., Tsukamoto, S., Naumann, M., Frechen, M., 2011. The potential of using feldspars for optical dating of young coastal sediments - a test case from Darss-Zingst peninsula (southern Baltic Sea coast). Quaternary Geochronology, in press.

Roberts, H. M., 2008. The development and application of luminescence dating to loess deposits: a perspective on the past, present and future. Boreas 37, 483-507.

Smolíková, L., 1994. Paleopedologický výzkum významných lokalit Paudorf, Göttweig, Krems a Stranzendorf. Zpr. Geol. Výzk. v Roce, 80.

Thiel, C., Buylaert, J. P., Murray, A. S., Terhorst, B., Hofer, I., Tsukamoto, S., Frechen, M., 2011. Luminescence dating of the Stratzing loess profile (Austria) - Testing the potential of an elevated temperature post-IR IRSL protocol. Quaternary International. doi:10.1016/j.quaint.2010.05.018.

Thiel, C., Buylaert, J. P., Murray, A. S., Tsukamoto, S., submitted. On the applicability of post-IR IRSL dating to Japanese loess. Geochronometria.

Thiel, C., Coltorti, M., Tsukamoto, S., Frechen, M., 2010. Geochronology for some key sites along the coast of Sardinia (Italy). Quaternary International 222, 36-47.

Thomsen, K. J., Bøtter-Jensen, L., Denby, P. M., Moska,, P., Murray, A. S., 2006. Developments in luminescence measurement techniques. Radiation Measurements 41, 768-773.

Thomsen, K. J., Murray, A. S., Jain, M., Bøtter-Jensen, L., 2008. Laboratory fading rates of various luminescence signals from feldspar-rich sediment extracts. Radiation Measurements 43, 1474-1486.

Wallinga, J., Bos, A. J. J., Dorenbos, P., Murray, A. S., Schokker, J., 2007. A test for anomalous fading correction in IRSL dating. Quaternary Geochronology 2, 216-221.

Wang, X. L., Lu, Y. C., Wintle, A. G., 2006. Recuperated OSL dating of fine-grained quartz in Chinese loess. Quaternary Geochronology 1, 89-100.

Watanuki, T., Murray, A. S., Tsukamoto, S., 2005. Quartz and polymineral luminescence dating of Japanese loess over the last 0.6 Ma: Comparison with an independent chronology. Earth and Planetary Science Letters 240, 774-789.

Wintle, A. G., Murray, A. S., 2006. A review of quartz optically stimulated luminescence characteristics and their relevance in single-aliquot regeneration dating protocols. Radiation Measurements 41, 369-391.

Zöller, L., Oches, E. A., McCoy, W. D., 1994. Towards a revised chronostratigraphy of loess in Austria with respect to key sections in the Czech Republic and in Hungary. Quaternary Geochronology (Quaternary Science Reviews) 13, 465-472.

IV

Testing the reliability of post-IR IRSL dating

IV.1 On the applicability of post-IR IRSL dating to Japanese loess

Thiel, C.[1,2], Buylaert, J.-P.[2,3], Murray, A. S.[2], Tsukamoto, S.[2]

[1] Leibniz Institute for Applied Geophysics, S3: Geochronology and Isotope Hydrology, Stilleweg 2, 30655 Hannover, Germany

[2] Nordic Laboratory for Luminescence Dating, Department of Earth Sciences, Aarhus University, Risø DTU, DK-4000 Roskilde, Denmark

[3] Radiation Research Division, Risø National Laboratory for Sustainable Energy, Technical University of Denmark, DK-4000 Roskilde, Denmark

Geochronometria, submitted in revised form (31.10.2010)

Abstract

Recent work on infrared stimulated luminescence (IRSL) dating has focussed on finding and testing signals which show less or negligible fading. IRSL signals measured at elevated temperature following IR stimulation at 50°C (post-IR IRSL) have been shown to be much more stable than the low temperature IRSL signal and seem to have considerable potential for dating. For Early Pleistocene samples of both European and Chinese loess natural post-IR IRSL signals lying in the saturation region of the laboratory dose response curve have been observed; this suggests that there is no significant fading in nature. As a contribution to the further testing of post-IR IRSL dating, we have used 18 samples from two Japanese loess profiles for which quartz OSL and tephra ages up to 600 ka provide age control. After a preheat of 320°C (60s), the polymineral fine grains (4-11 μm) were bleached with IR at 50°C (200 s) and the IRSL was subsequently measured at 290°C for 200 s. In general, the fading uncorrected post-IR IRSL ages agree with both the quartz OSL and the tephra ages. We conclude that the post-IR IRSL signal from these samples does not fade significantly and allows precise and accurate age determinations on these sediments.

Keywords: post-IR IRSL dating; fading; Japanese loess

Due to copyrights this manuscript is not included in the online version.
Please see the printed version or check the following webpage:
http://springerlink.com/content/1733-8387/

IV.2 IRSL and post-IR IRSL residual doses recorded in modern dust samples from the Chinese Loess Plateau

Buylaert, J.-P.[1,2,*], **Thiel, C**.[3], Murray, A. S.[1], Vandenberghe, D.[4], Yi, S. [5], Lu, H.[5]

[1] Nordic Laboratory for Luminescence Dating, Department of Earth Sciences, Aarhus University, Risø DTU, DK-4000 Roskilde, Denmark

[2] Radiation Research Division, Risø National Laboratory for Sustainable Energy, Technical University of Denmark, DK-4000 Roskilde, Denmark

[3] Leibniz Institute for Applied Geophysics, S3: Geochronology and Isotope Hydrology, 30655 Hannover, Germany

[4] Laboratory of Mineralogy and Petrology, Department of Geology and Soil Science, Ghent University, B-9000 Ghent, Belgium

[5] School of Geographical and Oceanographical Sciences, Nanjing University, Nanjing 210093, China

Geochronometria, submitted (08.10.2010)

Abstract

Using a set of modern/young (0 to about 200 years old) dust samples collected from the Chinese loess plateau the bleachability of IRSL measured at 50°C (IR_{50}) and post-IR_{50} elevated temperature IRSL (measured at 225°C and at 290°C) is investigated by measuring the apparent (residual) doses recorded by these signals. Doses recorded by quartz OSL are used as a reference. Allowing for differences in dose rates it seems that both IRSL and post-IR IRSL signals yield residual doses that are significantly larger than the doses measured in quartz. These residual doses can largely be explained by thermal transfer caused by preheating. Nevertheless, one probably should not use a low preheat (<200°C) with IR_{50} to date loess samples because, as has been reported before, the signal appears to be thermally unstable. In general, we conclude that it may not be advisable to apply post-IR IRSL dating to relatively young (Late Holocene) Chinese loess samples where residuals of up to ~20 Gy are a significant fraction of the total dose. However, these residuals quickly become unimportant when dating older loess, and this is the age range in which post-IR IRSL dating is likely to be most useful.

Keywords: modern dust, IRSL, polymineral fine-grains, post-IR IRSL, loess, China

Due to copyrights this manuscript is not included in the online version.
Please see the printed version or check the following webpage:
http://springerlink.com/content/1733-8387/

V

Summary and conclusions

V.1 Summary

The overall aim of this doctoral thesis was to test the applicability of post-IR IRSL dating to different environments in order to set up reliable geochronological framework especially for deposits older than Eemian. The study concentrated on coastal and shallow marine deposits from Sardinia as well as loess and loess like deposits from Austria, Japan and China.

Because most of the Sardinian coastal and shallow marine sediments under investigation showed either saturation for the quartz or feldspar inclusions, it was made use of post-IR IRSL dating (***Chapter II.1***). The fading rates could be reduced by a factor of two and the fading correction was thus less reliant on the untestable assumptions incorporated in the fading correction model (Huntley and Lamothe, 2001). The luminescence ages clearly point to deposition during MIS 5 for most of the investigated sedimentary units; some deposits are even older. Problems in this study arose due to significant disagreement of the luminescence ages with radiocarbon dating, which resulted in Holocene and slightly older ages. However, because the quartz dose response curves were clearly saturated for most of the samples, Holocene ages can be clearly excluded. The only cause of significant age overestimation in OSL dating is incomplete bleaching, which is typical for (glacio-)fluvial environments (e.g. Rittenour, 2008; Fuchs and Owen, 2008) but not coastal deposits (e.g. Jacobs, 2008). Incomplete bleaching could be excluded based on testing the dose distributions of small aliquots, which are able to reflect differences in signal resetting. Furthermore, both quartz OSL and feldspar post-IR IRSL, despite different luminescence behaviour, resulted in MIS 5 and older ages. It was hence concluded that the luminescence ages are more reliable than the radiocarbon ages, but it was acknowledged that further investigations are needed to clarify the discrepancies.

At the former brickyard in Langenlois (Lower Austria) fluvial deposits, loess derivatives and loess are exposed (***Chapter III.1***). The distinctively altering weathering degrees of the sediments at this site indicate different depositional ages and thus distinct landscape forming phases. Following the post-IR IRSL dating protocol proposed by Buylaert et al. (2009) one fluvial sample and five loess samples were dated to constrain the sedimentary and erosion processes in time.

The observed luminescence characteristics for the polymineral fine grain samples for both the IR_{50} signal and the $pIRIR_{225}$ signal were found to be equivalent to those of sand-sized potassium feldspar (Buylaert et al., 2009), and the obtained luminescence ages are considered reliable based on the good performance of standard laboratory tests (Murray and Wintle, 2003). The fading rate of the $pIRIR_{225}$ signal was measured to be reduced by at least 1%/decade compared to the IR_{50} signal. The fluvial layer and the underlying loess derivative, both showing very intense weathering, were dated to the Middle Pleistocene; this is coherent

with an interglacial fauna assemblage found in the fluvial layers. The loess deposits were dated to 35-55 ka, showing a great discontinuity and superposition of the much older slopes.

Making use of an enhanced post-IR IRSL dating protocol, which used higher preheat and correspondingly higher post-IR IR stimulation temperatures ($pIRIR_{290}$), nine samples from the loess/palaeosol sequence at the tennis court in Stratzing (Lower Austria) were dated (***Chapter III.2***). Based on the observations that the fading rate decreases with increasing stimulation temperatures (Thomsen et al., 2008) even lower fading rates for $pIRIR_{290}$ than for $pIRIR_{225}$ were expected. Most interestingly, using these temperature settings a sample from below the Brunhes/Matuyama boundary (~780 ka), which is expected to be in field saturation (expected dose ~2.7 kGy), was apparently in saturation on a laboratory generated growth curve. This implies that fading is negligible for $pIRIR_{290}$, i.e. this signal seems to be not dependent on any fading correction.

In contrast to these observations, a *g*-value of ~1-1.5%/decade was measured for the samples under investigation. To test whether these fading rates are meaningful, fading tests were conducted for fine grain quartz, which is known not to fade; the measurements resulted in *g*-values of ~1%/decade. It was concluded that the laboratory fading rate is not equivalent to the apparent fading rate, i.e. to the amount of anomalous fading that occurs on nature. Therefore the fading uncorrected $pIRIR_{290}$ ages were chosen as being the most reliable age estimates using polymineral fine grains. The choice was confirmed by the good agreement of the $pIRIR_{290}$ age with a radiocarbon age (cluster of many radiocarbon ages).

It could be shown that the pedocomplex found in the loess sequence is ≥ MIS 7, which indicates a prolonged discontinuity in this loess/palaeosol sequence.

Because nothing was known about the differences in equivalent doses, fading rates and correspondingly the ages of $pIRIR_{225}$ and $pIRIR_{290}$, in total twelve loess samples were dated making use of both measurement procedures (***Chapter III.3***). For comparison, the equivalent doses, the fading rates and the ages of IR_{50} (as part of the $pIRIR_{225}$ measurement cycle) were also investigated. The performance tests were all satisfactory, and the laboratory fading rates for $pIRIR_{290}$ have the tendency to be the lowest; in most cases they are below 1 %/decade. This is in agreement with the observations at Stratzing. It was hence concluded that no fading correction is needed for $pIRIR_{290}$, whereas for $pIRIR_{225}$ it ought to be applied. Unfortunately, the agreement of fading corrected $pIRIR_{225}$ ages with fading uncorrected $pIRIR_{290}$ ages was not satisfactory for all samples; there is a tendency for the $pIRIR_{225}$ to underestimate the $pIRIR_{290}$ ages (or the $pIRIR_{290}$ ages overestimate the $pIRIR_{225}$ ages). This could be either due to the limited range of the fading correction model (Huntley and Lamothe, 2001) or due to a larger residual signal for $pIRIR_{290}$, which would lead to an overestimation. The latter is less likely because by comparing the fading corrected IR_{50} ages of the young samples (for which the fading correction model is applicable) with the fading uncorrected $pIRIR_{290}$ ages it could

be shown that the $pIRIR_{290}$ signal can be reset in nature. However, at this stage it remained unclear to which extent thermal transfer influences the age estimates.

The dating results show that the pedocomplex 'Göttweiger Verlehmungszone' in Göttweig (Furth) is ≥ MIS 9. The Paudorfer Bodenbildung could be attributed to MIS 5, but it remains unclear whether this pedocomplex comprises all three substages, i.e. MIS 5e, MIS 5c, and MIS 5a. To address this question, luminescence dating at higher resolution is needed. It could also be shown that the pedocomplex exposed in Joching is equivalent to the Paudorfer Bodenbildung.

The studies in Sardinia and Austria were hampered by the lack of reliable independent age control, and thus post-IR IRSL dating was applied to two Japanese loess sequences for which reliable chronologies exist (***Chapter IV.1***).

Interestingly the fading measurements for IR_{50} resulted in negative *g*-values, which is indicating recuperation during storage of the aliquots. On the contrary, the dose recovery results are very satisfactory, which would imply that reliable ages can be obtained using this signal. However, the (fading uncorrected) IR_{50} ages largely underestimate the expected age. The fading rates for $pIRIR_{290}$ are close to zero, but due to recuperation observed for IR_{50} (measured on the same aliquots), these negligibly small *g*-values cannot be trusted even though they are equivalent to $pIRIR_{290}$ *g*-values observed in the other loess studies (Chapter 4 and 5). The argument of not correcting for any fading is, similar to the dating study in Stratzing (Chapter 4), based on the fact that a natural luminescence signal from a sample below B/M-boundary was found in saturation on a laboratory generated growth curve. The reliability of this observation and thus the reliability of the dating procedure were confirmed by the good agreement with independent age control. For the younger samples the $pIRIR_{290}$ slightly overestimated the expected ages, which could be due to a residual signal.

All of the post-IR IRSL dating studies had in common that a residual signal of up to 20 Gy was measured. It was not clear how much of this residual is a result from different bleaching behaviour of the various IRSL signals, and how much originates from thermal transfer. A set of modern dust samples from China was used to investigate these issues (***Chapter IV.2***).

It was found that there is clear evidence for thermal transfer in the IRSL signals from the polymineral fine grains. It was hence presumed that most of the residual dose recorded arises from thermal processes rather than from different bleaching behaviour; the latter cannot be completely excluded but will be of minor importance. The largest residual doses were recorded for $pIRIR_{290}$; on average the residual dose is 10 ± 2 Gy. Lower preheats, which might reduce thermal transfer, are not advisable for the post-IR IRSL measurements because there will be a TL contribution arising from the high temperature post-IR IR stimulation. Because of the apparent residual doses measured on modern material, post-IR IRSL dating in its current form is not applicable to (Late) Holocene Chinese loess samples.

V.2 Conclusions and future directions

In conclusion, post-IR IRSL dating is applicable to the environments under investigation, and it could be shown that it is also suitable for polymineral fine grain samples. The post-IR IRSL dating application in Sardinia showed that sedimentary units older than Eemian can now be dated. Due to the comparably large dose rate (~3.5-4 Gy) in European loess the dateable age limit is ~300-350 ka for this environment. The Japanese loess exhibited rather low dose rates and thus dating up to ~600 ka was feasible. Speaking in doses, which is more appropriate due to the dependency of dose rate on the dating limit, the dateable age range is equivalent to ~1500 Gy.

The lower age limit seems to be hampered due to thermal transfer, which results in artificial doses (residuals) on top of the natural doses. For older samples any residual will become of second order importance and thus it is clearly possible to use this technique to extend the age range in luminescence dating. However, the long term aim ought to be a dating procedure which can be applied to both young and old samples. Apart from addressing this issue in further research detailed investigations on the difference of the physical behaviour of pure K-feldspar and polymineral fine grain extracts are needed. For loess dating polymineral fine grains have been, and will be, the preferred material (e.g. Roberts, 2008). The mineralogical composition of loess is known to the extent that it is made up of quartz, feldspar, mica, carbonates and heavy minerals (e.g. Zheng et al., 1994). Prior to luminescence measurements the carbonates are removed with hydrochloric acid, and the quartz is not contributing to the IRSL signal measured in the blue emission spectrum (Aitken, 1998). Because the luminescence intensity of feldspar is large compared to other minerals, it can be confidentially assumed that the IRSL and thus the post-IR IRSL signal is dominated by feldspar. However, using fine grained material, not only K-feldspar but also sodium-rich (Na) and calcium-rich (Ca) feldspars (plagioclase) can be present. Little is known about the IRSL of these other feldspars (e.g. Krause et al., 1997) and as yet no studies exist on post-IR IRSL. Due to different thermal stabilities of Na- and K-feldspar, and polymineral fine grains and sand-sized K-feldspar (Li and Wintle, 1992) there is a need for investigating the post-IR IRSL behaviour of Na- and Ca-feldspars. The very satisfactory agreement of independent age control with the post-IR IRSL dating results of the Japanese loess gives confidence that the measurement conditions can be used for mixed feldspar extract despite different thermal stabilities.

Of great importance in further research will furthermore be investigations on the ideal way to conduct dose recovery tests. In quartz OSL dating it is generally accepted that any dose measurement protocol should be able to recover a known dose (Murray and Wintle, 2003). For some of the deposits investigated during the dissertation project the dose recovery experiments using laboratory bleached samples did not always produce satisfactory results. It seems that when working with post-IR IRSL dating (i.e. two IRSL signals in one measurement), dose recovery tests seem to be problematic. In some studies the dose recovery

for the IR_{50} is satisfactory but the same signal cannot be used for dating for several reasons (e.g. Japanese loess). It needs to be addressed how meaningful such dose recovery experiments are and to which degree we can trust these experiments. In general, it seems that the given doses can only be appropriately recovered for one of the signals (either IR_{50} or post-IR IRSL), but not for both. Parts of this may arise from different bleachability of the signals, and the problem that bleaching in the laboratory is not equivalent to bleaching in nature. Therefore, dose recovery experiments using naturally bleached samples, i.e. young samples or modern analogues to which a known dose is added, are usually much more satisfactory (cf. study on modern dust). This suggests that the laboratory bleaching experiments of the samples cannot reproduce natural conditions. To allow for post-IR IRSL dating without the repeated need of comparison with independent age control, a reliable and meaningful dose recovery procedure has to be found.

Following the above mentioned statements it can be concluded that post-IR IRSL dating is a very promising technique to extend the dateable age range. So far this method has only systematically been tested on aeolian and shallow marine deposits for which incomplete bleaching can be excluded. To be able to address whether this dating technique is applicable to the entire range of Quaternary deposits, further dating studies, preferentially with independent age control are needed.

References

Aitken, M. J., 1998. An Introduction to Optical Dating. Oxford University Press, Oxford, UK.

Buylaert, J.-P., Murray, A. S., Thomsen, K. J., Jain, M., 2009. Testing the potential of an elevated temperature IRSL signal from K-feldspar. Radiation Measurements 44, 560-565.

Fuchs, M., Owen, L. A., 2008. Luminescence dating of glacial and associated sediments: review, recommendations and future directions. Boreas 37, 636-659.

Huntley, D. J., Lamothe, M., 2001. Ubiquity of anomalous fading in K-feldspars and the measurement and correction for it in optical dating. Canadian Journal of Earth Science 38, 1093-1106.

Jacobs, Z., 2008. Luminescence chronologies for coastal and marine sediments. Boreas 37, 508-535.

Krause, W. E., Krbetschek, M. R., Stolz, W., 1997. Dating of Quaternary lake sediments from the Schirmacher Oasis (East Antartica) by infra-red stimulated luminescence (IRSL) detected at the wavelength of 560 nm. Quaternary Science Reviews 16, 387-392.

Li, S.-H., Wintle, A. G., 1992. A global view of the stability of luminescence signals from loess. Quaternary Science Reviews 11, 133-137.

Murray, A. S., Wintle, A. G., 2003. The single aliquot regenerative dose protocol: potential for improvements in reliability. Radiation Measurements 37, 377-381.

Rittenour, T. M., 2008. Luminescence dating of fluvial deposits: applications to geomorphic, palaeoseismic and archaeological research. Boreas 37, 613-635.

Roberts, H. M., 2008. The development and application of luminescence dating to loess deposits: a perspective on the past, present and future. Boreas 37, 483-507.

Zheng, H., Theng, B. K . G ., Whitton, J. S., 1994. Mineral Composition of Loess-Paleosol Samples from the Loess Plateau of China and Its Environmental Significance. Chinese Journal of Geochemistry 13(1), 61-72.

Acknowledgements/Danksagung

Die Liste derer, die mich während meiner Dissertation und darüber hinaus begleitet haben, ist lang - und ebenso vielfältig ist die Art der Unterstützung.

Allen vorab danke ich meinem Doktorvater Prof. Dr. Manfred Frechen für die fachliche Betreuung dieser Arbeit. Seine Offenheit hinsichtlich neuer Ideen und die damit verbundenen Freiheiten haben maßgeblich zum Gelingen dieser Arbeit beigetragen. Manfred, durch deine konstruktive Kritik fühle ich mich nun gestärkt für die weitere wissenschaftliche Laufbahn.

Weiterhin danke ich allen Mitgliedern des Prüfungsausschusses (FB Geowissenschaften) der Freien Universität Berlin für die Zeit und Arbeit, die sie in mein Dissertationsverfahren investiert haben.

I am thankful for all the opportunities I got at the Nordic Laboratory for Luminescence Dating. I would like to express my gratitude to Prof. Dr. Andrew Murray who strongly supported me. Andrew, your personal and scientific drive has inspired me - and your encouragement was crucial for my decision to continue in science!

I am very grateful to Dr. Jan-Pieter Buylaert for his never-ending support, his encouraging words and for the many cheerful moments we shared in Risø. Jan-Pieter, after several difficult months you were one of the first who had confidence in me and my work - I appreciate this a lot and I will never forget it!

Bei Dr. Sumiko Tsukamoto möchte ich mich für die Einführung in die Lumineszendatierung sowie für die kollegiale Unterstützung bedanken. Ohne dich, Sumiko, wäre es mir niemals gelungen, so schnell so viel über die methodischen Feinheiten der Lumineszenzdatierung zu lernen. Ich weiß es sehr zu schätzen, dass du oftmals deine eigenen Arbeiten nach hinten angestellt hast, um mal wieder einem meiner Anliegen nachzukommen.

Meine Arbeiten in Niederösterreich wurden von vielen lieben Menschen begleitet. Allen voran sei Prof. Dr. Birgit Terhorst gedankt, die mich nicht nur in die Lössstratigraphie Österreichs eingeführt, sondern auch durch viele Diskussionen meine Arbeiten unterstützt hat. Birgit, ich danke dir herzlich für die Möglichkeiten, die du mir geboten hast und für deine Geduld mit mir!
Dipl.-Geogr. Ingo Hofer und Dipl.-Geogr. Iva Jaburová danke ich für die Unterstützung im Gelände. Ingo, dir sei zudem gedankt für die Gastfreundschaft in Wien und die Gespräche über Gott und die Welt. Des Weiteren gilt mein Dank Dr. Reinhard Roetzel für die Privatexkursion zu Lössen Niederösterreichs und Dr. Florian Fladerer für die Einblicke in die Quartärpaläontologie. Prof. Dr. Bodo Damm danke ich sowohl für die Unterstützung bei Geländearbeiten als auch für die fachlichen Gespräche.

Besonderer Dank gilt Dr. Melanie Sierralta für ihr offenes Ohr und ihre weit über den kollegialen Alltag hinausgehende Unterstützung. Melanie, ich werde die vielen kurzen und langen Gespräche genauso vermissen wie die gemeinsamen Fahrten zur Arbeit.

Natürlich möchte ich mich auch ganz herzlich bei allen Techniker/innen der Sektion S3 am Leibniz-Institut für Angewandte Geophysik, Hannover, bedanken. Durch eure Unterstützung, sei es bei Computerproblemen oder bei analytischen Fragestellungen, wurde mir der Arbeitsalltag sehr erleichtert. Besonderer Dank gilt dabei Sonja Riemenscheider, die mich in die Aufbereitung der Lumineszenzproben eingeführt und mir zum Ende hin auch einen großen Teil der Laboranalytik abgenommen hat. Sonja, danke für die gute Zusammenarbeit, deine Hilfe bei Laborfragen und deine aufmunternden Worte. Gudrun Drewes sei neben technischer Unterstützung für ihre Herzlichkeit und ihre liebe Art gedankt. Durch dich, Gudrun, wurde mir so mancher Tag im Institut verschönert!

During my dissertation project I spent more than seven months in Risø, Denmark. I appreciated the welcoming atmosphere and the support of all technicians and engineers. Dr. Kristina Thomsen, Dr. Christina Ankjærgaard, Dr. Mayank Jain and Reza Sohbati are thanked for the encouragement and the constructive discussions - and, of course, for all the cheerful moments!

Bodil Graae warmly welcomed me and gave me a home in Denmark- inclusive of three cuddly cats! Bodil, I thank you so much for your heartiness, for the nice dinners and the inspiring discussions.

I am furthermore grateful to my luminescence and non-luminescence colleagues and friends for the constructive discussions during diverse conferences, workshops and field trips. Funnily enough, I am especially thankful to Prof. Dr. Mauro Coltorti, who, most likely unintentionally, strengthened my scientific opinion. Mauro, you once said that I have to learn a lot - and yes, I did learn a lot!

Manche Dinge lassen sich kaum in Wort fassen - und so ist es auch mit dem Folgenden: Meinen Eltern Monika und Gerhard und meinem Bruder Thomas möchte ich danken für das Vertrauen in mich und für all die Liebe, die sie mir zuteil kommen lassen. Was ich bin und wie ich bin, habe ich euch zu verdanken! Thomas, du hast mir zudem immer wieder gezeigt, dass Hürden im Leben da sind, um überwunden zu werden!

Mein Robin, ich danke dir für die unausgesprochene und unaussprechliche Unterstützung, vor allem jedoch für deinen immerwährenden Optimismus, der mich in schwierigen Zeiten jedes Mal wieder aufgebaut hat.

Curriculum vitae

Der Lebenslauf ist in der Online-Version aus Gründen des Datenschutzes nicht enthalten.

Publications and conference contributions

Peer-reviewed publications

(10) Buylaert, J.-P., **Thiel, C.**, Murray, A. S., Vandenberghe, D. A. G., Yi, S., Lu, H., submitted. IRSL and post-IR IRSL residual doses recorded in modern dust samples from the Chinese Loess Plateau. Geochronometria.

(9) **Thiel, C.**, Terhorst, B., Jaburova, I., Buylaert, J.-P., Murray, A. S., Fladerer, F. A., Damm, B., Frechen, M., Ottner, F., in press. Sedimentation and erosion processes in Middle to Late Pleistocene sequences exposed in the brickyard of Langenlois/Lower Austria. Geomorphology.

(8) **Thiel, C.**, Klotz, S., Uhl, D., in press. Palaeoclimate estimates for selected leaf floras from the Late Pliocene (Reuverian) of Central Europe based on different palaeobotanical techniques. Turkish Journal of Earth Science.

(7) Frank, C., Terhorst, B., Damm, B., **Thiel, C.**, Frechen, M., Peticzka, R., in press. Pleistocene loess deposits and mollusk assemblages in the Eastern Pre-Alps. Quaternary Science Journal (E&G).

(6) **Thiel, C.**, Buylaert, J.-P., Murray, A. S., Tsukamoto, S., submitted. On the applicability of post-IR IRSL dating to Japanese loess. Geochronometria.

(5) **Thiel, C.**, Buylaert, J.-P., Murray, A. S., Terhorst, B., Tsukamoto, S., Frechen, M., in press. Investigating the chronostratigraphy of prominent palaeosols in Lower Austria using post-IR IRSL dating. Quaternary Science Journal (E&G).

(4) **Thiel, C.**, Buylaert, J.-P., Murray, A.S., Terhorst, B., Hofer, I., Tsukamoto, S., Frechen, M., 2011. Luminescence dating of the Stratzing loess profile (Austria) - Testing the potential of an elevated temperature post-IR IRSL protocol. Quaternary International; doi: 10.1016/j.quaint.2010.05.018.

(3) **Thiel, C.**, Coltorti, M., Tsukamoto, S., Frechen, M., 2010. Geochronology for some key sites along the coast of Sardinia (Italy). Quaternary International 222, 36-47.

(2) Günther, A., **Thiel, C.**, 2009. Combined rock slope stability and landslide susceptibility assessment of the Jasmund cliff area (Rügen Island, Germany). Natural Hazards and Earth System Sciences 9, 687-698.

(1) Uhl, D., Klotz, S., Traiser, C., **Thiel, C.**, Utescher, T., Kowalski, E., Dilcher, D. L., 2007. Cenozoic paleotemperatures and leaf physiognomy - A European Perspective. - Palaeogeography, Palaeoclimatology, Palaeoecology 248, 24-31.

Other publications

(2) Günther, A., Obst, K., Schütze, K., **Thiel, C**., 2010. Erläuterungen zur Gefahrenhinweiskarte für gravitative Massenbewegungen am Steilufer von Jasmund (Rügen) 1:10 000, interner Bericht; Bundesanstalt für Geowissenschaften und Rohstoffe, Landesamt für Umwelt und Geologie Mecklenburg-Vorpommern**.**

(1) **Thiel, C.**, 2007. Vergleichende flächenhafte Modellierungen von Rutschungs-empfindlichkeiten der pleistozänen Sedimente an der Steilküste Jasmunds (Rügen/Deutschland). Diploma thesis, Geographisches Institut, Eberhard-Karls-Universität Tübingen (unpubl.).

Conference contributions

(35) **Thiel, C.**, Murray, A. S., Buylaert, J.-P., Schmidt, A., Steffensen, J. P., Willerslev, E., 2010. Post-IR IRSL dating of single grains embedded in ice - a challenging task. Leibniz Pakt Luminescence Workshop, 25.-26.10.2010; Hannover, Germany.

(34) **Thiel, C.**, Horváth, E., Frechen, M., Ostertag-Henning, C., 2010. n-alkane studies, grain size analysis and post-IR IRSL dating applied to Hungarian loess/palaeosol sequences. DAAD-Workshop "Traces of Quaternary Environmental changes preserved in loess of Hungary", 22.-23.10.2010; Budapest, Hungary.

(33) Novothny, Á., Horváth, E., Frechen, M., **Thiel, C.**, Wacha, L., Rolf, C., 2010. Investigating the penultimate and last glacial cycles of the Süttő loess section using luminescence dating, high-resolution grain size and palaeomagnetic data. DAAD-Workshop "Traces of Quaternary Environmental changes preserved in loess of Hungary", 22.-23.10.2010; Budapest, Hungary.

(32) **Thiel, C.**, Horváth, E., Frechen, M., Tsukamoto, S., 2010. Luminescence chronology and high-resolution grain size data for the loess section of Paks (Hungary). International Workshop on Loess Research and Geomorphology, 17.-21.10.2010; Pécs, Hungary.

(31) Novothny, Á., Horváth, E., Frechen, M., **Thiel, C.**, Wacha, L., Rolf, C., 2010. Complex investigation of the penultimate and last glacial cycles of the Süttő loess section

(Hungary). International Workshop on Loess Research and Geomorphology, 17.-21.10.2010; Pécs, Hungary.

(30) Novothny, Á., Horváth, E., Frechen, M., Königer, P., **Thiel, C.**, Wacha, L., Rolf, C., Krolopp, E., Barta, G., Bajnóczi, B., 2010. Detailed chronological and high resolution grain size, geochemical and palaeomagnetic study of the Süttő loess-palaeosol sequence, Hungary. XIX Congress of the Carpathian Balkan Geological Association, 23.-26.09.2010; Thessaloniki, Greece.

(29) **Thiel, C.**, Terhorst, B., Frechen, M., 2010. Chronostratigraphy of Lower Austrian loess/palaeosol sequences. 35th DEUQUA Conference, 13.-17.09.2010; Greifswald, Germany.

(28) **Thiel, C.**, Günther, A., Schütze, K., Obst, K., 2010. Geomorphological mapping as prerequisite for landslide susceptibility modelling of Pleistocene sediments along the coast of Jasmund/Rügen. 35th DEUQUA Conference, 13.-17.09.2010; Greifswald, Germany.

(27) Günther, A., **Thiel, C.**, 2010. An approach to assess the rock slope stability and shallow landslide susceptibility of the Jasmund cliff area (Rügen Island, Germany). 35th DEUQUA Conference, 13.-17.09.2010; Greifswald, Germany.

(26) **Thiel, C.**, Murray, A. S., Buylaert, J.-P., Schmidt, A., Steffensen, J. P., Willerslev, E., 2010. The dose rate to individual sand grains of feldspar embedded in ice. UK Meeting on Luminescence and Electron Spin Resonance Dating, 08.-10.09.2010; Oxford, England.

(25) **Thiel, C.**, Königer, P., Ostertag-Henning, C., Scheeder, G., Novothny, Á., Horváth, E., Wacha, L., Techmer, A., Frechen, M., 2010. Multi-proxy approach for palaeoclimate reconstruction using a loess-palaeosol sequence from Süttő, Hungary. EGU General Assembly, 02.-07.05.2010; Vienna, Austria.

(24) **Thiel, C.**, Terhorst, B., Jaburova, I., Buylaert, J.-P., Murray, A., Frechen, M., 2010. Landscape evolution in Lower Austria: Geodynamic processes comprised in time based on luminescence dating of loess. EGU General Assembly, 02.-07.05.2010; Vienna, Austria.

(23) Hofer, I., **Thiel, C.**, Terhorst, B., Jaburova, I., Buylaert, J.-P., Murray, A., Frechen, M., 2010. The story of landscape evolution in Lower Austria told by sedimentological analysis and luminescence dating. EGU General Assembly, 02.-07.05.2010; Vienna, Austria.

(22) **Thiel, C.**, Buylaert, J.-P., Murray, A., Tsukamoto, S., 2010. On the applicability of post-IR IRSL dating to Japanese loess. 10th International Conference on Methods of Absolute Chronology, 22.-25.04. 2010; Gliwice, Poland.

(21) Königer, P., Wacha, L., **Thiel, C.**, Ostertag-Henning C., Scheeder, G., Novothny, Á., Bajnóczi, B., Horváth, E., Techmer, A., Frechen, M., 2010. Evaluation of bulk carbonate stable isotope composition from the Süttő loess sequence (Hungary) - What can we interpret with an existing chronology? 10th International Conference on Methods of Absolute Chronology, 22.-25.04. 2010; Gliwice, Poland.

(20) **Thiel, C.**, Murray, A. S., Buylaert, J.-P., Schmidt Grene, A., Willerslev, E., Steffensen, J. P., Jain, M., Frechen, M., 2009. Dating the Arctic Ice Cap: an elevated temperature post-IR IRSL protocol applied to ice-embedded single grains of feldspar. German Meeting on Luminescence and Electron Spin Resonance Dating (German LED08), 9.-11.10.2009; Hannover, Germany.

(19) Jahnke, W., Rebens, M., **Thiel, C.**, Tsukamoto, S., Frechen, M., Wagner, B., 2009. Lumineszenz-Datierung an Lössen im Göttinger Raum. German Meeting on Luminescence and Electron Spin Resonance Dating (German LED08), 9.-11.10.2009; Hannover, Germany.

(18) **Thiel, C.**, Klotz, S., Uhl, D., 2009. Palaeotemperature estimates for selected leaf-floras from the Middle Pliocene of Central Europe based on different techniques. NECLIME Annual Meeting, 28.09.-1.10.2009; Izmir, Turkey.

(17) Coltorti, M., Frechen, M., **Thiel, C.**, Tsukamoto, S., 2009. Controversial dating of Late-Middle Pleistocene key deposits of Sardinia. 27th IAS Meeting of Sedimentologists, 20.-23.09.2009; Alghero, Italy.

(16) **Thiel, C.**, Ostertag-Henning, C., Riss, W., Strauß, H., 2009. The ageing of an unusual lake system seen through geochemical glasses. 24th International Meeting on Organic Geochemistry (IMOG), 06.-11.09.2009; Bremen.

(15) **Thiel, C.**, Buylaert, J.-P., Murray, A. S., Terhorst, B., Tsukamoto, S., Frechen, M., 2009. Beyond the Eemian: The application of an enhanced elevated temperature infra-red stimulated luminescence measurement protocol for Late and Middle Pleistocene Danube loess. Loessfest, 31.08.-03.09.2009, Novi Sad, Serbia.

(14) **Thiel, C.**, Murray, A. S., Buylaert, J.-P., Schmidt Grene, A., Willerslev, E., Steffensen, J. P., Jain, M., Frechen, M., 2009. Dating the Arctic Ice Cap: an elevated

temperature post-IR IRSL protocol applied to ice-embedded single grains of feldspar. UK Meeting on Luminescence and Electron Spin Resonance Dating, 26.-28.08.2009; London, England.

(13) **Thiel, C.**, Buylaert, J.-P., Murray, A. S., Elmejdoub, N., 2009. Optically stimulated luminescence dating of Middle to Late Pleistocene marine terraces on the Cap Bon peninsula, N-E Tunisia. UK Meeting on Luminescence and Electron Spin Resonance Dating, 26.-28.08.2009; London, England.

(12) Thomsen, K. J., Murray, A. S., **Thiel, C.**, Derese, C., Jain, M., 2009. Progress towards a non-fading luminescence signal from feldspar. UK Meeting on Luminescence and Electron Spin Resonance Dating, 26.-28.08.2009; London, England.

(11) **Thiel, C.**, Terhorst, B., Hofer, I., Jaburova, I., Buylaert, J.-P., Murray, A. S., Frechen, M., 2009. New insights into landscape evolution of Lower Austria based on luminescence dating of loess. 7th International Conference on Geomorphology (ANZIAG), 06.-11.07.2009; Melbourne, Australia.

(10) **Thiel, C.**, Frechen, M., 2009. Aktuelle Fortschritte aus dem Bereich Lumineszenzdatierung und die Bedeutung dessen für die Paläopedologie und Quartärforschung. 28. Jahrestagung der AG Paläopedologie der DBG, 21.-23.05.2009, Vienna, Austria.

(9) **Thiel, C.**, Buylaert, J.-P., Murray, A. S., Tsukamoto, S., Jain, M., Frechen, M., 2009. Dating loess with high temperature IRSL signals from polymineral fine grains - Luminescence characteristics and comparison with conventional techniques. EGU General Assembly, 19.-24.04.2009; Vienna, Austria.

(8) **Thiel, C.**, Hofer, I., Jaburova, I., Terhorst, B., Buylaert, J.-P., Murray, A. S., Tsukamoto, S., Frechen, M., 2009. Luminescence Dating of the Stratzing Loess Profile (Austria) - New Insights into Landscape Evolution. EGU General Assembly, 19.-24.04.2009; Vienna, Austria.

(7) **Thiel, C.**, Tsukamoto, S., Coltorti, M., Melis, E., Patta, D., Frechen, M., 2008. Radiometric dating of the San Giovanni di Sinis section (western Sardinia, Italy). German Meeting on Luminescence and Electron Spin Resonance Dating (German LED08), 31.10.-02.11.2008; Leipzig, Germany.

(6) **Thiel, C.**, Coltorti, M., Melis, E., Patta, D., Tsukamoto, S., Frechen, M., 2008. New Dating of Late Pleistocene and Holocene Deposits in Sardinia (Italy): Consequences for Coastal Dynamics, Sea Level Change and Neotectonics. 12th International Conference on Luminescence and Electron Spin Resonance Dating (LED08), 18.-22.09.2008; Beijing, China.

(5) **Thiel, C.**, Coltorti, M., Melis, E., Patta, D., Tsukamoto, S., Frechen, M., 2008. A higher sea level during the Holocene in Sardinia? - New findings based on 14C and OSL dating. 34th DEUQUA Conference, 31.08.-06.09.2008; Vienna, Austria.

(4) **Thiel, C.**, Günther, A., Schütze, K., Lange, C., Bibus, E., 2007. Results of geomorphological mapping and landslide susceptibility modelling of Pleistocene sediments along the coast of Jasmund/Rügen. GeoPomerania, 24.-26.09.2007; Stettin, Poland.

(3) Günther, A., **Thiel. C.**, Lange, C., Schütze, K., Kuhn, D., Obst, K., Balzer, D., 2007. An integrated approach to assess slope stability and landslide susceptibility of the Jasmund cliff (Rügen, Germany). GeoPomerania, 24.-26.09.2007; Stettin, Poland.

(2) **Thiel, C.**, Günther, A., Schütze, K., Bibus, E., 2007. Shallow landslide susceptibility modelling - A comparison of different approaches for the coast of Jasmund Peninsula (Rügen/Germany). Pedometrics, 27.-30.08.2007; Tübingen, Germany.

(1) Günther, A., **Thiel, C.**, 2007. Integrated slope stability and sliding susceptibility assessment of the Jasmund cliff area (Rügen Island, Germany). EGU General Assembly, 15.-20.04.2007; Vienna, Austria.

Selbständigkeitserklärung

Hiermit erkläre ich, Christine Thiel,
dass ich die Arbeit eigenständig angefertigt habe. Alle Stellen, die dem Wortlaut oder dem Sinn nach anderen Werken entnommen sind, wurden durch Angabe der Quellen als solche kenntlich gemacht.

Hannover, 4. November 2010